Copyright

by

Minta Carol Akin

2008

The Dissertation Committee for Minta Carol Akin certifies that this is the approved version of the following dissertation:

LOW-ENERGY ELECTRON DRIVEN REACTIONS IN LAYERED METHANOL/AMORPHOUS SOLID WATER FILMS

Committee:

C. Buddie Mullins, Supervisor

Graeme Henkelman

Keith J. Stevenson

Thomas M. Truskett

David A. Vanden Bout

LOW-ENERGY ELECTRON DRIVEN REACTIONS IN LAYERED METHANOL/AMORPHOUS SOLID WATER FILMS

by

Minta Carol Akin, B.S.

Dissertation

Presented to the Faculty of the Graduate School of

The University of Texas at Austin

in Partial Fulfillment

of the Requirements

for the Degree of

Doctor of Philosophy

The University of Texas at Austin

May 2008

Dedication

To Jesse

Acknowledgements

Many people helped me during graduate school, and I will probably not manage to include everybody. Foremost, I would like to thank my advisor, Buddie Mullins, who gave generously of his time and advice to make me a better researcher and teacher, and was always supportive of new ideas. I especially appreciate the flexibility he showed over the last few months that let me cope with my pregnancy as I wrote. I could not have asked for a better mentor, and am extremely grateful to him.

I would also like to thank the members of my doctoral committee, Graeme Henkelman, Keith Stevenson, Thomas Truskett, and David Vanden Bout, for all of their hard work on my behalf and their helpful comments. Jennifer Brodbelt, Ruth Shear, and Harriet Dinerstein also helped me in graduate school in many ways. Thank you.

The research described in this dissertation was performed at the William R. Wiley Environmental Molecular Sciences Laboratory (EMSL) at Pacific Northwest National Laboratory (PNNL) in Richland, Washington, as part of the Summer Research Institute. While there, I worked with Nick Petrik and Greg Kimmel, without whom this dissertation would not exist (or would certainly have a different form). Scott Smith, Mike White, and Russ Tonkyn gave additional support, encouragement, and help troubleshooting. The Department of Energy and the National Science Foundation provided funding for the summer. The Texas Space Grant Consortium provided additional partial funding for the 2007-2008 year.

Finally, I'd like to thank my family and friends—you know who you are. A special thanks goes to Maryam Ali for her wonderful advice about writing and not

panicking. I'd also like to thank my husband, Jesse Pino, for keeping me well-supplied with ondansetron and clean bowls, doing all the housework, proofreading chapter drafts, and the million other things he took care of so I could write. The help from Jesse, Buddie, my committee, Nick, and Greg eliminated many poorly written sentences and typos; any faults remaining in this dissertation are strictly due to me.

LOW-ENERGY ELECTRON DRIVEN REACTIONS IN LAYERED METHANOL/AMORPHOUS SOLID WATER FILMS

Minta Carol Akin, Ph. D.

The University of Texas at Austin, 2008

Supervisor: C. Buddie Mullins

Understanding the radiolysis of impure water and resulting reactions is crucial to many fields. Reactions driven by low energy electrons (LEE) are of special interest, as high-energy radiation generates large quantities of these electrons, which then provide the energy for most subsequent reactions. Interfacially located reactions are also of particular interest, both as models for heterogeneously distributed reactions occurring during radiolysis, and in their own right, as radiation-driven reactions at interfaces are responsible for key processes such as corrosion and DNA damage. To study LEE-driven reactions at interfaces, thin-layered films of amorphous solid water (ASW) and methanol were grown under ultra-high vacuum conditions using molecular beam techniques. The

films were exposed to a beam of low-energy (100eV or less) electrons, and studied using electron-stimulated desorption (ESD) and temperature programmed desorption (TPD).

ESD studies indicated that methanol moves through a water film during deposition at 80 K but not at 50 K. This transport was not seen during thermal annealing, but radiation-induced mixing was observed at all temperatures. Major and minor LEE radiation products of pure methanol films were identified and found to be consistent with previous results. Products of LEE irradiated layered methanol/water films were determined for the first time using ESD and TPD spectra, and found to be limited to H_2, O, O_2, CH_2O, C_2H_6, CO, CO_2, CH_3OCH_3, and CH_3CH_2OH.

The effect of adding methanol to an ASW film on the production in ASW of H_2 and O_2 was also examined. The interface created by the addition of CH_3OH to ASW was found to generate H_2 in previously non-reactive regions of the water film by increasing water-water and water-methanol reactions. Radiative mixing of CH_3OH and ASW enhanced this effect, presumably by increasing the region of disrupted H-bonding in the ASW. In contrast, the addition of CH_3OH at low coverages suppressed O_2 production in both unprocessed and preprocessed ASW layers. Modeling indicates that methanol scavenging of the O_2 precursor OH and of the reaction-driving electrons is responsible for this reduction in O_2 signal.

Table of Contents

List of Tables xi

List of Figures xii

Chapter 1: Introduction 1

Why use ASW? 2

Thermal processes in ASW 4

Thermal processes in mixed water/methanol systems 6

Basic radiation-driven mechanisms in pure water films 9

H_2 and O_2 production in pure water 10

Radiation-driven products in pure methanol 11

An increasingly complicated system: Radiation-driven processes in doped water films 13

Dissertation Overview 15

References 19

Chapter 2: Observations on electron-driven reactions between methanol and ASW 25

Introduction 25

Methods 26

Results and Discussion 29

Conclusions and Future Work 44

References 45

Chapter 3: The effect of creating chemical interfaces in amorphous solid water/methanol films on electron-stimulated H_2 production 47

Introduction 47

Previous Work....48
Methods....49
Results and Discussion....52
Conclusions and Future Work....66
References....68
Chapter 4: Suppression of electron stimulated O_2 production from amorphous solid water by CH_3OH....70
Introduction....70
Methods....72
Results and Discussion....75
Conclusions and Future Work....87
References....88
Chapter 5: Closing Remarks....90
Summary....90
Future Work....96
References....98
Tables and Figures....100
Appendix....154
Bibliography....155
Vita....162

List of Tables

2.1: Experimental cracking fractions for methanol..... 100

2.2: Major desorption peaks during TPD from 30 ML unprocessed CH_3OH 104

2.3: Pure methanol TPD products..... 120

2.4: TPD products, methanol-capped films..... 121

2.5: TPD products, sandwich films..... 122

3.1: Sources of hydrogen species from each isotopologue of methanol 127

List of Figures

2.1: Deposition of ASW over CH_3OH at T=80K leads to an increased concentration of CH_3OH at the sample surface. 101

2.2: O_2 production from a methanol-capped water film deposited at 50 K and irradiated at 80K. 102

2.3: O_2 production from a methanol-capped water film deposited and irradiated at 80K. 103

2.4: ESD products of 30 ML CH_3OH. 105

2.5: Selected ESD products of 30 ML CH_3OH, 2μA. 106

2.6: ESD products of 30 ML CH_3OH, 20eV. 107

2.7: TPD products after irradiation of 30 ML CH_3OH using 20eV electrons. 108

2.8: TPD spectra of 30 ML CH_3OH following irradiation with 100 eV electrons. 109

2.9: TPD products after irradiation of 30 ML CH_3OH at different temperatures..... 110

2.10: Increasing the irradiation temperature to 80K increases the pure water signal. 111

2.11: CO desorption during ESD from n ML CH_3OH on 80 ML H_2O..... 112

2.12: Methanol desorption from a water film before and after irradiation 113

2.13: The addition of methanol to a water film creates additional atomic oxygen, detected in the TPD. 114

2.14: Major TPD peaks of a) 4 ML b) 10 ML and c) 30 ML CH OH on 80 ML ASW after irradiation. 115

2.15: Minor TPDs of a) 4 ML b) 10 ML and c) 30 ML CH_3OH on 80 ML ASW after irradiation. 116

2.16: 31 amu TPD from selected sandwich films. 117

2.17: Surface area measurements using Kr. 118

2.18: CO_2 surface area measurements. 119

3.1: Hydrogen production from H_2O and D_2O is similar. 123

3.2: Temperature affects H_2 formation and desorption from CH_3OH. 124

3.3: Molecular hydrogen isotopologues desorbing from CD_3OH. 125

3.4: Molecular hydrogen isotopologues desorbing from CD_3OD. 126

3.5: D_2 produced in methanol (CD_3OD) layer. 128

3.6: D_2 produced from water beneath a methanol cap. 129

3.7: The addition of CH_3OH to the surface of D_2O inhibits D_2 formation. 130

3.8: Integral of D_2 signal showing reduction of D_2 production by CH_3OH. 131

3.9: D_2 produced during ESD of CD_3OD on D_2O. 132

3.10: D_2 produced at the methanol/water interface. 133

3.11: Integrals of D_2 produced at methanol/water interface, peaking at ~1 ML methanol coverage. 134

3.12: The addition of methanol can increase the availability of D in water to form D_2. 135

3.13: Methanol is a more efficient suppressant than H_2O of D_2 production from D_2O. 136

3.14: Total D_2 production from D_2O decreases greatly when the capping layer includes CH_3OH. 137

3.15: Methanol may act as an internal interface. 138

3.16: Saturation of D_2 production. 139

4.1: Suppression of O_2 production by CH_3OH capping layer. 140

4.2: Time delay in O_2 production caused by methanol. 141

4.3: $^{18}O_2$ Suppression kinetics. 142

4.4: Sandwich films of water and 1 ML CH_3OH. 143

4.5: $^{16}O_2$ production during ESD from isotopically labeled sandwich films. 144

4.6: $^{16}O^{18}O$ production during ESD from isotopically labeled sandwich films. 145

4.7: $^{18}O_2$ production during ESD from isotopically labeled sandwich films. 146

4.8: Dose dependence of oxygen suppression by buried methanol. 147

4.9: O_2 production from capped pre-irradiated $H_2{}^{18}O$ films..... 148

4.10: O_2 production dependence on surface MeOH concentration..... 149

4.11: Effect of a $H_2{}^{16}O$ spacer layer on O_2 suppression by methanol..... 150

4.12: Suppression of water by CH_3OH. 151

4.13: Model 2 predictions compared to data from Figure 4.1. 152

4.14: A comparison of Model 3 with the data. 153

Chapter 1: Introduction

An understanding of the mechanisms underlying the radiolysis of water is crucial in many fields, including biology, medicine, atmospheric sciences, nuclear reactor design, nuclear waste storage and remediation, clean energy sources, astrochemistry, and astrophysics. The radiolysis of water leads to both ions and radicals, which lead to subsequent reactions. The damage done by radiation and resulting free radicals in cells to macromolecules such as DNA is well known, and is used to sterilize biological work hoods. It is of critical importance in medicine as well, as such damage can be responsible for cellular aging and certain cancers. Further advances in treating these problems and developing new radiation-based therapies will require a thorough understanding not only of the mechanisms of radiolysis in pure water, but dilute aqueous solutions of organic compounds as well. In the upper atmosphere, radiation-driven reactions are extremely common. Photolytically generated radicals often drive such reactions, some of which act to deplete ozone concentrations or form acid rain, and many of which are thought to occur on ice nanoparticles in cirrus clouds.

Inside a water-cooled nuclear reactor, energetic particle bombardment leads to the formation of corrosive H_2O_2 and OH radicals that damage the reactor's structure. To reduce the corrosion rate, H_2 gas is injected into the water to scavenge the H_2O_2, but significantly greater amounts of H_2 are needed than predicted by theory.[1] In nuclear waste tanks, the opposite problem may arise; decaying radiation generates an excess of H_2 gas. This additional H_2 poses an increased risk to the tanks' stability and to any workers attempting to clean up or control the waste. As in biological systems, the presence of

organic compounds in the tanks increases the complexity of the system and likely contributes to the excess H_2. However, there is a silver lining; this excess production of H_2 may point the way to a cheap H_2 source that could be used in a hydrogen economy.[1] This potential application is increasingly important as the rising environmental and monetary costs of fossil fuels drives greater interest in such clean alternative energy systems.

Finally, astrobiologists, astrochemists, and astrophysicists must also consider and understand the radiolysis of water. In space, water is the most common solid compound[2] and is a necessary criterion in determining where to look for life outside our own planet. Energy is needed to drive any biological or prebiotic reactions, and highly energetic radiation is a major (and sometimes only) source. Radiation-driven reactions, and especially those in amorphous solid water (ASW), have been shown to generate necessary biological precursors for earth-like life,[3-6] including homochiral amino acids.[7, 8] ASW-catalyzed reactions are also responsible for the generation and destruction of H_2 on grain surfaces,[3] which must be considered in determining the origins and evolution of many objects, including molecular clouds and the interstellar medium.

Why use ASW?

Previous work has studied radiolysis of vapor, liquid, and solid phases of water.[1] In the applications mentioned above, the condensed phases are of greatest concern. In the work presented in this dissertation, we limit ourselves to ASW films, and neglect liquids and crystalline solids. ASW is an eminently suitable medium for this work. It is directly

applicable to the astronomical applications, as it is the form predominantly found in those environments. It is also directly applicable to biological research, as the formation of ASW in tissue samples can lead to problems in preserving sample structure.[9] However, ASW's defining lack of long-range order also makes it an excellent model for crystalline ice surfaces,[10, 11] liquids, and glasses[12, 13] considered in other fields. The unique characteristics of ASW make it a preferred medium, as reactions can be slower compared to liquid water, easing measurements, and some data are available in the condensed phase only for ASW.[1] Additionally, the slower mixing of ASW compared to liquid water is an advantage in studying heterogeneously distributed reactions, such as those occurring at interfaces or along particle tracks. For this purpose, ASW is preferred over crystalline ice (CI), as the defect-laden structure better mimics liquid structure and provides greater mobility to guest molecules.[14]

However, studying these reactions in ASW is not without its complications. Considerable debate about the phase state (i.e., if it is a supercooled liquid, a true solid, or both) and other fundamental data such as the glass transition temperature exists in the literature.[15-31] Like crystalline ices, ASW has multiple forms, which are generally determined by the growth conditions. For example, the density of ASW can vary from 0.16 g/cc in porous structures to 1.31 g/cc in films grown at high pressure.[32] Such variation in density is exaggerated by the introduction of pores or voids to the ASW structure, which can contain up to 80 % of the solid's volume. The most common form of ASW is called "low-density" ASW, even though its density is comparable to that of cubic ice, ~0.94 g/cc,[33] to contrast it with the high-pressure forms. Low-density ASW is grown

by vapor deposition at temperatures less than ~120K under UHV conditions and in space, making it the most common form of water in the universe. This form is the focus of our work, and is the form referred to in this document. The various forms of ASW have required the development of new techniques to grow a consistent dense, non-porous ASW film for experimental purposes. Care must be employed in growing the films, as templating the surface with crystalline ice prevents the growth of ASW.[34] The preferred method, used in our experiments, requires that a molecular beam of water molecules be dosed perpendicularly to the supporting substrate held at T less than 90 K. This method creates films of uniform, maximum density[35] and minimum porosity[36] without requiring annealing and prevents the growth of CI. For our purpose, this is ideal, as the development of a porous or otherwise rough surface will affect the amount of methanol deposited, the extent of the methanol/water interface, and the mobility of the methanol in the ASW.

Thermal processes in ASW

To understand the non-thermal effects discussed later, a brief summary of thermal processes in pure and doped ASW is given here. As mentioned previously, there is extensive debate in the literature about fundamental characteristics of ASW, such as its phase, the nature of the crystallization transition, and the glass temperature. There is evidence that ASW is a glassy solid,[2, 15, 37, 38] and additional evidence that it is a liquid (or very liquid-like) instead.[16, 17, 21, 30, 39-41] Further debate about whether water is a strong or weak liquid complicates the matter. However, there is a growing body of evidence that if

water is a liquid, it is a strong liquid at T less than 160 K, and cannot be a fragile liquid.[20, 26, 42-44]

As the ASW is heated, it crystallizes into cubic ice at ~160 K (exact crystallization temperature varies with heating histories). At this time, the increased mobility of the ASW increases mixing of the water with itself, as seen by isotopic labeling.[24, 40] Structural changes occur simultaneously as crystallization begins via small-domain nucleation.[44] Crystallization is not complete, as the crystal domains coexist with ASW domains that can trap volatiles during crystallization if the volatile concentration smaller than 10 %.[44] The coexisting ASW and crystal grains, and the stresses induced by crystallization, lead to the development of cracks in the water film, through which trapped species can explosively desorb, and which also provide a major transport mechanism for water.[26, 42] These trapped molecules would normally have desorbed at much lower temperatures, and therefore the explosive desorption marker is usually a very sharp desorption peak occurring at the water crystallization shoulder, as water desorption slows.[45] Similar results have been seen with molecules dosed onto porous ASW films that become trapped as the pores collapse during annealing to be released later,[46-48] indicating that ASW can retain possible reactants at temperatures greater than would be predicted.

The additional motion of the water molecules at the crystallization temperature increases the likelihood of reaction in the ASW. However, the effect of adding dopants to the film has been studied in only a limited manner, primarily to gather infrared (IR) spectra for astronomical surveys, rather than information on transport via diffusion or cracking channels or to gather information about reaction pathways. Studies on the

formation of clathrate hydrates, for example, have only included a few acids in the context of adsorption on stratospheric ice particle surfaces. McClure *et al.* showed that the addition of HNO_3 in small quantities to ASW reduced the degree of fracture, and the associated transport, while accelerating crystallization.[42] Souda[49] found that formic acid and propanol dosed on a D_2O surface were hydrated, and suggests that these compounds quench the crystal transition by remaining on the surface and reducing surface tension.

Thermal processes in mixed water/methanol systems

Gunster *et al.* [50] used metastable impact electron spectroscopy (MIES) and ultraviolet photoelectron spectroscopy (UPS) to study the interaction of thin films (2-10 ML) of CH_3OH and D_2O on MgO(100). MIES is a surface-sensitive technique while UPS signals incorporate some of the bulk response, so the combination of these two techniques enabled the researchers to determine the location of each chemical, and to describe qualitatively the mixing at the surface and in the bulk. Their results indicate that a near monolayer of methanol on 6 ML water was sufficient to cover the water surface, indicating a slightly higher sticking probability of MeOH on D_2O than on MgO or MeOH. At the same time, methanol did not penetrate into the bulk of D_2O, but remained localized on the surface. Heating the $CH_3OH/D_2O/MgO$ sample led to mixing beginning at about 140K, with desorption complete by ~165K. However, if methanol was pre-deposited and water dosed on top of it, mixing appeared to occur at 100K, the dosing temperature. Even dosing 8 ML D_2O atop 2 ML CH_3OH led to a surface layer that was mixed methanol/water, apparently driven by the energetic cost of solvating the

hydrophobic methyl group. Smaller changes were observed upon heating this pre-mixed sample, but at 155K the two were both comparably mixed. For contrast, films of methanol and ethanol, where both molecules are amphiphilic, were observed to intermix completely prior to the onset of desorption at ~120K by Ayotte and coworkers.[51]

Temperature Programmed Desorption (TPD) of 8 ML D_2O/2 ML CH_3OH/MgO shows two methanol peaks, occurring at 162 K, approximately the crystallization temperature of D_2O, and at 175K, when desorption of D_2O/CH_3OH is complete.[50] In contrast, TPD of 8 ML D_2O/3.5 ML CH_3OH/MgO shows two methanol peaks at 145K and 174K. While the 174 K peak is again due to completing desorption, the 145K peak shows different characteristics, including a sharp rise beginning at 140K and the appearance of a water signal at the same temperature not present in the 8 ML D_2O/2 ML CH_3OH/MgO sample. This temperature is too low to be caused by the ASW to cubic ice phase transition. Gunster *et al.* argue that the higher mobility of the capping water layers at 140K is responsible for the sudden appearance of CH_3OH, and the associated water peak results from entrainment by methanol desorption.

However, they do not address the likelihood, based on the observed mixing, that methanol is already present at the surface of the water multilayer. We cannot eliminate the possibility that this 140K peak is surface desorption of methanol from an enriched methanol/water surface, which would also lead to an entrained water peak, consistent with results by Wolff, Carlstedt, and Brown.[52] It is clear that during deposition of water, methanol is sufficiently mobile to act as a surfactant, moving to (or remaining at) the surface to minimize the total energy by placing the hydrophobic methyl group at the

surface. Any resulting "capping water layer" is likely a mixture of water and methanol. This mix would have increased mobility, leading to the lower desorption temperature, resulting from a decreased mean number of H-bonds per molecule and increased disruptions by the hydrophobic methyl group. However, the degree of mixing that occurs in sub-surface layers (e.g., if lower layers are mixed to a greater or lesser degree than the surface) when water is the capping film is unknown, and has not yet been studied.

The orientation of methanol on the surface of ice Ih (0001) at 0K was simulated by Picaud, Toubin, and Giradet.[53] They also found that the interaction between water and methanol is stronger than the interaction between methanol and methanol. Two probable adsorption sites for methanol on Ih were found, in which the more stable (-442meV vs. –427meV) is oriented such that the OH bond points to a water oxygen and the methyl group lies over a cavity in the ice crystal. Additional simulations by Collignon and Picaud [54] focused on mobile surface layers as opposed to rigid layers. Not surprisingly, the methyl groups of CH_3OH are tilted away from the ice surface, and CH_3OH acts to hydrogen bond (by donation and acceptance of H) with both water and other methanol molecules.

Unlike mixed alcohol films, water and methanol mixed films do not mix when the methanol is dosed at the surface. Methanol acts as a surfactant when water is dosed atop it at 100 K, moving to the surface and increasing its local concentration. This transport only occurs during deposition, and not during subsequent heating.

Basic radiation-driven mechanisms in pure water films

Experiments on the radiolysis of liquid water showed that high energy particles (γ rays, α particles, neutrons, and highly energetic electrons, for example) generate large quantities of lower-energy electrons by ionization, both directly by stripping an electron to form an energetic ion, and through subsequent collisions of that ion.[1] Secondary ion collisions in particular yield large quantities of these lower energy electrons, which have an average energy less than 100eV. These ~100eV electrons generate yet lower energy electrons, of average energy less than 10eV,[55] through a similar ionization mechanism. Both the first and second series of ionization events are localized in the water structure, and the subsequent excitations and newly formed ions have a localized distribution in the water, concentrated near the original particle's path, as these processes happen on a femto- to pico-second time scale.[1] The resulting ionized and excited water molecules can follow several reaction pathways to form H_3O^+, OH-, O-, and H-, OH, H, solvated electrons, H_2, O, and H. These species in turn can form new species such as H_2O_2 and HO_2. Our full understanding of the processes leading to these products is complicated by the strong intermolecular interactions of water molecules and its high polarity, and a lack of knowledge about how these characteristics impact the structure and formation of ions and excitons.

H_2 and O_2 production in pure water

To better understand the radiation chemistry of the reactions, research has focused on the reactions driven by the ~100eV electrons. In water films, the main molecular products are O_2 and H_2 but H, O, and H_2O_2 have also been observed.[56] Photoionization studies have observed mainly H^+ at 21eV (584Å), and H^+ and H_3O^+ at higher energies (41eV, or ~300 Å).[57] Anionic H and D have been found to desorb from ASW surfaces at very low electron energies of 5.5 eV, with maximum anionic yield peaking at ~7.4 eV, comparable to the first water excitation at 7.3 eV. [58] These anions have a very high probability of trapping on the ASW surface,[58] where they were later found to be the source of D_2 production at 6.3 eV, by reaction with H_2O (D_2O).[59] At higher energies, additional reactions are available, including that of H_3O^+ with trapped electrons, and direct formation from excited water states.[60] Petrik and Kimmel [61] later examined the production of H_2 from water films using ~100eV electrons. H_2 production is confined to the interfaces, in this case the water/vacuum interface and the water/Pt (111) interface. No H_2 was produced in the bulk regions of the water. However, the bulk region is the main region of energy absorption, indicating that excited water molecules must diffuse to the interfaces before they can react. The implications of these results are discussed in Chapter 3, where we examine the effect the addition of H-rich methanol on H_2 production.

O_2 production was previously characterized by Petrik, Kavetsky, and Kimmel,[62] and found to increase with exposure until it saturates. This increase in O_2 production is the result of several electron-driven reactions that yield increasing quantities of O_2

precursors such as OH, H_2O_2, and HO_2. These precursors are then consumed in O_2 production and saturation correlates to a steady-state process. The details of this multi-step reaction are discussed in Chapter 4. Briefly, using isotopically labeled water ($H_2{}^{16}O$, $H_2{}^{18}O$, and D_2O), O_2 production results from HO_2 dissociation occurring at the water/vacuum interface only during exposure. No reactions occurred if the electron beam was turned off. If the beam was restarted, O_2 production immediately resumed at saturation levels. The surface concentration of HO_2 and other precursors (H_2O_2 and OH) at saturation were predicted by kinetic modeling to be ~0.01 to 0.03 ML relative to the water coverage (1 ML).

Radiation-driven products in pure methanol

Stockbauer, Bertel, and Madey used variable UV photoemission and photon stimulated desorption to study pure MeOH films.[63] They found that the primary desorbed ions were H^+, which accounted for over 98% of the total ion yield. Electron stimulated desorption (ESD) experiments and isotopic labeling confirmed that in condensed films, the dominant source of H^+ is due to CH bond cleavage (as compared to the gas phase, where both CH and OH bond cleavage contribute) when the electron energy is 30-70 eV, consistent with the results of Burrows *et al.*[64] Stockbauer and coworkers state that the onset of proton desorption was ~21eV, and suggest that these protons originate from excitation of the 4a′ orbital, focused on the methyl group.[63] The emission of anions occurs at much lower energies; Parenteau, Jay-Gerin, and Sanche [65] detected H- as low as 6 eV, with the signal peaking around 8.3 eV, indicating that in a mixed film both

methanol and water may generate anionic hydrogen at very low energies. By using CH_3OD and CD_3OH, they found that the hydrogens originated from the methyl and hydroxyl groups. Dissociation of the hydroxyl group is similar to that seen in water, and is primarily responsible for anion production at energies lower than 9 eV, while CH scission is the main source of H- at energies greater than 9 eV.[66] Neutral CO was also generated at these energies as a result of dissociation.[67]

As with water, the products of pure methanol films are interface sensitive and dependent on the film thickness. Working on an Ar substrate, Kawanowa *et al.* [68] found that methyl ion fragments, hydronium ions, CHO^+, and $CH3O^+$ ions were emitted, with the highest yields seen at the lowest coverages. From a thick layer, only protons were observed. Henderson, Otero-Tapia, and Castro[69] studied the electron induced decomposition of methanol monolayers on TiO_2 (110) using TPD and ESD. Major post-irradiation (100eV) *ion* fragments were D^+, O^+, and OD^+; neutrals were not reported but the authors speculated that they are major channels. Work by Schwaner and White[70] examined the low energy electron induced fragmentation of methanol on silver (111). As on TiO_2 (110),[69] methanol was not observed to thermally decompose. Following irradiation, primary products were water, methane, hydrogen, formaldehyde, and glycoaldehyde, the latter observed only from multilayers. CH bond dissociation was found to be the primary route to H_2CO formation, while CO bond dissociation led to CH_3 and OH groups; OH bond dissociation was found to occur only at long irradiation times.[70] Of particular interest to our work with oxygen-rich water, Sasaki, Itai, and Iwasawa [71] studied the decomposition of methanol on Ru (001) precovered with O. The

presence of the oxygen enhanced selective CH scission and suppressed CO scission, promoting the formation of CO relative to Ru (001) not precovered with O. These results lead us to expect large quantities of H or H_2 from our methanol-doped water films, as well as significant CO and CH_2O signals. However, results of electron-induced reactions (EIR) and TPD experiments by Harris *et al.* [72] indicate that C_2H_4, $(CH_2OH)_2$, CH_3OCH_2OH, CH_3OCH_3, H_2CO, and CH_3CH_2OH are also possible products, and that detection of CH_3 and CH_4 is likely. A more thorough discussion of observed products and possible mechanisms will be given in Chapter 2.

An increasingly complicated system: Radiation-driven processes in doped water films

As mentioned previously, most work with water/organic mixed films has focused on IR spectra for astronomical identification or to determine possible products, many of which have produced methanol or methanol fragments. [73-80] However, despite the ubiquity of methanol/water mixes in astronomical and terrestrial environments, limited work has been completed examining processes of these mixed or layered films. Much of the work that has been done has focused on very energetic ions or specific photoemission lines common in space.

Palumbo, Castorina, and Strazzulla examined the effects of ion irradiation of 3-30keV ions on pure methanol and mixed methanol-water ices using IR spectroscopy. While they found that the pure methanol produced significant water during irradiation, the methanol-water mixes showed much smaller changes, although some CO and CO_2

was detected.[81] Likewise, Brunetto *et al.* [80] examined the radiolysis products of methanol and water-methanol mixtures exposed to 30 keV and 200 keV ion radiation, and found CO and CH_4 to be the primary products. Wu, Yang, and Judge determined the ion desorption yields of pure water, pure methanol, and mixed water-methanol ices at 77K caused by radiation at 58.4 nm (21.2 eV). [82] They found that the mixed ices showed enhanced ion desorption yields compared to the pure ices, possibly due to greater disruption of H-bond network or to reduced ionization potentials previously observed in the condensed phase.[83]

Radiation-driven processes in pure ASW and in pure methanol have been examined, but work so far on mixtures of the two has been limited and has neglected the role of the methanol/water interface. However, such mixtures are extremely common in many settings where ASW research has applications: comets and icy bodies, clouds, cells, and retired nuclear reactors. In these circumstances, the role of the interface can be crucial, as the introduction of any interface disrupts the H-bonding network of ASW and changes its reactivity. Major products of ASW radiolysis, H_2 and O_2, are formed primarily at such interfaces. These reactions require both matter and energy transfer across that interface. Studying these mixed films and their interfaces will improve our understanding fundamental topics such as hydrogen-bonding networks, mixing at low temperatures, and energy transport.

Dissertation Overview

This dissertation examines radiation-driven processes in mixed methanol-water films. Extra attention is given to the generation and destruction of molecular hydrogen and molecular oxygen due to the importance of these species in environments of interest, nuclear waste tanks and astronomical ices. In the former, the presence of H_2 poses a serious hazard to attempts to clean up contaminated sites. The build up of gases in these waste tanks also increases the risk of developing a leak in the tank, especially in the case of older, single-walled tanks. Previous studies have found greater quantities of H_2 present in these tanks than predicted by theory. Our research shows that this excess H_2 is likely due to the presence of small quantities of organic compounds, a factor that must be included in future models of nuclear waste storage and treatment. The formation of O_2 from water present in these tanks only increases the combustion and containment hazards posed by H_2 build up, and consequently must be considered.

Water and methanol mixes are common in astronomical ices of many types, including comet nuclei, interstellar dust grain mantles, asteroids, and moons/planetary bodies. Depending on the particular ice environment, the motivation for understanding these processes changes. In a comet, we are most interested in reaction byproducts and the possible formation of organic compounds relevant to life's origins. On a grain mantle or in a gas cloud, both possible organic compounds and the creation and destruction of H_2 are of importance.

All of the experiments described in this dissertation were performed using an ultra-high vacuum chamber and molecular beam techniques to grow smooth, dense, non-porous ASW, CH_3OH, and layered films. A TiO_2 (110) crystal was used as the growth substrate. However, some of the experiments reference ASW films grown on a Pt (111) crystal under the same conditions. In very thin films (40 ML or less), the substrate does play a role in determining reaction products and promoting reactions. However, in our experiments, we focused on relatively thick films of 80 ML or more, rendering the nature of the substrate irrelevant. Experiments with thick ASW films on TiO_2 (110) and Pt (111) yield very similar ESD spectra and are comparable. TPD peaks from these experiments are not compared to those using a Pt (111) substrate, although the basic shape of the water desorption peak is similar.

Chapter 2 comprises an overview of the results from these experiments. ESD and TPD spectra are analyzed to determine major products and processes of irradiation. Pure methanol, methanol-capped water films (methanol/water/TiO_2 structures), and methanol-sandwiched films (water/methanol/water/TiO_2 structures) are discussed. These experiments show that methanol is quite mobile during deposition at 80 K, acting as a surfactant, but immobile at 50 K. We also find that the methanol-water films, even for 30 ML thick methanol layers, produce fewer product species. The kinetics of desorption are not discussed, as up to 4 peaks overlap during desorption. The TPD data indicate that methanol and water co-desorb over a broad temperature range, and are mixed during the irradiation cycle.

Chapter 3 discusses how methanol changes H_2 production from water films. H_2 generation in both methanol and water begins immediately with the onset of radiation. Methanol generates copious quantities of hydrogen compared to pure water. Although the CH bond is slightly weaker than the OH bond as described above, we find that the main difference at the energy levels examined is not the quantity of H generated at each functional group, but the sustainability of H_2 production by that group, with H_2 production from the CH_3 group persisting longer. Capping layers of methanol on ASW quickly block the prompt H_2-forming water-vacuum interface. However, at sub-monolayer doses, methanol increases the ability of water to generate H_2 by increasing H_2 production at later times. This increase appears to be due to the creation of an extended methanol/water/vacuum interface. Similar results were seen with buried methanol/water interfaces, where the H_2 signal from water was observed to increase by as much as 40%. This increase is due to the creation of a reactive methanol/water interface in regions of the bulk water that are typically unreactive. When the effect of mixing between the water and methanol layers is considered, i.e., at longer irradiation exposures, the increase is greatest. We propose that these new interfaces increase the number of dangling bonds, more easily trapping the excitons that drive the reaction. The disruption of ASW's H-bonding network by methanol may also increase the mobility of water molecules near the interface and aid H_2 production.

The fourth chapter covers the suppression of O_2 production from water and explores the mechanisms by which methanol interrupts this multi-step reaction process. In water, O_2 is known to form at the vacuum interface. We find that the addition of

methanol to this interface, even at very low (0.05 ML) coverages, suppresses the production of O_2 from water in an unprocessed film. Similarly, a monolayer of methanol in the upper 30 layers of a water film also suppresses O_2 production, with greater suppression observed as the methanol was placed closer to the vacuum interface, and no O_2 produced during the radiation cycle when it was in the uppermost 10 layers. Unlike H_2 production, in which hydrogen formed at the methanol/water interface could come from either source, the little O_2 that was observed to form is almost exclusively (more than 95%) from water, with very little O mixing between the two layers. We found that methanol was similarly opaque to O_2 produced below the methanol layer, with nearly all of the detected O_2 resulting from water capping layers. Again, buried methanol layers act as an internal interface in a manner strongly resembling the interface created by Pt or TiO_2, creating a reactive interface in the normally non-reactive bulk water. These results, and O_2 suppression, are even more noticeable in pre-processed water films that have a saturation concentration of O_2 precursor molecules (HO_2, H_2O_2, and OH). We confirm that the O_2 suppression ability of methanol is a long-range effect that does not require methanol to be present at the precursor-saturated interface. These results all suggest that methanol is preferentially trapping excitons and reacting with OH at the vacuum interface, preventing the formation of the necessary O_2 precursors HO_2 and H_2O_2 in the film. Expanding upon the kinetic model used by Petrik *et al.*,[62, 84] we show that the reactions of methanol with electrons, HO_2, and OH account for the O_2 suppression in the unprocessed and preprocessed films.

In the final chapter, the major findings, and possible applications, of these experiments are summarized. Future avenues of research are also discussed.

References

1. Garrett, B. C.; Dixon, D. A.; Camaioni, D. M.; Chipman, D. M.; Johnson, M. A.; Jonah, C. D.; Kimmel, G. A.; Miller, J. H.; Rescigno, T. N.; Rossky, P. J.; Xantheas, S. S.; Colson, S. D.; Laufer, A. H.; Ray, D.; Barbara, P. F.; Bartels, D. M.; Becker, K. H.; Bowen, H.; Bradforth, S. E.; Carmichael, I.; Coe, J. V.; Corrales, L. R.; Cowin, J. P.; Dupuis, M.; Eisenthal, K. B.; Franz, J. A.; Gutowski, M. S.; Jordan, K. D.; Kay, B. D.; LaVerne, J. A.; Lymar, S. V.; Madey, T. E.; McCurdy, C. W.; Meisel, D.; Mukamel, S.; Nilsson, A. R.; Orlando, T. M.; Petrik, N. G.; Pimblott, S. M.; Rustad, J. R.; Schenter, G. K.; Singer, S. J.; Tokmakoff, A.; Wang, L. S.; Wittig, C.; Zwier, T. S., Role of water in electron-initiated processes and radical chemistry: Issues and scientific advances. *Chem. Rev.* **2005,** 105, (1), 355-389.
2. Angell, C. A., Amorphous water. *Annu. Rev. Phys. Chem.* **2004,** 55, 559-583.
3. Duvernay, F.; Chiavassa, T.; Borget, F.; Aycard, J. P., Experimental study of water-ice catalyzed thermal isomerization of cyanamide into carbodiimide: Implication for prebiotic chemistry. *J. Am. Chem. Soc.* **2004,** 126, (25), 7772-7773.
4. Takano, Y.; Tsuboi, T.; Kaneko, T.; Kobayashi, K.; Marumo, K., Pyrolysis of high-molecular-weight complex organics synthesized from a simulated interstellar gas mixture irradiated with 3 MeV proton beam. *Bull. Chem. Soc. Jpn.* **2004,** 77, (4), 779-783.
5. Walch, S. P.; Bauschlicher, C. W.; Ricca, A.; Bakes, E. L. O., On the reaction CH_2O+NH_3 -> CH_2NH+H_2O. *Chem. Phys. Lett.* **2001,** 333, (1-2), 6-11.
6. Woon, D. E., Pathways to glycine and other amino acids in ultraviolet-irradiated astrophysical ices determined via quantum chemical modeling. *Astrophys. J.* **2002,** 571, (2), L177-L180.
7. Bernstein, M. P.; Dworkin, J. P.; Sandford, S. A.; Cooper, G. W.; Allamandola, L. J., Racemic amino acids from the ultraviolet photolysis of interstellar ice analogues. *Nature* **2002,** 416, (6879), 401-403.
8. Caro, G. M. M.; Meierhenrich, U. J.; Schutte, W. A.; Barbier, B.; Segovia, A. A.; Rosenbauer, H.; Thiemann, W. H. P.; Brack, A.; Greenberg, J. M., Amino acids from ultraviolet irradiation of interstellar ice analogues. *Nature* **2002,** 416, (6879), 403-406.
9. Al-Amoudi, A.; Dubochet, J.; Studer, D., Amorphous solid water produced by cryosectioning of crystalline ice at 113 K. *J. Microsc.-Oxford* **2002,** 207, 146-153.
10. Delzeit, L.; Powell, K.; Uras, N.; Devlin, J. P., Ice surface reactions with acids and bases. *J. Phys. Chem. B* **1997,** 101, (13), 2327-2332.

11. Buch, V.; Bauerecker, S.; Devlin, J. P.; Buck, U.; Kazimirski, J. K., Solid water clusters in the size range of tens-thousands of H_2O: a combined computational/spectroscopic outlook. *Int. Rev. Phys. Chem.* **2004,** 23, (3), 375-433.
12. Yue, Y. Z.; Angell, C. A., Water behaviour - Reply. *Nature* **2005,** 435, (7041), E1-E2.
13. Morishita, T., Anomalous diffusivity in supercooled liquid silicon under pressure. *Phys. Rev. E* **2005,** 72, (2).
14. Devlin, J. P., Structure, spectra, and mobility of low-pressure ices: Ice I, amorphous solid water, and clathrate hydrates at T < 150 K. *J. Geophys. Res.-Planet* **2001,** 106, (E12), 33333-33349.
15. Yue, Y. Z.; Angell, C. A., Clarifying the glass-transition behaviour of water by comparison with hyperquenched inorganic glasses. *Nature* **2004,** 427, (6976), 717-720.
16. Jenniskens, P.; Banham, S. F.; Blake, D. F.; McCoustra, M. R. S., Liquid water in the domain of cubic crystalline ice I-c. *J. Chem. Phys.* **1997,** 107, (4), 1232-1241.
17. Johari, G. P., State of water at 136 K determined by its relaxation time. *Phys. Chem. Chem. Phys.* **2005,** 7, (6), 1091-1095.
18. Koza, M. M.; Geil, B.; Schober, H.; Natali, F., Absence of molecular mobility on nanosecond time scales in amorphous ice phases. *Phys. Chem. Chem. Phys.* **2005,** 7, (7), 1423-1431.
19. La Spisa, S.; Waldheim, M.; Lintemoot, J.; Thomas, T.; Naff, J.; Robinson, M., Infrared and vapor flux studies of vapor-deposited amorphous and crystalline water ice films between 90 and 145 K. *J. Geophys. Res.-Planet* **2001,** 106, (E12), 33351-33361.
20. Minoguchi, A.; Richert, R.; Angell, C. A., Dielectric studies deny existence of ultraviscous fragile water. *Phys. Rev. Lett.* **2004,** 93, (21).
21. Minoguchi, A.; Richert, R.; Angell, C. A., Dielectric relaxation in aqueous solutions of hydrazine and hydrogen peroxide: Water structure implications. *J. Phys. Chem. B* **2004,** 108, (51), 19825-19830.
22. Mitlin, S.; Leung, K. T., Temporal evolution of an ultrathin, noncrystalline ice deposit at crystallization near 160 K studied by FT-IR reflection-absorption spectroscopy. *Can. J. Chem.* **2004,** 82, (6), 978-986.
23. Daschbach, J. L.; Schenter, G. K.; Ayotte, P.; Smith, R. S.; Kay, B. D., Helium diffusion through H_2O and D_2O amorphous ice: Observation of a lattice inverse isotope effect. *Phys. Rev. Lett.* **2004,** 92, (19).
24. Smith, R. S.; Huang, C.; Kay, B. D., Evidence for molecular translational diffusion during the crystallization of amorphous solid water. *J. Phys. Chem. B* **1997,** 101, (32), 6123-6126.
25. Hornekaer, L.; Baurichter, A.; Petrunin, V. V.; Luntz, A. C.; Kay, B. D.; Al-Halabi, A., Influence of surface morphology on D_2 desorption kinetics from amorphous solid water. *J. Chem. Phys.* **2005,** 122, (12).
26. McClure, S. M.; Barlow, E. T.; Akin, M. C.; Safarik, D. J.; Truskett, T. M.; Mullins, C. B., Transport in amorphous solid water films: Implications for self-diffusivity. *J. Phys. Chem. B* **2006,** 110, (36), 17987-17997.

27. Poole, P. H.; Sciortino, F.; Grande, T.; Stanley, H. E.; Angell, C. A., Effect of Hydrogen-Bonds on the Thermodynamic Behavior of Liquid Water. *Phys. Rev. Lett.* **1994,** 73, (12), 1632-1635.
28. Poole, P. H.; Sciortino, F.; Essmann, U.; Stanley, H. E., Phase-Behavior of Metastable Water. *Nature* **1992,** 360, (6402), 324-328.
29. Liu, L.; Chen, S. H.; Faraone, A.; Yen, C. W.; Mou, C. Y., Pressure dependence of fragile-to-strong transition and a possible second critical point in supercooled confined water. *Phys. Rev. Lett.* **2005,** 95, (11).
30. Kohl, I.; Bachmann, L.; Mayer, E.; Hallbrucker, A.; Loerting, T., Water behaviour - Glass transition in hyperquenched water? *Nature* **2005,** 435, (7041), E1-E1.
31. Brovchenko, I.; Geiger, A.; Oleinikova, A., Liquid-liquid phase transitions in supercooled water studied by computer simulations of various water models. *J. Chem. Phys.* **2005,** 123, (4).
32. Mishima, O.; Calvert, L. D.; Whalley, E., An Apparently 1st-Order Transition between 2 Amorphous Phases of Ice Induced by Pressure. *Nature* **1985,** 314, (6006), 76-78.
33. Givan, A.; Loewenschuss, A.; Nielsen, C. J., FTIR studies of annealing processes in low temperature pure and mixed amorphous ice samples. *J. Phys. Chem. B* **1997,** 101, (43), 8696-8706.
34. Smith, R. S.; Zubkov, T.; Kay, B. D., The effect of the incident collision energy on the phase and crystallization kinetics of vapor deposited water films. *J. Chem. Phys.* **2006,** 124, (11).
35. Dohnalek, Z.; Kimmel, G. A.; Ayotte, P.; Smith, R. S.; Kay, B. D., The deposition angle-dependent density of amorphous solid water films. *J. Chem. Phys.* **2003,** 118, (1), 364-372.
36. Kimmel, G. A.; Stevenson, K. P.; Dohnalek, Z.; Smith, R. S.; Kay, B. D., Control of amorphous solid water morphology using molecular beams. I. Experimental results. *J. Chem. Phys.* **2001,** 114, (12), 5284-5294.
37. Velikov, V.; Borick, S.; Angell, C. A., The glass transition of water, based on hyperquenching experiments. *Science* **2001,** 294, (5550), 2335-2338.
38. Fisher, M.; Devlin, J. P., Defect Activity in Amorphous Ice from Isotopic Exchange Data - Insight into the Glass-Transition. *J. Phys. Chem.* **1995,** 99, (29), 11584-11590.
39. Johari, G. P., Dielectric relaxation time of bulk water at 136-140 K, background loss and crystallization effects. *J. Chem. Phys.* **2005,** 122, (14).
40. Smith, R. S.; Kay, B. D., The existence of supercooled liquid water at 150 K. *Nature* **1999,** 398, (6730), 788-791.
41. Smith, R. S.; Dohnalek, Z.; Kimmel, G. A.; Stevenson, K. P.; Kay, B. D., The self-diffusivity of amorphous solid water near 150 K. *Chem. Phys.* **2000,** 258, (2-3), 291-305.
42. McClure, S. M.; Barlow, E. T.; Akin, M. C.; Tanaka, P. L.; Safarik, D. J.; Truskett, T. M.; Mullins, C. B., Effect of dilute nitric acid on crystallization and fracture of amorphous solid water films. *Journal of Physical Chemistry C* **2007,** 111, (28), 10438-10447.

43. McClure, S. M.; Safarik, D. J.; Truskett, T. M.; Mullins, C. B., Evidence that amorphous water below 160 K is not a fragile liquid. *J. Phys. Chem. B* **2006,** 110, (23), 11033-11036.
44. Jenniskens, P.; Blake, D. F., Crystallization of amorphous water ice in the solar system. *Astrophys. J.* **1996,** 473, (2 Pt 1), 1104-13.
45. Smith, R. S.; Huang, C.; Wong, E. K. L.; Kay, B. D., The molecular volcano: Abrupt CCl_4 desorption driven by the crystallization of amorphous solid water. *Phys. Rev. Lett.* **1997,** 79, (5), 909-912.
46. Collings, M. P.; Dever, J. W.; Fraser, H. J.; McCoustra, M. R. S.; Williams, D. A., Carbon monoxide entrapment in interstellar ice analogs. *Astrophys. J.* **2003,** 583, (2), 1058-1062.
47. Sadtchenko, V.; Knutsen, K.; Giese, C. F.; Gentry, W. R., Interactions of CCl_4 with thin D_2O amorphous ice films, part I: A nanoscale probe of ice morphology. *J. Phys. Chem. B* **2000,** 104, (11), 2511-2521.
48. Notesco, G.; BarNun, A., Trapping of methanol, hydrogen cyanide, and n-hexane in water ice, above its transformation temperature to the crystalline form. *Icarus* **1997,** 126, (2), 336-341.
49. Souda, R., Hydration of polar and nonpolar molecules at the surface of amorphous solid water. *Phys. Rev. B* **2004,** 70, (16).
50. Gunster, J.; Liu, G.; Stultz, J.; Goodman, D. W., Interaction of methanol and water on MgO(100) studied by ultraviolet photoelectron and metastable impact electron spectroscopies. *J. Chem. Phys.* **1999,** 110, (5), 2558-2565.
51. Ayotte, P.; Smith, R. S.; Teeter, G.; Dohnalek, Z.; Kimmel, G. A.; Kay, B. D., A Beaker without walls: Formation of deeply supercooled binary liquid solutions of alcohols from nanoscale amorphous solid films. *Phys. Rev. Lett.* **2002,** 88, (24).
52. Wolff, A. J.; Carlstedt, C.; Brown, W. A., Studies of binary layered CH_3OH/H_2O ices adsorbed on a graphite surface. *Journal of Physical Chemistry C* **2007,** 111, (16), 5990-5999.
53. Picaud, S.; Toubin, C.; Girardet, C., Monolayers of acetone and methanol molecules on ice. *Surf. Sci.* **2000,** 454, 178-182.
54. Collignon, B.; Picaud, S., Comparison between methanol and formaldehyde adsorption on ice: a molecular dynamics study. *Chem. Phys. Lett.* **2004,** 393, (4-6), 457-463.
55. Pimblott, S. M.; LaVerne, J. A., Production of low-energy electrons by ionizing radiation. *Radiat. Phys. Chem.* **2007,** 76, (8-9), 1244-1247.
56. Zheng, W. J.; Jewitt, D.; Kaiser, R. I., Formation of hydrogen, oxygen, and hydrogen peroxide in electron-irradiated crystalline water ice. *Astrophys. J.* **2006,** 639, (1), 534-548.
57. Baggott, S. R.; Kolasinski, K. W.; Perdigao, L. M. A.; Riedel, D.; Guo, Q. M.; Palmer, R. E., Vacuum ultraviolet surface photochemistry of water adsorbed on graphite. *J. Chem. Phys.* **2002,** 117, (14), 6667-6672.
58. Rowntree, P.; Parenteau, L.; Sanche, L., Electron-Stimulated Desorption Via Dissociative Attachment in Amorphous H_2O. *J. Chem. Phys.* **1991,** 94, (12), 8570-8576.

59. Kimmel, G. A.; Orlando, T. M.; Cloutier, P.; Sanche, L., Low-energy (5-40 eV) electron-stimulated desorption of atomic hydrogen and metastable emission from amorphous ice. *Journal of Physical Chemistry B* **1997,** 101, (32), 6301-6303.
60. Kimmel, G. A.; Orlando, T. M.; Vezina, C.; Sanche, L., Low-Energy Electron-Stimulated Production of Molecular-Hydrogen from Amorphous Water Ice. *J. Chem. Phys.* **1994,** 101, (4), 3282-3286.
61. Petrik, N. G.; Kimmel, G. A., Electron-stimulated reactions at the interfaces of amorphous solid water films driven by long-range energy transfer from the bulk. *Phys. Rev. Lett.* **2003,** 90, (16).
62. Petrik, N. G.; Kavetsky, A. G.; Kimmel, G. A., Electron-stimulated production of molecular oxygen in amorphous solid water. *J. Phys. Chem. B* **2006,** 110, (6), 2723-2731.
63. Stockbauer, R.; Bertel, E.; Madey, T. E., The Origin of H^+ in Electron-Stimulated Desorption of Condensed CH_3OH. *J. Chem. Phys.* **1982,** 76, (11), 5639-5641.
64. Burrows, M. D.; Ryan, S. R.; Lamb, W. E.; McIntyre, L. C., Studies of H^+, H^{+2}, and H^{+3} Dissociative Ionization Fragments from Methane, Ethane, Methanol, Ethanol, and Some Deuterated Methanols Using Electron-Impact Excitation and a Time-of-Fight Method Incorporating Mass Analysis. *J. Chem. Phys.* **1979,** 71, (12), 4931-4940.
65. Parenteau, L.; Jaygerin, J. P.; Sanche, L., Electron-Stimulated Desorption of H^- Ions Via Dissociative Electron-Attachment in Condensed Methanol. *J. Phys. Chem.* **1994,** 98, (40), 10277-10281.
66. Parenteau, L.; Sanche, L., Low-Energy Dissociative Electron-Attachment (0-20 Ev) on Methanol and Some Organic-Molecules. *J. Chim. Phys. Phys.-Chim. Biol.* **1994,** 91, (7-8), 1237-1242.
67. Lepage, M.; Michaud, M.; Sanche, L., Low energy electron total scattering cross section for the production of CO within condensed methanol. *J. Chem. Phys.* **1997,** 107, (9), 3478-3484.
68. Kawanowa, H.; Hanatani, K.; Gotoh, Y.; Souda, R., Electron-stimulated desorption of positive ions from methanol adsorbed on a solid Ar substrate. *Surf. Rev. Lett.* **2003,** 10, (2-3), 271-275.
69. Henderson, M. A.; Otero-Tapia, S.; Castro, M. E., Electron-induced decomposition of methanol on the vacuum-annealed surface of TiO_2(110). *Surf. Sci.* **1998,** 413, 252-272.
70. Schwaner, A. L.; White, J. M., Electron-induced chemistry of methanol on Ag(111). *J. Phys. Chem. B* **1997,** 101, (49), 10414-10422.
71. Sasaki, T.; Itai, Y.; Iwasawa, Y., Real-time observation of the dehydrogenation processes of methanol on clean Ru(001) and Ru(001)-p(2x2)-O surfaces by a temperature-programmed electron-stimulated desorption ion angular distribution/time-of-flight system. *Surf. Sci.* **1999,** 443, (1-2), 44-56.
72. Harris, T. D.; Lee, D. H.; Blumberg, M. Q.; Arumainayagam, C. R., Electron-Induced Reactions in Methanol Ultrathin Films Studied by Temperature-Programmed Desorption - a Useful Method to Study Radiation-Chemistry. *J. Phys. Chem.* **1995,** 99, (23), 9530-9535.
73. Schutte, W. A., Production of organic molecules in interstellar ices. In *Space Life Sciences: Extraterrestrial Organic Chemistry, Uv Radiation on Biological Evolution, and*

Planetary Protection, Pergamon-Elsevier Science Ltd: Oxford, 2002; Vol. 30, pp 1409-1417.
74. Beltran, F. J.; Ovejero, G.; Rivas, J., Oxidation of polynuclear aromatic hydrocarbons in water .3. UV radiation combined with hydrogen peroxide. *Industrial & Engineering Chemistry Research* **1996,** 35, (3), 883-890.
75. Woon, D. E.; Park, J. Y., Photoionization of benzene and small polycyclic aromatic hydrocarbons in ultraviolet-processed astrophysical ices: A computational study. *Astrophys. J.* **2004,** 607, (1), 342-345.
76. Yamamoto, S.; Beniya, A.; Mukai, K.; Yamashita, Y.; Yoshinobu, J., Low-energy electron-stimulated chemical reactions of CO in water ice. *Chem. Phys. Lett.* **2004,** 388, (4-6), 384-388.
77. Wu, C. Y. R.; Judge, D. L.; Cheng, B. M.; Yih, T. S.; Lee, C. S.; Ip, W. H., Extreme ultraviolet photolysis of CO_2-H_2O mixed ices at 10 K. *J. Geophys. Res.-Planet* **2003,** 108, (E4).
78. Wu, C. Y. R.; Judge, D. L.; Cheng, B. M.; Shih, W. H.; Yih, T. S.; Ip, W. H., Extreme ultraviolet photon-induced chemical reactions in the C_2H_2-H_2O mixed ices at 10 K. *Icarus* **2002,** 156, (2), 456-473.
79. Hidaka, H.; Watanabe, N.; Shiraki, T.; Nagaoka, A.; Kouchi, A., Conversion of H_2CO to CH_3OH by reactions of cold atomic hydrogen on ice surfaces below 20 K. *Astrophys. J.* **2004,** 614, (2), 1124-1131.
80. Brunetto, R.; Baratta, G. A.; Domingo, M.; Strazzulla, G., Reflectance and transmittance spectra (2.2-2.4 _m) of ion irradiated frozen methanol. *Icarus* **2005,** 175, (1), 226-232.
81. Palumbo, M. E.; Castorina, A. C.; Strazzulla, G., Ion irradiation effects on frozen methanol (CH_3OH). *Astron. Astrophys.* **1999,** 342, (2), 551-562.
82. Wu, C. Y. R.; Yang, B. W.; Judge, D. L., Total Ion Desorption Yields of H_2O, D_2O, CH_3OH, CD_3OD and Water-Methanol Mixed Ices Irradiated at 584 Angstrom. *Planet. Space Sci.* **1994,** 42, (4), 273-277.
83. Woon, D. E., Photoionization in ultraviolet processing of astrophysical ice analogs at cryogenic temperatures. In *Space Life Sciences: Steps toward Origin(S) of Life*, 2004; Vol. 33, pp 44-48.
84. Petrik, N. G.; Kavetsky, A. G.; Kimmel, G. A., Electron-stimulated production of molecular oxygen in amorphous solid water on Pt(111): Precursor transport through the hydrogen bonding network. *J. Chem. Phys.* **2006,** 125, (12).

Chapter 2: Observations on electron-driven reactions between methanol and ASW

Introduction

A significant body of literature studying pure water and pure methanol exists, including both radiation-driven and thermal processes. Mixed water/organic systems, such as are found in cells, the atmosphere, nuclear waste tanks, and comets, have been studied less. However, understanding these mixed systems is necessary to accurately model many systems of interest, such as protein folding and DNA damage in cells, or the origins of prebiotic chemistry in space. Radiation-driven processes are of particular interest for these systems, as they are either responsible for the more pertinent consequences (e.g., accelerating cellular aging or creating tumors) or are the major source of energy (e.g., nuclear waste tanks and astrophysical environments). To model these non-thermal processes in mixed water/organic solutions, we use low energy electrons and layered films of methanol and amorphous solid water (ASW). Low energy electrons are generated in copious quantities by the radiolysis of water and drive most of the subsequent reactions.[1] Methanol is used as a model organic compound because it is known to be present in many of the environments mentioned above, is a common product of radiolytic reactions between water and simpler organics such as CH_4,[2] and does not irreversibly thermally decompose.[3] While some studies have been performed on the thermal processes occurring in mixed methanol/ASW films,[4, 5] no previous works have been published regarding low-energy electron-driven processes in solid mixes of methanol and water at cryogenic temperatures.

Methods

Chamber Set Up

Experiments were done in an ultra-high vacuum (UHV) chamber, equipped with a closed cycle helium cryostat, low-energy electron gun, quadrupole mass spectrometer, and a molecular beam line. Median base pressure for the system was ~1.1E-10 torr and base sample temperature was ~22K. Films were grown on a clean TiO_2 (110) crystal approximately 10 mm in diameter and 0.5mm thick. The crystal was cleaned by neon ion sputtering, followed by annealing at 850 K in vacuum, to yield a consistent TiO_2 (111) surface. The sample was resistively heated, and the temperature measured by a type K thermocouple spot-welded to the back of the sample.

Deposition and Growth Conditions

High-Pressure Liquid Chromatography-grade CH_3OH, distilled, deionized H_2O, and their isotopologues (CD_3OH, CD_3OD, D_2O, and $H_2{}^{18}O$) were freeze-pump-thawed prior to use to remove dissolved gases and to ensure purity. All films were dosed at temperatures colder than 100 K by molecular beams at normal incidence to the sample, creating a dense non-porous film.[6, 7] The films did not cover the entire substrate surface, but were centered on the TiO_2. Water coverage calibration was based on previous calculations using a coverage of 1 x 10^{15} molecules*cm^{-2}.[8] Direct measurements of methanol saturation coverage on ASW for calibration purposes are difficult due to mixing processes during desorption. Instead, methanol coverage was calibrated based on the integration of the first monolayer peak in the temperature programmed desorption spectra

from a *bare* TiO_2 crystal. Based on the relative coverage of methanol on bare TiO_2 (110), 3.2 x 10^{14} molecules cm^{-2},[9] one monolayer of methanol on ASW was defined to be roughly three times the exposure needed for one monolayer on methanol on TiO_2. This definition of a CH_3OH monolayer on ASW has a comparable coverage to that of a water monolayer on ASW, 1 x 10^{15} molecules*cm^{-2}. The same exposure definition (in torr s) was used for each of the isotopically labeled varieties of methanol used, CH_3OH, CD_3OH, and CD_3OD, although the calibration was performed only for CH_3OH. We must emphasize that our monolayer definition is strictly to make comparing the effects of a monolayer of methanol with those of a water monolayer easier on a per-molecule basis, and is not based on any measurement of the actual coverage of CH_3OH on ASW. Estimates of CH_3OH coverage on crystalline ice surfaces (none are available for ASW surfaces) range in value, but are comparable to its coverage on TiO_2 (110).[10-12]

The structured methanol/water films in our experiments often required different growth temperatures for different layers. Underlying foundational water layers (in contact with the TiO_2 surface) were grown at 80K, conditions known to produce consistently dense and smooth ASW surfaces. [6, 7] Surfaction, or the phase separation and resulting movement of methanol to the vacuum interface, was observed during deposition of upper water layers in "sandwich" experiments. In these experiments, layers of water are dosed atop methanol to isolate it from the vacuum interface, creating a layered film with a sandwich-like structure of water/methanol/water/TiO_2. When the upper layers were deposited at 80K, the methanol promptly appeared on the surface in subsequent electron stimulated desorption (ESD) experiments. When the upper layers were dosed at 50K or

less, it eliminated the prompt appearance of methanol from subsequent ESD experiments, even if the film was heated to 80 K from the lower dose temperature. Heating gently to 80K and irradiating had no effect on the ESD signal structure compared to irradiation at 50 or 25K. (For details, see results section.) To eliminate the effects of such surfaction in studies of ESD and temperature-programmed desorption (TPD) products in mixed films, all upper films were grown at 80K or less, depending on their position in the final film structure. Capping water layers, or layers dosed atop methanol, were grown at 50K or less to minimize the surfactant properties of methanol. Methanol films were grown at 80K or less if their final position was located at the vacuum interface (i.e., an "open-faced" sandwich structure, also referred to in this paper as a methanol-capped film), and at 50K or less if in the interior (i.e., in a "sandwich" experiment).

Radiation Conditions

To eliminate the effects of thermal mixing and focus on radiative mixing and reaction products, all irradiation was performed at 80 K or colder; changes in the ESD temperature do not appear to change the signal structure, although it may affect the signal intensity (See results section). Capped films were irradiated at 80 K, when the surfactant properties of methanol could be neglected. Sandwich films were irradiated at their growth temperature unless otherwise noted. The electron beam was incident at 35° to the sample normal. The films were irradiated with 100 eV electrons at a current of ~2 μA for 100 scan cycles (for a total exposure of ~97 s) unless otherwise noted. A scan-averaging mode was used that samples the signal repeatedly within a single cycle, rastering across

the film sample to generate "pixels." The pixels were then averaged to generate a single data point per cycle with a very high signal-to-noise ratio, as described in detail in Petrik *et al.* [8]

Experimental cracking fractions in our system were determined during isothermal measurements of CH_3OH and are given in Table 2.1. These cracking fractions are used instead of literature cracking fractions (e.g., NIST) for the purpose of making assignments of ESD and TPD products.

Results and Discussion

Surfaction

Methanol has been previously observed to act as a surfactant,[4] meaning that the methanol molecules preferentially congregate at the water/vacuum interface. The presence of methanol at the vacuum interface suppresses O_2 production from water even at low (<0.1ML) concentrations (See Chapter 4). Therefore, we can use the O_2 ESD signal as a tracer of methanol's presence at the surface. To examine the ability of methanol to surfact, we used sandwiches of 30 ML H_2O/1 ML CH_3OH/ 50 ML H_2O/TiO_2 (110). This structure was chosen for several reasons. For films of this total thickness (81 ML), there should be no detectable products from the TiO_2/ASW interface,[8, 13] allowing us to focus on surfaction at the vacuum interface. Methanol buried under 30 ML of H_2O should not receive significant energy from impinging electrons that would allow the molecule to react,[14] avoiding any effects caused by methanol by-products. Finally, we found that O_2 production saturates when 30 or more ML H_2O are deposited atop CH_3OH

(See Chapter 4), giving us a large control signal for easy comparison. The sandwich films were grown and irradiated at various temperatures, allowing us to explore the effect of temperature on the ability of methanol to move through the film. Our data show (Figure 2.1) that while methanol does act as a surfactant, it does so only under certain conditions.

The lowest available temperature of the chamber is ~22K. To best exclude any possible thermal effects on surfaction, the sandwich film was grown and irradiated at 25 K. Results are shown in Figure 2.1. In this "ideal" case, O_2 production begins immediately with the onset of irradiation, and grows until saturation, consistent with O_2 production from a pure water film. Repeating the experiment with a growth temperature of 25 K and irradiation temperatures of 50 and 80 K yielded nearly identical line shapes, once they were scaled for differing saturation values. The key characteristic, prompt production of O_2, was still present. Therefore, diffusion of methanol to the surface during heating is slow enough that it does not cause surfaction. Similar results were obtained when the growth temperature was 50 K and the irradiation temperature was 50 or 80 K. However, when the sandwich film was grown at 80 K, the prompt O_2 production signal vanishes, indicating that methanol is present at the vacuum interface at the beginning of the ESD. During deposition at 80 K, CH_3OH is mobile enough to move to or remain at the surface, where the hydrophobic methyl groups' solvation energy can be minimized. At deposition temperatures less than or equal to 50 K, methanol is immobilized, and no surfaction is detected.

Deposition temperature appears to have little effect on the ESD signal shape and intensity. For example, if capping layers of methanol that are deposited at 50 K and

irradiated at 80 K show very similar H_2 and other signals as capping layers deposited and irradiated at 80 K. The greatest difference is seen in the 32 amu signal, especially at very low coverages (Figures 2.2 and 2.3). When CH_3OH is deposited on 80 ML ASW at 80 K, the O_2 signal recovers sooner than when methanol is deposited at 50 K, implying that less methanol is on the surface when deposited at 80K. This difference is only apparent when 0.35 ML CH_3OH or less are deposited, and is most obvious at near-zero coverages. It is unlikely that the sticking coefficient for methanol on ASW changes greatly over this temperature range. The supporting ASW layers were grown at 80 K in both cases and therefore have similar morphologies. Instead, increased mixing during deposition effectively moves small quantities of the methanol into the water layer, causing the reduced apparent surface concentration of methanol when deposited at 80 K. This mixing may be due to stronger H-bonding interactions between methanol and water than between methanol and methanol,[15] but appears to be a weaker effect than the surfaction-inducing forces that move buried methanol to the ASW surface.

Deposition of pure methanol

30 ML of CH_3OH were deposited at 80K and then heated at a ramp rate of 2 K/s. One major peak at 172K was detected (See Table 2.2), and is assigned to the molecularly desorbing CH_3OH multilayer. Only masses resulting from CH_3OH fragmentation are observed at this peak. Greater quantities of masses 18 and 28 are observed than are predicted by methanol cracking fragments, the result of background H_2O and CO in the chamber. We use our experimentally defined cracking fragments shown in Table 2.1 in

assigning peaks and compounds in subsequent experiments. Additional minor peaks were observed at ~315 K and ~550 K. The latter peak lacks a 31 amu signal but is consistent with the presence of small quantities of CH_2O. These results are consistent with those of Henderson, Otero-Tapia, and Castro,[3] who examined the surface chemistry of thin layers of pure methanol deposited on TiO_2 (110). Four major temperature programmed desorption (TPD) peaks were identified, including a multilayer peak at 150K and a peak associated with molecular desorption of the CH_3OH monolayer at 295K.

ESD and TPD of pure methanol

As with water, the main irradiation product of 30 ML CH_3OH is H_2. Other products include H_2O, CH_3OH, CH_2O, CH_4, CO, and CO_2, and likely C_2H_4 and C_2H_6, which are convoluted with the larger signals from CO and CH_2O respectively. Heavier mass products such as HCOOH are also detected, but in very small quantities. Methanol fragments (masses 31, 32, and 15, and a portion of the mass 29 signal) start at a high initial, or "prompt," signal, and then rapidly decay as methanol is consumed. Fragments of methanol byproducts such as H_2CO and C_2H_6 (masses 2, 29, and 30) also decrease with time, but the decrease is less rapid as additional byproducts are generated by the consumption of methanol. In contrast, the production rates of H_2O, CO, C_2H_4, and CO_2 (masses 18, 28, and 44) increase with radiation exposure. These signals do not increase when pure water is irradiated, and are not due to changing background levels of these molecules in the experimental chamber, but to the formation of these species in the

methanol film. Their increase with respect to time is unsurprising given the additional steps required to generate these products compared to CH_3 or H_2CO. Reducing the electron flux (from 5μA to 2μA) does not change these general trends, although they become less pronounced and overall signal intensity decreases (Figures 2.4 and 2.5). Similar effects are seen when the electron energy is reduced from 100 eV to 20 eV (Figure 2.6).

As in unprocessed methanol films, the major TPD peak in processed films occurs at ~170K. Methanol cracking fragments 15, 29, 31, and 32 dominate this peak, consistent with the desorption of the methanol multilayer and byproducts such as CH_2O (Figure 2.7). However, several additional peaks at temperatures ranging from ~110 to ~200 K are also present. CH_4 and CH_3OCH_3 (dimethyl ether) are observed desorbing in a two-peak system at ~109 and ~128 K after irradiation using 20eV electrons at 2 μA (Figure 2.7A). Small, minor peaks are also observed at higher temperatures for masses 27, 28, 29, and 30, indicating the presence of H_2CO at ~550 K and C_2H_4 at ~650 K.

Increasing the total energy dosed, as in Figure 2.8, which used 100 eV electrons at 5 μA, leads to both larger signals and additional product species. As with lower energy doses, the main peak remains at ~170 K and is dominated by the same species, but is smaller in relative size when compared to other peaks than it is in the lower-energy case. Besides the main peak at 170K, additional peaks are present at 125, 139, 153, 180, and 232K. The two-peak system found at 125 and 139 K (Figure 2.8A) is similar in peak structure to the one found at 109 and 128 K in the low-energy experiment (Figure 2.7A), but is shifted to higher temperatures and results from a more complex origin. The peak

found at 125 K is due to desorbing dimethyl ether, while the peak at 139K is due to CH_4, CO, CO_2, CH_3OOCH_3, and a combination of ethanol, HCOOH, CH_3OCH_3, C_2H_6, and $(CH_2OH)_2$ that cannot be determined from the TPD data. Of these, ethanol fits the data while only requiring one species to form and so is the presumptive source. However, combinations of C_2H_6 + $(CH_2OH)_2$ + HCOOH and C_2H_6 + $(CH_2OH)_2$ + CH_3OCH_3 also fit the data, about as well as ethanol alone. Measuring additional TPD masses could help resolve the source(s), but the signals from the additional masses (12, 13, 25, 26, and 62) are expected to be quite small, so a spectroscopic method would be preferred. The peak at 153 K is due to desorbing ethylene glycol, while the peaks at 180, 232, and 480 K are due to water (for comparison, a thick water film has a distinct shoulder at 180K and peaks at ~193 K). Additional very small peaks are present at 585 and 610 K, possibly artifacts.

Temperature effects in irradiated pure methanol films

Increasing the ESD temperature T_{irr} of 30 ML CH_3OH from 25 to 50 K made no significant difference in the methanol signal during ESD. However, the temperature increase led to a total increase in signal from methanol products (masses 2, 15, and 28) during the ESD, primarily in the prompt region. Saturation levels were similar except in the case of 2 amu, where saturation at 50 K is difficult to determine. The final data point for 2amu at 50 K was roughly double that at 25K. A further increase to 80K led to a very large increase in the 15, 29, and 32 amu signals, especially in the prompt region. H_2 and CO production at 80 K is at least double that at 50 K. These results—that increasing T_{irr}

leads to increased signal intensities—are consistent with increases in the H_2O, H_2, and O_2 signals observed in ESDs of pure water films with increasing T_{irr}.

No difference was observed in the location of subsequent TPD peaks and only a small difference in the intensity of TPD peaks for the monitored masses (12,13,14,15,16,18 28, 29, 30, 31, 32, 33, 44, 45, and 46 amu) when the irradiation temperature was increased from 25 to 50 K. When the temperature is increased to 80 K, a number of changes appear, although the main peak at 170 K remains constant. These changes include a 7-9 K increase in the desorption temperature of most of the methanol products. A methane + CO_2 TPD peak at 130K (masses 12, 13, 14, 16, 44, 45, and 46 amu) shifts to 139 K when T_{irr} is increased from 50 to 80K. The CO_2 peak resulting from irradiation at 80 K is also ~4 times larger than that from irradiation at 50K, while the corresponding peak at 170 K is about half the size it was at 50 K. A similar relative increase of the ~139K peak relative to the 170K peak is observed in methane desorption, but is not as pronounced as in the 44 amu channel. The 45 and 46 amu signals show a similar shift, and a small concomitant increase, from 130 to 139 K, but the peaks at 170 K did not change in intensity. A second H_2O TPD peak (18 amu) appears at 178K when T_{irr} is increased to 80 K (Figure 2.10). At T_{irr} = 50 K, there is only one major peak for water, occurring at 170K. This new peak at 178 K indicates increased water production from methanol irradiated at 80 K and is comparable to water desorption temperatures from bare TiO_2 (110). For H_2CO (masses 15, 29, and 30), a TPD peak at 110 K disappears when T_{irr} is raised from 50 to 80 K (Figure 2.9); it may be converted to other products. Another H_2CO peak at 132 K shifts to 139 K (15, 28, 29, and 30 amu). Methanol

fragment CH_2 (mass 14) shows the disappearance of a small peak at 525 K when T_{irr} is increased to 80 K. No major changes are observed in the TPD signal for mass 32 (CH_3OH and O_2), although there is an increase in the high-temperature shoulder signal at ~200-250 K, and none are observed for masses 31 or 33 (a major and minor methanol signal, respectively). These results suggest increased production of methanol products in the film during irradiation at higher temperatures, in agreement with the increased signals observed during ESD. However, the lack of major changes in the main methanol signals (31 and 32 amu) indicates that the products are still a relatively small component, forming in a film that remains mostly methanol. The 7-9 K increase in desorption temperatures of the methanol products observed after irradiation at 80 K may be the result of several processes. The products may form at or diffuse to greater depths in the methanol film (further from the vacuum interface), or may be better trapped by accelerated electron-induced annealing at higher irradiation temperatures.

ESD products in layered methanol/water films

Capped films

In capped films, major methanol ESD products H_2, CH_3OH, CH_2O, CO, and CO_2 increased as expected with increasing methanol dose, as shown in Figure 2.13 for CO, while the H_2O and O_2 signals, resulting from water, decreased. Thorough discussions of H_2, O_2, and CH_3OH products, and the processes affecting them, are included in Chapters 3 and 4.

Sandwich films

As increasing quantities of water are deposited atop methanol, the signals from methanol and its major products, CO and CH_2O, decrease. This decrease is only noticeable at 2 or more capping layers of water; a single layer appears to make no difference in the ESD signal, even at the earliest times when mixing is minimized and capping water quantity is maximized. These signals all reach their minimum when the capping water layer is greater than 20 ML thick, and show an exponential decay in total signal with increasing water dose. Only one notable difference appears between the expected signals based on pure methanol ESDs and signals from capped films: the CH_2O signal is as big as, or bigger than, the CH_3OH signal at each of these buried depths. This result may be due to reactions at the water interface, or simply due to retaining greater quantities of methanol for the longer periods needed to generate H_2CO.

TPD products after irradiation in layered methanol/water films

Capped films

TPDs from non-irradiated films of 1 ML CH_3OH on 80 ML H_2O (Figure 2.12) show a consistent peak structure common to all of the methanol-dominated channels (15, 29, 30, 31, and 32amu). Onset of methanol desorption occurs at 140K, approximately the same temperature as it does from pure methanol films. The peak structure consists of a major peak at 195 K with two low temperature shoulders resulting from peaks at 161 and 179K. The major peak at 195 K coincides with the major water desorption peak, has a

similar structure (Figure 2.12C), and is likely due to entrained methanol during water desorption. The shoulder located at ~179 K coincides with a similar shoulder observed in processed pure ASW films. It is also coincident with the major methanol peak from irradiated 1 ML CH_3OH/80 ML H_2O films, suggesting that its origins may be methanol in contact with ASW. The origin of the shoulder at 160 K is less clear. As it is not present in irradiated films of 1 and 4 ML CH_3OH/80 ML H_2O, in which less than 1 ML CH_3OH are calculated to remain after sputtering, but is present in irradiated films of 10 ML CH_3OH/80 ML H_2O, we assign it to the desorption of a methanol multilayer from the water surface. This temperature is ~10 K higher than Henderson *et al.*'s observed first methanol multilayer desorption temperature from bare TiO_2 (110), and ~5 K lower than the desorption temperature for H-bonded CH_3OH on bare TiO_2 (110).[3] However, it is lower than our observed peak desorption temperature for processed 30 ML methanol films, and has a similar onset temperature, as would be expected for a partial multilayer.

These channels also show a small broad peak at ~340K in the unprocessed film. Although methanol on bare TiO_2(110) recombinatively desorbs at ~350 K,[9] the thick water layer is expected to prevent the methanol from contacting the TiO_2 surface. The peak is not due to CH_2O, O_2, or another species, as it shifts in all methanol channels to ~316K after processing. The same data indicate that it is not an artifact of deposition, as the small quantity of methanol that might deposit on the bare TiO_2 would be removed or converted to CH_2O by electron sputtering. In irradiated films of 4, 10, and 30 monolayers of methanol on ASW, this peak becomes difficult to isolate as it appears convoluted with the tail of the major desorption signal, becoming a high-temperature shoulder. However,

it is present as a high-temperature shoulder in the same channels (15, 29, 30, 31, and 32amu) but not higher mass channels (e.g., 44 or 46 amu), which suggests that it is due to methanol desorption and not the desorption of a newly formed heavier species, such as formic acid or ethanol.

The signal from 1 ML CH_3OH on 80 ML H_2O is reduced by ~93% after irradiation (Figure 2.12A), indicating that nearly all of the methanol is removed electron-induced desorption. The remainder is likely protected by mixing to some degree with the water layer, as ESDs indicate that ~3 ML of CH_3OH are sputtered during irradiation under these conditions. (For comparison, ~2.3 ML of H_2O are sputtered from a pure water film under the same conditions.) This degree of sputtering is also observed in processed films of 4 ML CH_3OH on ASW, where integration of the 31amu channel shows that less than a monolayer of methanol desorbs during the TPD. TPDs of mass channels 15, 31, and 32 show the same structure, with two peaks located at ~180 and 193 K. The peak at 193 K is of similar intensity as peaks observed during desorption of pure water films and is due to background/residual methanol desorption during desorption of the water peak. The peak at 180K is the main peak, due to methanol desorption.

Note that the 32 amu signal is a special case, as it is the mass channel for both methanol and molecular oxygen generated during the ESD. When pure water is irradiated, this channel shows three peaks—the background water desorption peak at 195K, and two additional peaks of comparable intensity at 180 and 170 K (Figure 2.12B). However, due to the different peak structure and earlier onset of O_2 desorbing from water, it is plain that no or little O_2 is desorbing from the processed film of 1 ML

CH_3OH/ASW. This result is consistent with our other results (Chapter 4) showing that the addition of methanol suppresses the production of O_2 at the water/vacuum interface.

Other products include CH_2O, which was detected desorbing in a broad peak centered at ~265K that overlaps with methanol desorption observed at 315K. We note the appearance of another broad peak, centered at ~625K, consistent with the appearance of small quantities of ethane. The 16 amu channel was also monitored, and in the unprocessed film largely overlaps with O desorption from processed and unprocessed water films, peaking at ~194K (Figure 2.13). However, in the processed 1 ML CH_3OH/ASW film, a low-temperature shoulder appears, indicating an additional source at ~187 K. While most of the 16 amu signal bears the characteristics of O desorbing from H_2O, a small fraction appears to be sourced in methanol. This contribution to the 16 amu signal is not due to CH_4, as it occurs at a much higher temperature than observed from a pure methanol film, and is many times larger than the 15amu signal. Therefore, this is additional atomic O resulting either from the irradiated methanol, or from water at the methanol/water interface.

Similar films of 4, 10, and 30 ML CH_3OH were deposited on 80 ML ASW and irradiated at 80K using 100 eV electrons at 5 μA. In all cases, the main water peak remains located at 195 K, and small but significant quantities of methanol are commingled with the water desorption at each coverage (Figure 2.14). At 4 ML coverage, the main methanol desorption peak is located at 170K (Figure 2.14A). As the methanol dose increases, this peak first grows (Figure 2.14B) and then shifts to 180K (Figure 2.13C). As the methanol dose increases, water begins to co-desorb with the methanol, as

observed in Figure 2.14C. The multilayer peak assigned to 160 K also grows and shifts to higher temperatures with increasing methanol dose, ending at ~168 K for a 30 ML CH_3OH dose. CO and CO_2 desorb with the water and main methanol peaks at all coverages. Low levels of H_2CO are again observed in a broad peak ranging from ~220 to ~320K (Figure 2.15A) at 4 and 10 ML CH_3OH coverages, but a large tail prevents observation at the 30 ML CH_3OH dose.

At 10 ML CH_3OH coverage, a new peak appears at 187K (Figures 2.14B and 2.15B). This peak is particularly noticeable in the 15, 16, 28, 44, 45, and 46 amu channels, but also increases the signal in the 29 and 31 amu channels so that the "valley" between the 170 and 195 K peaks is higher than would be expected for two Gaussian or exponential curves. The cracking patterns of these 44-46 amu channels are consistent with the desorption of small amounts of dimethyl ether and/or ethanol. The remaining channels indicate additional methanol; the location suggests that this methanol may be well mixed with water. This peak disappears or combines with other peaks at the 30 ML dose, as would be expected if only limited quantities of methanol near the methanol/ASW interface are radiatively mixed. Another new peak is present at 125 K in both the 10 and 30 ML CH_3OH covered films (Figures 2.15B and 2.15C). The cracking patterns for 44, 45, and 46 amu present at 125 K are similar to those described above, again suggesting dimethyl ether or ethanol; as dimethyl ether is observed desorbing at this temperature from an irradiated pure methanol film, we assign it to this peak. Finally, at the 30 ML CH_3OH coverage, a peak at 158K, again with a similar cracking pattern, is present (Figure 2.15C).

Sandwich films

Films of n ML H_2O on 1 ML CH_3OH on 80-n ML H_2O on TiO_2 were studied as well. The upper layers of these films were grown at 25 K to minimize surfaction, and irradiated at 25 K using 100eV electrons at ~2μA current. These films were then heated at a rate of 2 K/s to gather TPD data on several species. Figure 2.16 shows the TPD data for mass 31, representing methanol desorption. Multiple peaks are present, including the main water desorption peak at ~193 K and an analogue to the main methanol desorption peak at 165-170K. As the methanol is placed deeper in the film, the entrained methanol peak at ~195K grows. Increasing burial depths of methanol decrease the quantity that is removed by electron sputtering during ESD, leading to a growing total signal.

The evolution of the main methanol peak at 165-170 K is particularly interesting, although somewhat difficult to interpret. For coverages of 0-5 capping ML H_2O (that is, thin "upper slices"), the leading edge of the peak does not shift from its onset temperature of ~150K. This indication that methanol is still near the vacuum interface is consistent with the expectation that ~2.3 ML of H_2O are removed during the ESD. As the capping water layer thickness n increases, the onset of desorption is delayed, slightly at n = 10 ML, and by ~15 K at n = 20 ML, whereupon it rises sharply. Thicker capping layers of 30 ML H_2O do not further increase this onset temperature of ~165 K, indicating that the appearance of methanol is not the result of simple diffusion through the thicker capping layers. The sharp rise is reminiscent of species that are released by crystallization processes, which may occur in the 10-20 ML of H_2O directly atop the methanol. The

overall result is that the main methanol peak at 165K grows in intensity with increasing capping water layer thickness to 10 ML, but then is quickly suppressed and shifted at thicknesses greater than 20 ML. Related methanol signals (15, 28, 29, 30, and 32 amu) are similar in this range, indicating that nearly all of the products desorbing at 165-170 K are due to methanol. Small quantities of CH_2O are detected at ~270 K, decreasing slightly in temperature with increasing capping water layer thickness, and peaking in intensity at 20 ML capping water layer thickness. There is also a small O_2 signal at 550 K that increases as the capping water layer grows. Extremely small peaks corresponding to heavier products are detected at 90 K (up to capping water layer thicknesses of 10 ML), 130K (up to thicknesses of 5 ML), and 160 K (thicknesses greater than or equal to 10 ML). These peaks also shift to higher temperatures with increasing depths.

Surface Area Measurements

The surface area of various methanol/water layered films was measured using Kr. The films were prepared at 80K, and Kr was dosed at less than 30 K. TPDs monitoring Kr were then taken using a ramp rate of 2 K/s. The TPDs are shown in Figure 2.17. The desorption onset of Kr begins and peaks at approximately the same temperatures (25 and 33K respectively) regardless of the amount of water or methanol at the surface. The clearest trend is observed at temperatures greater than ~37K, where increasing surface concentration of methanol corresponds to completion of Kr desorption at lower temperatures, suggesting that the water-dominated surface may be slightly rougher. Annealing the films made little difference in the structure or intensity of the Kr

desorption peak. Performing similar experiments using CO_2 as the probe molecule yielded similar results. Sandwich films of n ML H_2O/1 ML CH_3OH/80-n ML H_2O/TiO_2 (110) were grown at 80 K and then dosed with 120 torr*s of CO_2 at 21 K. When grown in this manner, surfaction will cause decreasing amounts of methanol to appear at the surface as n increases. The results, shown in Figure 2.18, indicate that as more water is present at the surface, more total CO_2 is adsorbed, and remains adsorbed to higher temperatures. While this result is consistent with the Kr desorption results, we must be cautious in drawing any further conclusions, as the CO_2 may H-bond more effectively and in larger numbers with a water-dominated surface, and that may be the cause of its higher desorption temperature and intensity rather than surface roughness.

Conclusions and Future Work

Methanol surfaction is minimized for deposition temperatures less than or equal to 50 K. At deposition temperatures of 80 K, the methanol is mobile enough to move to the surface. However, this mobility exists only during deposition; heating a film deposited at 25 K to 80 K does not lead to an increased concentration of methanol at the surface. Products other than methanol appear only after radiative processing. From a pure methanol film, these include H_2, CH_2O, CO, CO_2, H_2O, CH_4, C_2H_6, C_2H_4, and heavier species such as HCOOH, CH_3OCH_3 , CH_3OOCH_3 , CH_3CH_2OH, and $(CH_2OH)_2$. The variety and quantity of products increases as the total energy deposited increases. From a mixed methanol/water film, fewer products are seen, with CH_3OH and H_2O dominating TPDs. Observed products from these films included H_2, O, CH_2O, C_2H_6, CO, CO_2,

CH_3CH_2OH, CH_3OCH_3 , and O_2. TPDs indicate significant mixing in the layered films due to radiative processing during ESD. Surface area measurements suggest that water-dominated surfaces are marginally rougher than methanol-dominated surfaces. Confirmation of these products by spectroscopic methods (e.g., infrared spectroscopy), improved surface area measurements, and the effects of extended irradiation exposures will be included in future work.

1. Garrett, B. C.; Dixon, D. A.; Camaioni, D. M.; Chipman, D. M.; Johnson, M. A.; Jonah, C. D.; Kimmel, G. A.; Miller, J. H.; Rescigno, T. N.; Rossky, P. J.; Xantheas, S. S.; Colson, S. D.; Laufer, A. H.; Ray, D.; Barbara, P. F.; Bartels, D. M.; Becker, K. H.; Bowen, H.; Bradforth, S. E.; Carmichael, I.; Coe, J. V.; Corrales, L. R.; Cowin, J. P.; Dupuis, M.; Eisenthal, K. B.; Franz, J. A.; Gutowski, M. S.; Jordan, K. D.; Kay, B. D.; LaVerne, J. A.; Lymar, S. V.; Madey, T. E.; McCurdy, C. W.; Meisel, D.; Mukamel, S.; Nilsson, A. R.; Orlando, T. M.; Petrik, N. G.; Pimblott, S. M.; Rustad, J. R.; Schenter, G. K.; Singer, S. J.; Tokmakoff, A.; Wang, L. S.; Wittig, C.; Zwier, T. S., Role of water in electron-initiated processes and radical chemistry: Issues and scientific advances. *Chem. Rev.* **2005,** 105, (1), 355-389.
2. Wada, A.; Mochizuki, N.; Hiraoka, K., Methanol formation from electron-irradiated mixed H2O/CH4 ice at 10 K. *Astrophys. J.* **2006,** 644, (1), 300-306.
3. Henderson, M. A.; Otero-Tapia, S.; Castro, M. E., The chemistry of methanol on the surface: the TiO_2 (110) influence of vacancies and coadsorbed species. *Faraday Discuss.* **1999**, (114), 313-329.
4. Gunster, J.; Liu, G.; Stultz, J.; Goodman, D. W., Interaction of methanol and water on MgO(100) studied by ultraviolet photoelectron and metastable impact electron spectroscopies. *J. Chem. Phys.* **1999,** 110, (5), 2558-2565.
5. Wolff, A. J.; Carlstedt, C.; Brown, W. A., Studies of binary layered CH_3OH/H_2O ices adsorbed on a graphite surface. *Journal of Physical Chemistry C* **2007,** 111, (16), 5990-5999.
6. Dohnalek, Z.; Kimmel, G. A.; Ayotte, P.; Smith, R. S.; Kay, B. D., The deposition angle-dependent density of amorphous solid water films. *J. Chem. Phys.* **2003,** 118, (1), 364-372.
7. Kimmel, G. A.; Stevenson, K. P.; Dohnalek, Z.; Smith, R. S.; Kay, B. D., Control of amorphous solid water morphology using molecular beams. I. Experimental results. *J. Chem. Phys.* **2001,** 114, (12), 5284-5294.
8. Petrik, N. G.; Kavetsky, A. G.; Kimmel, G. A., Electron-stimulated production of molecular oxygen in amorphous solid water. *J. Phys. Chem. B* **2006,** 110, (6), 2723-2731.

9. Henderson, M. A.; Otero-Tapia, S.; Castro, M. E., Electron-induced decomposition of methanol on the vacuum-annealed surface of TiO_2(110). *Surf. Sci.* **1998,** 413, 252-272.
10. Collignon, B.; Picaud, S., Comparison between methanol and formaldehyde adsorption on ice: a molecular dynamics study. *Chem. Phys. Lett.* **2004,** 393, (4-6), 457-463.
11. Winkler, A. K.; Holmes, N. S.; Crowley, J. N., Interaction of methanol, acetone and formaldehyde with ice surfaces between 198 and 223 K. *Phys. Chem. Chem. Phys.* **2002,** 4, (21), 5270-5275.
12. Hudson, P. K.; Zondlo, M. A.; Tolbert, M. A., The interaction of methanol, acetone, and acetaldehyde with ice and nitric acid-doped ice: Implications for cirrus clouds. *J. Phys. Chem. A* **2002,** 106, (12), 2882-2888.
13. Petrik, N. G.; Kimmel, G. A., Electron-stimulated reactions at the interfaces of amorphous solid water films driven by long-range energy transfer from the bulk. *Phys. Rev. Lett.* **2003,** 90, (16).
14. LaVerne, J. A.; Pimblott, S. M., Effect of elastic collisions on energy deposition by electrons in water. *J. Phys. Chem. A* **1997,** 101, (25), 4504-4510.
15. Picaud, S.; Toubin, C.; Girardet, C., Monolayers of acetone and methanol molecules on ice. *Surf. Sci.* **2000,** 454, 178-182.

Chapter 3: The effect of creating chemical interfaces in amorphous solid water/methanol films on electron-stimulated H_2 production

Introduction

In a broad spectrum of research fields, including biology, energy research, and astrophysics, the mechanisms of non-thermal reactions in condensed water phases are of critical importance. Reactions occurring at interfaces, such as water solvating a DNA molecule or corrosion reactions, are of special importance. However, studying these reactions using liquid water, where the interface constantly changes, is difficult. To understand the role of the interface and study heterogeneously located reactions, amorphous solid water (ASW) serves as a model. Transport processes are slower in ASW, easing determination of the processes involving interfacial molecules and the extent of the interface.

Previous work with water showed that as high-energy radiation passes through water, lower-energy secondary electrons, of energy less than 100 eV, form in large quantities along the ray's path.[1] These electrons are the primary drivers of subsequent reactions, including the production of H_2, O_2, H, O, and H_2O_2.[2] H_2 production is of particular interest, as excessive H_2 production in nuclear waste tanks poses increased hazards associated with waste storage and environmental clean-up efforts.[1] H_2 creation and destruction, especially on ice-coated grains, is also of critical interest to astrophysicists, who use it to determine stars' and clouds' origins and evolution. Finally, cheap H_2 production is of the utmost importance to all who would like to decrease

reliance on fossil fuels by switching to a hydrogen economy. To model the effects of interfaces with organic compounds on non-thermal H_2 production from water, we use 100 eV electrons to study reactions occurring in layered methanol/ASW systems.

Previous Work

Petrik and Kimmel[3] found that hydrogen is formed in ASW at the films' interfaces with the supporting Pt (111) substrate and the vacuum, although the energy to drive these reactions is absorbed in the bulk of the film. The total H_2 yield peaked in films of about 25 ML ASW, decreasing with increasing thickness until ~70 ML, when it reached a constant level that was ~30% of the peak value. The contributions from each interface were observed to appear at different times after the electron beam was turned on, allowing the yield from each interface to be determined. At coverages greater than ~60 ML, virtually all of the H_2 was generated at the vacuum interface, and the Pt interfacial contribution was negligible. However, at coverages less than ~50 ML, the contribution from Pt was significant; isotopic labeling showed that the Pt interface was responsible for about 80 % of H_2 produced during the peak production level at ~25 ML thickness. Isotope labeling also determined that almost no H_2 was produced in the film region greater than ~3 ML from the substrate and more than ~10 ML from the vacuum interface. While no molecular hydrogen was produced in this "dead" region and it did not contribute any reactive species such as OH or H, energy was absorbed in this region and transferred to the interfaces. Evidence of this energy transfer lies in D_2 produced at the

substrate interface in 30-50 ML thick films, as Laverne and Pimblott found the penetration depth of 100 eV electrons in water not to exceed 30 ML.[4]

To avoid complications of H_2 production from the substrate interface, we studied thick (80 ML) films, allowing us to focus on the water/vacuum, methanol/vacuum, and water/methanol interfaces. At these thicknesses, contributions from the water/substrate interface are negligible, while the water/vacuum interface contributions are nearly constant. By imposing these experimental limits to eliminate contributions from the TiO_2 substrate, we focus on the methanol-induced changes to the film-vacuum interface. We also examine the effect of creating interior interfaces in the "dead" region by placing layers of methanol in this portion of the ASW film in a sandwich structure (described in detail later). If H_2 is produced at depths greater than ~10 ML from the vacuum interface, then we know that the addition of methanol forms a separate interface similar in some respects to the Pt interface used previously.

Methods

Chamber Set Up

Experiments were done in an ultrahigh vacuum (UHV) chamber, equipped with a closed cycle helium cryostat, low-energy electron gun, quadrupole mass spectrometer, and a molecular beam line. Median base pressure for the system was ~1.1E-10 torr and base sample temperature was ~22K. Films were grown on a clean TiO_2 (110) crystal approximately 10 mm in diameter and 0.5mm thick. The crystal was cleaned by neon ion

sputtering, followed by annealing at 850 K in vacuum, to yield a consistent TiO_2 (111) surface. The sample was resistively heated, and the temperature measured by a type K thermocouple spot-welded to the back of the sample.

Deposition and Growth Conditions

High-Pressure Liquid Chromatography-grade CH_3OH, distilled, deionized H_2O, and their isotopologues (CD_3OH, CD_3OD, D_2O, and $H_2{}^{18}O$) were freeze-pump-thawed prior to use to remove dissolved gases and to ensure purity. All films were dosed at temperatures colder than 100 K by molecular beams at normal incidence to the sample, creating a dense non-porous film.[5, 6] The films did not cover the entire substrate surface, but were centered on the TiO_2. Water coverage calibration was based on previous calculations using a coverage of 1 x 10^{15} molecules*cm^{-2}.[7] Direct measurements of methanol saturation coverage on ASW for calibration purposes are difficult due to mixing processes during desorption. Instead, methanol coverage was calibrated based on the integration of the first monolayer peak in the temperature programmed desorption spectra from a *bare* TiO_2 crystal. Based on the relative coverage of methanol on bare TiO_2 (110), 3.2 x 10^{14} molecules cm^{-2},[8] one monolayer of methanol on ASW was defined to be roughly three times the exposure needed for one monolayer on methanol on TiO_2. This definition of a CH_3OH monolayer on ASW has a comparable coverage to that of a water monolayer on ASW, 1 x 10^{15} molecules*cm^{-2}. The same exposure definition (in torr s) was used for each of the isotopically labeled varieties of methanol used, CH_3OH, CD_3OH, and CD_3OD, although the calibration was performed only for CH_3OH. We must

emphasize that our monolayer definition is strictly to make comparing the effects of a monolayer of methanol with those of a water monolayer easier on a per-molecule basis, and is not based on any measurement of the actual coverage of CH_3OH on ASW. Estimates of CH_3OH coverage on crystalline ice surfaces (none are available for ASW surfaces) range in value, but are comparable to its coverage on TiO_2 (110).[9-11]

The structured methanol/water films in our experiments often required different growth temperatures for different layers. Underlying foundational water layers (in contact with the TiO_2 surface) were grown at 80K, conditions known to produce consistently dense and smooth ASW surfaces.[5, 6] Surfaction, or the phase separation and resulting movement of methanol to the vacuum interface, was observed during deposition of upper water layers in "sandwich" experiments. In these experiments, layers of water are dosed atop methanol to isolate it from the vacuum interface, creating a layered film with a sandwich-like structure of water/methanol/water/TiO_2. When the upper layers were deposited at 80K, the methanol promptly appeared on the surface in subsequent electron stimulated desorption (ESD) experiments. When the upper layers were dosed at 50K or less, it eliminated the prompt appearance of methanol from subsequent ESD experiments, even if the film was heated to 80 K from the lower dose temperature. Heating gently to 80K and irradiating had no effect on the ESD signal structure compared to irradiation at 50 or 25K. (For details, see Chapter 2.) To eliminate the effects of such surfaction, all upper films were grown at 80K or less, depending on their position in the final film structure. Capping water layers, or layers dosed atop methanol, were grown at 50K or less to minimize the surfactant properties of methanol. Methanol layers were grown at

80K or less if their final position was located at the vacuum interface (i.e., an "open-faced" sandwich structure, also referred to in this paper as a methanol-capped film), and at 50K or less if in the interior (i.e., in a "sandwich" experiment).

Radiation Conditions

To eliminate the effects of thermal mixing and focus on radiative mixing and reaction products, all irradiation was performed at 80 K or colder; changes in the ESD temperature do not change the signal structure, although it may affect the signal intensity (See Chapter 2). Capped films were irradiated at 80 K, when the surfactant properties of methanol could be neglected. Sandwich films were irradiated at their growth temperature unless otherwise noted. The electron beam was incident at 35° to the sample normal. The films were irradiated with 100 eV electrons at a current of ~2 μA for 100 scan cycles (for a total exposure of ~97 s) unless otherwise noted. A scan-averaging mode was used that samples the signal repeatedly within a single cycle, rastering across the film sample to generate "pixels." The pixels were then averaged to generate a single data point per cycle with a very high signal-to-noise ratio, as described in detail in Petrik *et al.* [7]

Results and Discussion

Relative sensitivity of H_2 and D_2 in the QMS

The QMS showed different sensitivity to H_2 than to D_2. To determine the ratio of these sensitivities, H_2 and D_2 gases were leaked in at various pressures and the signal measured. After correcting for the ionization sensitivity of the ion gauge used to measure

the leaked gas pressure (Stanford Research, error ~10%), we found that the quadrupole was roughly twice (2.04 times) as sensitive to H_2 detection than D_2 detection. That is, for the same gas pressure, the H_2 signal appears twice as large as the D_2 signal. To determine mass balance from water and methanol films, we set the quadrupole sensitivity to HD to be the average of the H_2 and D_2 sensitivities, or 1.52. Doing so allows us to compare the hydrogen produced from an H_2O film with that from a D_2O film by weighting the HD and D_2 signals appropriately. For example, to determine the total hydrogen signal from a D_2O film, we measured the H_2 (background hydrogen), HD (primarily desorbed D atoms reacting with background H), and D_2 (molecularly formed in D_2O film) signals. If we perform a weighted sum of these signals such that

$$\text{total hydrogen} = H_2 \text{ signal} + 1.52\ (\text{HD signal}) + 2.04\ (D_2 \text{ signal}),$$

we find that the total hydrogen signal from D_2O is nearly identical (within typical variation in signal during ESD) in intensity and shape to the total hydrogen signal from H_2O (Figure 3.1). We will use these weightings to determine hydrogen production from various layers of water/methanol films, and in each figure with multiple isotopologues, we have weighted the HD and D_2 signals accordingly. However, we use D_2 as our signal of choice, as it has a single source, unlike the H_2 and HD signals, which can be affected by background levels of hydrogen and are observed during ESD of bare TiO_2.

Production of H_2, HD, and D_2 from pure water and pure methanol films

In pure water, the hydrogen signal initially spikes and then returns to a nearly constant rate (Figure 3.1). As determined previously,[3] the hydrogen signal in water arises from H_2 produced at the water/vacuum interface in films thicker than 60 ML, and it is this interface that is responsible for the prompt signal.

Methanol often behaves similarly to H_2O, and it is expected that the methanol/vacuum interface also plays an important role in H_2 production from pure methanol. Figures 3.2, 3.3, and 3.4 show the production of H_2, HD, and D_2 from 30 ML CH_3OH, 10 ML CD_3OH, and 10 ML CD_3OD respectively. Although these thinner layers of methanol may be affected by the TiO_2 interface, they should serve as an adequate point of comparison for later mixed methanol/water structures.

As in pure water, hydrogen production in thin pure methanol films promptly appears after the electron beam turns on. The H_2 signal from methanol quickly rises and then declines steadily when irradiated at warm temperatures (Figure 3.2 shows the results of irradiating the film at 50 K. Similar results are observed for temperatures greater than 50K). In contrast, hydrogen formation in CH_3OH at 25 K increases slowly, and the large signal remaining after the electron beam is turned off indicates that a significant portion of the detected hydrogen must diffuse out of the methanol film, suggesting that the majority of H_2 formed at this temperature is not formed at the methanol/vacuum interface. It is unclear if the H_2 is forming in the bulk, or, as in water films of similar thickness, at the substrate. We focused on thick mixed films of water and methanol to simplify the number of interfaces, and so our primary concern is establishing that pure

methanol also generates a prompt H_2 (D_2) signal to determine the signal source in mixed films.

After accounting for the different sensitivity of the QMS to each isotopologue, the total signal intensity (H_2 + 1.52HD + 2.04D_2) of CD_3OH is about 25% larger than the total signal intensity of CD_3OD, suggesting an isotope effect. By comparing the three signals, it is clear that substituting D for H ($H_2 \rightarrow$ HD, HD$\rightarrow D_2$) leads to a decrease in the signal intensity by a factor of 0.68. This factor is likely the result of both reduced formation rates and reduced desorption rates of the heavier molecules.

Previous work suggests that at these electron energies, methanol contributes H primarily from its methyl group. [12-14] To determine the contribution of the methyl and alcoholic hydrogens to hydrogen production from methanol films, we compare the H_2, HD, and D_2 signals. Examining the D_2 signal from CD_3OH (Figure 3.3), which has a single source, we see that the contribution from methyl Ds reacting to form D_2 is nearly constant over the radiation scan. The H_2 signal from CD_3OH, which is the result of alcoholic hydrogens reacting with each other, or desorbing to react with adsorbed H on the chamber walls, is also nearly constant. However, the D_2 signal from CD_3OD, resulting from three sources (two methyl Ds, two alcoholic Ds, or one methyl D and one alcoholic D) rapidly declines. We posit that the decrease observed is due to a reduction in the formation of D_2 from one methyl D and one alcoholic D.

This hypothesis is reinforced when one examines the HD signals from CD_3OH and CD_3OD. HD from CD_3OD, which results from the desorption of D atoms that react with H adsorbed on the chamber walls, is a relatively small signal, and decreases slowly.

The HD from CD_3OH is the result of both desorbing D atoms reacting with H present in the chamber, and D atoms reacting with alcoholic H atoms in the film. Its initial signal is roughly six times larger than the HD signal from CD_3OD, an increase which must be due to methyl-alcoholic HD formation since fewer D atoms are available to desorb and react with chamber H. It also decreases quickly, like the additional D_2 signal from CD_3OD that can be attributed to methyl-alcoholic D_2 formation. Addition of the three weighted signals for CD_3OH and CD_3OD yields two curves with the same shapes, showing that no major additional processes (e.g., hot D_2 reacting with H adsorbed to chamber walls to form HD) are occurring. Because the D_2 and H_2 signals from CD_3OH are nearly constant, the decrease seen in D_2 from CD_3OD is not from reactions of two methyl deuteriums or two alcoholic deuteriums, but from a decrease in the reaction rate of methyl deuterium with alcoholic deuterium. The mechanism responsible is unclear; if it were the result of consuming either the alcoholic or methyl D atoms, we would expect to see a decrease in the D_2 and H_2 signals from CD_3OH.

Production of H_2, HD, and D_2 from layered water/methanol films: Capped films, a.k.a. "open-faced sandwiches"

Because thick films of pure water and pure methanol both show a prompt hydrogen production signal, we cannot use different time scales to determine the kinetics of each species. Instead, we must focus on results from isotopic labeling. As shown in Table 3.1, H_2 and HD are more likely to have non-zero background levels or to be formed by desorbed atoms reacting with hydrogen present in the chamber. D_2 has no effective

background level and in many isotopic films has only one possible source, making it the signal of choice for determining the methanol- or water-based origins of hydrogen production.

The simplest layered water/methanol film is the capped film. A large quantity of water was deposited, typically 80 ML, to eliminate the effects of the water/substrate reactions. A thinner layer of methanol varying in thickness was grown atop the water, resulting in two interfaces: the methanol/vacuum interface, and the water/methanol interface.

Figure 3.5 shows the D_2 signal from an isotopically labeled layered film of n ML CD_3OD on 80 ML H_2O. The D_2 signal arises solely from the methanol portion of the film, showing an increase in total D_2 as more CD_3OD is dosed. The signal rapidly rises as soon as the beam is turned on, and then continues to rise slightly before decreasing with time; the time of peak signal intensity increases as the CD_3OD dose increases, with the signal peaking about 10 seconds after the beam starts for the thickest dose, 5 ML CD_3OD. In this respect, the signal from n ML CD_3OD/80 ML H_2O acts more like the thicker pure methanol films, as the shape of the D_2 curve is comparable to the H_2 curve from 30 ML CH_3OH. However, it is quite different from the D_2 signal from 10 ML CD_3OD (Figure 3.4). While both curves show a prompt increase in the signal, that from 10 ML CD_3OD immediately begins to decrease. This difference in shape, and the similarity of the very thin capping layer signals to the thicker pure methanol film, suggests that the substrate may be affecting the signal in the 10 ML pure methanol films, but does not affect a thin film of methanol on a thick water base, as expected. The total

D_2 signal increases linearly with CD_3OD thickness. This increase is observed over both short (3 s) and long (100 s) integration periods.

Figure 3.6 shows the D_2 signal from a labeled, layered film of n ML CH_3OH on 80 ML D_2O, irradiated at 50K. In this case, the D_2 signal arises solely from the water layers of the film, and allows us to determine how methanol acts as a barrier to D_2 formation and diffusion from the film. The addition of methanol, even in submonolayer quantities, suppresses the prompt formation of D_2 in the film associated with the water/vacuum interface. As more methanol is added, this effect becomes greater and lasts for longer periods. Integrating the D_2 signal over the first 3 seconds of irradiation to reflect this prompt D_2 formation shows that the D_2 signal decays exponentially with increasing CH_3OH coverage, with a 1/e constant of 1.14 ML (1.56 ML at 80K, likely due to an increased CH_3OH desorption rate). In comparison, the D_2 signal from pure water produced at the vacuum interface decays with a constant of 2.7 ML, suggesting that CH_3OH effectively eliminates the water/vacuum interface at lower coverages. Integration over the 100 second irradiation cycle is more complicated. At low doses of methanol, the D_2 signal from water increases by up to 40% when irradiated at 50K, as a result of increased D_2 production at later times. This increase persists until about 0.6 ML of CH_3OH are dosed, after which the total D_2 signal also decays exponentially, with a 1/e constant of 1.04 ML CH_3OH. There appears to be some temperature dependence in this process. When the experiment is repeated at 80K, the increase over the 100s integration period is much smaller, persisting to only 0.2 ML, after which it decays with a 1/e constant of 2.28 ML.

While submonolayer coverages of CH_3OH decreased the prompt portion of the D_2 signal, they also increased the long-term production of D_2 in the upper layers (Figures 3.7 and 3.8) above that seen from a pure D_2O film. The mechanism for this increase is unclear, but as it is the result of later production, it may be due to a methanol/water/vacuum interface with an increased number of dangling bonds to localize excitations and to higher mobility. The post-irradiation D_2 signal (after the beam is turned off) from these submonolayer coverages, which results from D_2 diffusing out of the film, is higher than for the pure D_2O film. Surface roughening is another possibility, though unlikely; measurements of surface roughening of methanol/water films showed little difference (see Chapter 2).

Coverages greater than a monolayer suppress both early and late D_2 production in the D_2O that recovers only as the capping methanol layer is sputtered away. A number of causes may lead to this suppression. First, the addition of the methanol layer moves the uppermost layers of water deeper into the film, where they receive lower levels of energy and are less likely to be excited. However, as this suppression occurs even when the water has been moved away from the vacuum interface by only a few monolayers, another mechanism is more probable. Second, the water/methanol interface may be less reactive, mimicking the behavior of a water/water interface in the bulk, where reactions do not occur. We will show later that this is also unlikely. Third, the methanol layer may act to trap the energetic electrons and/or the resulting excitations, therefore reacting at a higher rate than D_2O , explaining the disproportionately high quantities of D_2 generated in the CD_3OD/H_2O film. Petrik and Kimmel showed that only the uppermost 10 layers

are involved in generating H_2 from H_2O at the vacuum interface. For comparison, ~1.2-1.3 monolayers of CD_3OD at the vacuum interface generates the same quantity of D_2 as a pure 80 ML D_2O film over the course of the radiation scan and during the prompt regime. Finally, it is possible that D_2 is forming in the water layer or at the water/methanol interface and being physically trapped by multiple monolayers of CH_3OH and prevented from diffusing. However, this idea conflicts with the higher diffusion levels seen in films capped with submonolayers of CH_3OH.

To elucidate the nature of the water/methanol interface and determine if it may be more reactive, fully deuterated films of n ML CD_3OD/80 ML D_2O were dosed and irradiated. In these films, the addition of methanol increased the D_2 production (Figure 3.9), even at low coverages. This increase is greater than can be attributed to either methanol or water, in both the prompt and later time periods. For example, the addition of 0.6 ML CD_3OD to the D_2O surface led to an increase of roughly 0.1 units at each point during the full scan of the ESD (Figure 3.9), while the contribution from purely methanol peaks at only 0.05 units (Figure 3.5). Clearly, the methanol/water interface is responsible for some of the D_2 production. To determine how much, the D_2 signals from the labeled films CD_3OD/H_2O (D_2 solely from methanol) and CH_3OH/D_2O (D_2 solely from water) were subtracted from the D_2 signals from the CD_3OD/D_2O films, with the difference attributed to D_2 that is formed from both methanol and water. For ease in referring to these species, D from methanol is labeled here as “Dm” and D from water as “Dw.” This “interfacial” signal is shown for selected methanol doses in Figure 3.10. The small signal seen for the 0 ML methanol dose is due to variation in ESD signals between two pure

D_2O films. We can see that the interfacial contribution is significantly larger than this variation signal, indicating that it is a real effect and not due to changes in the chamber conditions over the course of the experiments, such as increased background D levels due to repeated D_2O dosing. The interfacial contribution rises promptly for submonolayer coverages, with the peak signal time increasing as the methanol dose is increased. The prompt signal seen with submonolayer coverages is consistent with Dm_2 and Dw_2 production from the methanol and water layers, which both contain rapid rises. The increasing delay in the time of peak signal for the interface is also consistent with the delays seen in Dw_2 production as the methanol layer thickens and the water/methanol interface moves away from the vacuum interface and receives less energy. The DmDw signal peaks at 1 ML CD_3OD coverage, where there is the greatest interaction of water and methanol molecules, least distance to the vacuum interface and the desorbing surface, and a high electron flux. This prompt peak at 1 ML coverage occurs at both 50 and 80 K (Figure 3.11). If the integration range is expanded to include the full ESD, and any mixing effects, the peak occurs at ~2 ML methanol coverage at both temperatures, suggesting that the second monolayer of methanol is mixing and reacting as the first monolayer is sputtered away. It is possible that even greater coverages of methanol would show an interfacial peak if the ESD was extended to longer times to allow for greater mixing.

The interfacial signal calculated previously was used to determine the total D contribution from D_2O, by adding the DmDw signal to twice the Dw_2 signal. The Dw contribution from capped methanol/water films was compared to the Dw signal from pure

D_2O using two integration ranges, the first three seconds of irradiation (no mixing effects) and the full scan (~100 seconds, and affected by mixing). Although the peak Dw signal occurs at different coverages due to mixing during the 100s integration, in both cases the addition of small quantities of methanol increased the Dw contribution (Figure 3.12). At 80K, this increase compared to a pure D_2O film was approximately 8% when mixing effects were minimal, and approximately 20% when they were considered. Larger increases were observed when the experiment was repeated at 50 K, with a 40% increase seen over the full, mixed scan integral (100s); however this may be due to the fact that the basis of comparison, a D_2O film irradiated at 50K, has a smaller signal than when irradiated at 80K. The presence of methanol causes a greater number of deuterium atoms in D_2O to react than would be seen in a pure D_2O film. This result has broad implications, especially if it holds true at higher temperatures. If so, it could lead to another route to H_2 production for a future hydrogen economy, and may be a hazard in nuclear waste tanks where the presence of well-mixed organics exposed to radiation over long periods could lead to excess H_2. Dw production is maximized when there is 0.5 ML methanol on the surface when using a 3 s integration period. At this point, the methanol/water interface is presumably half complete, allowing water to be at the surface and creating a methanol/water/vacuum interface. This complex interface allows both water and methanol to have a high number of dangling bonds exposed to many available electrons, excitons, and ions to drive the D_2 producing reactions. Water molecules may react at this interface through multiple reaction paths (water-water, water-vacuum, and water-methanol). At lower methanol coverages, only the water-water and water-vacuum

reactions are available, and at higher coverages only the water-methanol reactions. As the integration time increases and radiative mixing occurs, we see that the peak Dw signal shifts to higher coverages.

Production of H_2, HD, and D_2 from layered water/methanol films: Sandwich films

Data from capped films suggests that the methanol/water interface promotes the formation of D_2 in a manner similar to substrates such as Pt(111) and TiO_2(110). To determine the nature of the buried methanol/water interface, the ability of methanol to act as a substrate, and the opacity of the methanol layer to excitons or electrons, we use sandwich structures.

While it is clear that the methanol/water interface is reactive, it is unclear if both sides of the interface are equally so. The "opacity" of the methanol layer is a consequence of its ability to reduce the D_2 signal from the lower methanol/water interface, either by blocking the formation of D_2 in buried layers or the diffusion of D_2 from those layers to the vacuum surface. To determine this opacity and find if any detectable D_2 was formed at the lower interface, 8 ML of D_2O were placed either above or below 6 ML of CH_3OH on an 80 ML H_2O base. These structures were then capped with varying amounts of H_2O to determine how much H_2O, alone or with the addition of CH_3OH, would reduce detectable D_2 (Figure 3.13). Not surprisingly, D_2O at the vacuum interface had the highest initial D_2 signal. Placing H_2O atop the D_2O decreased the prompt D_2 signal and shifted peak signal intensity to later times as the D_2O layer was moved away from the vacuum interface and received fewer excitations. The addition of a water capping layer

reduced the prompt signal with a 1/e constant of 5.6 ML, twice that in a pure water film [Note: this value integrated over 3 s; 2.7 ML value integrated over 17.2 s. Each used different amounts of D_2O, 8 ML vs. 2 ML.],[3] suggesting that the methanol interface beneath the D_2O may actually promote D_2 production in the D_2O layer. This idea is supported by the increase in total D_2 production that is observed when the H_2O capping layer is increased from 0 to 4 ML (Figures 3.13 and 3.14). In a pure water film, moving the D_2O layer away from the vacuum interface strictly decreases the total signal, as the more distant layer both receives less energy/excitations, and any excited D_2O must move to the reactive interface. Therefore, the 20% increase seen in D_2 production of the 4 ML H_2O/8 ML D_2O/6 ML CH_3OH film compared to the 0 ML H_2O/8 ML D_2O/6 ML CH_3OH film indicates that the D_2O/CH_3OH interface promotes D_2 production. However, this total increase is due to increased D_2 production at later times, suggesting that the D_2 may form at the D_2O/CH_3OH interface, and then diffuse to the surface. The lower signal seen at 0 ML $H_2O/D_2O/CH_3OH$ may also be the result of most of the D_2 reacting at the vacuum interface and a higher flux of desorbing D atoms from the interface, reducing the D_2O reservoir available to react at the CH_3OH interface. Future work using the direct measurements of desorbing D_2O and examining the HD signal from the system may help to resolve the observed increase.

If D_2O is placed beneath CH_3OH, the prompt D_2 signal is completely quenched (Figure 3.13). As expected, no D_2 forms at the vacuum interface. The appearance of the D_2 signal is slowed in time by the presence of a CH_3OH capping layer, and when it does recover, remains small by comparison. The largest D_2 signal observed, when 6 ML of

CH_3OH and 0 ML of H_2O capped the D_2O, is comparable to 16-18 ML of H_2O capping D_2O. The addition of H_2O to the 6 ML CH_3OH capping layer serves to reduce the D_2 signal further, but not as strongly as the original 6 ML CH_3OH. It appears that the majority of the D_2 signal reduction is caused the presence of the methanol layer, which either does not permit D_2 formed beneath it to diffuse to the vacuum surface, or effectively quenches D_2 formation reactions, perhaps by trapping excitons.

When 6 ML CH_3OH are deposited between n and 80-n ML of D_2O at 50 K and then irradiated, we observe that the total D_2 signal has two components, prompt and late, as before (Figure 3.15). The prompt portion, reflecting D_2 produced at the water/vacuum interface, of the signal rapidly increases, with an early peak occurring within 10 seconds of turning on the electron beam. Early production of D_2 saturates once n = 10, as it does in pure water, suggesting that production of D_2 in this earliest regime occurs at the vacuum/water interface (Figure 3.16). As the upper water dose of n ML increases, the time of peak signal shifts to later ranges as D_2 products from greater depths increase. Notably, late-stage production of D_2 rises steadily as more water is deposited but peaks at n = 20, decreasing with greater capping layer thickness until n = 30, at which point late-stage D_2 production saturates and the signal is similar to that seen from a pure D_2O film (e.g., Figure 3.6). This saturation at $n \geq 30$ suggests that the D_2 produced in this region is due to reactions occurring within the first 30 layers of the surface, but not directly at the vacuum interface. The difference between late stage D_2 production at n = 20 and n = 30 suggests that when the methanol/water interface is in this region, it plays some role in D_2 production, in a manner similar to the role played by Pt(111) in thin

films of pure water. Future experiments will test this idea by examining D_2 production from films of n ML H_2O/2 ML D_2O/18-N ML H_2O/6 ML CH_3OH/60 ML H_2O.

Conclusions and Future Work

The addition of a methanol layer to an ASW film increases the total electron-driven hydrogen production during ESD. Part of this increase is due to contributions from the H-rich methanol, as similar to one capping monolayer of methanol can produce as much H_2 as a thick pure water film. The increase is not solely due to contributions from methanol, however, as isotopic labeling showed that coverages of less than 0.6 ML methanol on ASW at the vacuum interface increase D_2 production occurring strictly in the amorphous D_2O film (that is, both D atoms come from a water source). At these submonolayer coverages the production of D_2 from ASW at the vacuum interface is initially reduced, while later D_2 production is increased. This later increase (and overall) suggests that the methanol may disrupt the hydrogen-bonding network of the ASW as it is radiatively mixed and sputtered, creating more dangling bonds that can react.

Thicker capping layers of CH_3OH decrease the D_2 formed exclusively in the labeled water film because the water layer is located deeper in the film, where it receives a lower electron flux. Isotopic labeling shows that as the methanol/water interface becomes more complete, more molecular hydrogen is formed at the interface. This H_2 (D_2) has two sources, with one atom coming from the methanol layer and one from the water layer. Increasing quantities of this interfacially produced hydrogen are observed with increasing methanol coverage until the prompt (unaffected by mixing or sputtering)

signal peaks at 1 ML, when the interface is complete, nearest the desorbing surface, and receiving the highest electron flux. Greater coverages of methanol do not increase the prompt interfacial signal, but do increase the signal at later times, when mixing effects become important. Radiatively driven mixing in the film effectively increases interfacial contact between methanol and ASW, as more layers of ASW are penetrated by a methanol molecule that can disrupt its H-bonding network. The addition of methanol in these films, while decreasing the H_2 produced only in the water layer, increased the measured total H contribution from water due to interfacially formed D_2 .

The reactivity of the methanol-water interface was confirmed by growing $H_2O/D_2O/CH_3OH/H_2O/TiO_2$ "sandwich" films. In thick films of pure water, H_2 is produced only in the 10 ML closest to the vacuum interface. In constructing these sandwich films, a methanol layer was placed in this non-reactive region, creating a D_2O/CH_3OH interface. The D_2 signal was found to be 20% larger when this interface was placed 12 ML away from the vacuum interface than when it was only 8 ML distant. The increase was due to D_2 production at later times, which is associated with production at a buried interface where D_2 must diffuse to the vacuum surface. However, thick layers of methanol were found to effectively block D_2 production from buried D_2O layers, so the methanol layer is semi-opaque to either diffusing D_2, or more likely, to excitons. Therefore, the methanol-water interface is both opaque and reactive, similar to a buried Pt-water or TiO_2-water interface. This result suggests that to maximize electron-driven H_2 production in water films at long times, a mixed film will be most effective.

Additional work with pure methanol films of varying thickness will enable us to isolate any existing methanol/substrate reactions in Figures 3.2, 3.3, and 3.4. If methanol acts as water does in these thin films, doing such experiments may enable us to determine the contribution of methanol and water to the prompt D_2 signal in mixed films. We also plan to find the "length" of the methanol/water interface, that is, how close a layer of water must be to a layer of methanol in order to see the methanol-induced results discussed above. These experiments will primarily involve isotopically labeling 1-2 water layers with D_2O, and separating the labeled layers from CH_3OH with spacer layers of H_2O. For example, the length of a methanol-water interface placed 30 ML from the vacuum interface would be studied by irradiating a film of 28-n ML H_2O/2 ML D_2O/n ML H_2O/1 ML CH_3OH/50 ML H_2O/TiO_2. The ideal depth of a buried methanol interface for increasing D_2 production, and the relationship between a methanol layer's thickness and its opacity, will also be explored.

References

1. Garrett, B. C.; Dixon, D. A.; Camaioni, D. M.; Chipman, D. M.; Johnson, M. A.; Jonah, C. D.; Kimmel, G. A.; Miller, J. H.; Rescigno, T. N.; Rossky, P. J.; Xantheas, S. S.; Colson, S. D.; Laufer, A. H.; Ray, D.; Barbara, P. F.; Bartels, D. M.; Becker, K. H.; Bowen, H.; Bradforth, S. E.; Carmichael, I.; Coe, J. V.; Corrales, L. R.; Cowin, J. P.; Dupuis, M.; Eisenthal, K. B.; Franz, J. A.; Gutowski, M. S.; Jordan, K. D.; Kay, B. D.; LaVerne, J. A.; Lymar, S. V.; Madey, T. E.; McCurdy, C. W.; Meisel, D.; Mukamel, S.; Nilsson, A. R.; Orlando, T. M.; Petrik, N. G.; Pimblott, S. M.; Rustad, J. R.; Schenter, G. K.; Singer, S. J.; Tokmakoff, A.; Wang, L. S.; Wittig, C.; Zwier, T. S., Role of water in electron-initiated processes and radical chemistry: Issues and scientific advances. *Chem. Rev.* **2005,** 105, (1), 355-389.

2. Zheng, W. J.; Jewitt, D.; Kaiser, R. I., Formation of hydrogen, oxygen, and hydrogen peroxide in electron-irradiated crystalline water ice. *Astrophys. J.* **2006,** 639, (1), 534-548.
3. Petrik, N. G.; Kimmel, G. A., Electron-stimulated production of molecular hydrogen at the interfaces of amorphous solid water films on Pt(111). *Journal of Chemical Physics* **2004,** 121, (8), 3736-3744.
4. LaVerne, J. A.; Pimblott, S. M., Effect of elastic collisions on energy deposition by electrons in water. *J. Phys. Chem. A* **1997,** 101, (25), 4504-4510.
5. Dohnalek, Z.; Kimmel, G. A.; Ayotte, P.; Smith, R. S.; Kay, B. D., The deposition angle-dependent density of amorphous solid water films. *J. Chem. Phys.* **2003,** 118, (1), 364-372.
6. Kimmel, G. A.; Stevenson, K. P.; Dohnalek, Z.; Smith, R. S.; Kay, B. D., Control of amorphous solid water morphology using molecular beams. I. Experimental results. *J. Chem. Phys.* **2001,** 114, (12), 5284-5294.
7. Petrik, N. G.; Kavetsky, A. G.; Kimmel, G. A., Electron-stimulated production of molecular oxygen in amorphous solid water. *J. Phys. Chem. B* **2006,** 110, (6), 2723-2731.
8. Henderson, M. A.; Otero-Tapia, S.; Castro, M. E., Electron-induced decomposition of methanol on the vacuum-annealed surface of TiO_2(110). *Surf. Sci.* **1998,** 413, 252-272.
9. Collignon, B.; Picaud, S., Comparison between methanol and formaldehyde adsorption on ice: a molecular dynamics study. *Chem. Phys. Lett.* **2004,** 393, (4-6), 457-463.
10. Winkler, A. K.; Holmes, N. S.; Crowley, J. N., Interaction of methanol, acetone and formaldehyde with ice surfaces between 198 and 223 K. *Phys. Chem. Chem. Phys.* **2002,** 4, (21), 5270-5275.
11. Hudson, P. K.; Zondlo, M. A.; Tolbert, M. A., The interaction of methanol, acetone, and acetaldehyde with ice and nitric acid-doped ice: Implications for cirrus clouds. *J. Phys. Chem. A* **2002,** 106, (12), 2882-2888.
12. Stockbauer, R.; Bertel, E.; Madey, T. E., The Origin of H^+ in Electron-Stimulated Desorption of Condensed CH_3OH. *J. Chem. Phys.* **1982,** 76, (11), 5639-5641.
13. Burrows, M. D.; Ryan, S. R.; Lamb, W. E.; McIntyre, L. C., Studies of H^+, H^{+2}, and H^{+3} Dissociative Ionization Fragments from Methane, Ethane, Methanol, Ethanol, and Some Deuterated Methanols Using Electron-Impact Excitation and a Time-of-Fight Method Incorporating Mass Analysis. *J. Chem. Phys.* **1979,** 71, (12), 4931-4940.
14. Parenteau, L.; Sanche, L., Low-Energy Dissociative Electron-Attachment (0-20 Ev) on Methanol and Some Organic-Molecules. *J. Chim. Phys. Phys.-Chim. Biol.* **1994,** 91, (7-8), 1237-1242.

Chapter 4: Suppression of electron stimulated O_2 production from amorphous solid water by CH_3OH

Introduction

Most recent work on supercooled thin water films has focused on amorphous solid water (ASW) due that material's importance in multiple fields. Radiation-driven processes in pure ASW and pure methanol have been described elsewhere,[1] but these processes in mixed and layered films have not. However, such mixes are common in many settings where ASW research has applications, including comets and icy bodies, clouds, cells, and retired nuclear reactors and waste tanks.[1-8] Such mixed and layered films also have applications on a broader scale, by clarifying energy transfer, leading to new synthetic processes, and clarifying mechanisms in water-based reactions. Our understanding of H-bonding networks, interfacially controlled reactions, and mixing at low temperatures needs to be improved by studying such combinations.

In pure ASW, the major molecular products of non-thermal processes are H_2 and O_2, although H_2O_2 and atomic products have also been described. [9-12] Our focus in this chapter is limited to O_2 production in the layered CH_3OH/H_2O films. Sieger, Simpson, and Orlando examined the production of O_2 from ASW and determined that the threshold energy required for production was ~10 eV.[13] As they found that O_2 production was not immediate, but required an initial dose, they determined that the O_2 production mechanism must require the formation of a stable precursor molecule, implying a two-step process. While the precursor-forming step was found to be temperature dependent,

the reaction of the precursor to form O_2 is temperature independent. The behaviors of both the precursor formation step and the precursor → O_2 step are inconsistent with older interpretations requiring thermal diffusion of radicals. Sieger *et al.* proposed instead that O_2 production begins with reactions of excited water molecules, and that the observed temperature dependency of O_2 production is accounted for by the lifetimes of excited water molecules.

Petrik, Kavetsky, and Kimmel[14] further characterized radiation-driven O_2 production in ASW. In films that were not previously irradiated (also called "unprocessed" or "raw" films), O_2 production grew with time until production was saturated. When the electron beam was stopped after saturation, the sample was allowed to "rest" at the same temperature, and the electron beam was restarted, O_2 production resumed immediately at the previous saturation level, regardless of the length of resting time. Using isotopically labeled water ($H_2{}^{16}O$ and $H_2{}^{18}O$), Petrik *et al.* determined that O_2 production was localized at the water-vacuum interface and ultimately resulted from HO_2 after a series of reactions:

1. $e^- + H_2O_{\ bulk} \rightarrow H_2O^+ + 2e^-$
2. $H_2O^+ + e^- \rightarrow H_2O^*_{bulk}$
3. $H_2O^*_{bulk} \rightarrow H_2O^*_{vac}$
4. $H_2O^*_{vac} \rightarrow H_{des} + OH_{vac}$
5. $2\ OH_{\ vac} \rightarrow H_2O_{2\ vac}$
6. $H_2O_{2\ vac} + OH_{\ vac} \rightarrow HO_{2\ vac} + H_2O$

7. $HO_{2\,vac} + A \rightarrow O_2$ + other products

In reaction 7, A is unknown, and may be another precursor molecule, an exciton, or an impinging electron. The surface coverage of HO_2 and other precursors (H_2O_2, OH) at saturation was found by modeling the reaction series to be ~0.01 to 0.03 ML relative to the water coverage (1 ML). Here we present the results of a study of the effects of O_2 production in H_2O by the addition of methanol, focusing on reactions at the vacuum interface.

Methods

Chamber Set Up

Experiments were done in an ultrahigh vacuum (UHV) chamber, equipped with a closed cycle helium cryostat, low-energy electron gun, quadrupole mass spectrometer, and a molecular beam line. Median base pressure for the system was ~1.1E-10 torr and base sample temperature was ~22K. Films were grown on a clean TiO_2 (110) crystal approximately 10 mm in diameter and 0.5mm thick. The crystal was cleaned by neon ion sputtering, followed by annealing at 850 K in vacuum, to yield a consistent TiO_2 (111) surface. The sample was resistively heated, and the temperature measured by a type K thermocouple spot-welded to the back of the sample.

Deposition and Growth Conditions

High-Pressure Liquid Chromatography-grade CH_3OH, distilled, deionized H_2O, and their isotopologues (CD_3OH, CD_3OD, D_2O, and $H_2{}^{18}O$) were freeze-pump-thawed prior to use to remove dissolved gases and to ensure purity. All films were dosed at temperatures colder than 100 K by molecular beams at normal incidence to the sample, creating a dense non-porous film.[15, 16] The films did not cover the entire substrate surface, but were centered on the TiO_2. Water coverage calibration was based on previous calculations using a coverage of 1 x 10^{15} molecules*cm^{-2}.[14] Direct measurements of methanol saturation coverage on ASW for calibration purposes are difficult due to mixing processes during desorption. Instead, methanol coverage was calibrated based on the integration of the first monolayer peak in the temperature programmed desorption spectra from a *bare* TiO_2 crystal. Based on the relative coverage of methanol on bare TiO_2 (110), 3.2 x 10^{14} molecules cm^{-2},[17] one monolayer of methanol on ASW was defined to be roughly three times the exposure needed for one monolayer on methanol on TiO_2. This definition of a CH_3OH monolayer on ASW has a comparable coverage to that of a water monolayer on ASW, 1 x 10^{15} molecules*cm^{-2}. The same exposure definition (in torr s) was used for each of the isotopically labeled varieties of methanol used, CH_3OH, CD_3OH, and CD_3OD, although the calibration was performed only for CH_3OH. We must emphasize that our monolayer definition is strictly to make comparing the effects of a monolayer of methanol with those of a water monolayer easier on a per-molecule basis, and is not based on any measurement of the actual coverage of CH_3OH on ASW.

Estimates of CH_3OH coverage on crystalline ice surfaces (none are available for ASW surfaces) range in value, but are comparable to its coverage on TiO_2 (110).[18-20]

Underlying foundation water films (in contact with the TiO_2 surface) were grown at 80K, conditions known to produce consistently dense and smooth ASW surfaces. [15, 16] Surfaction, or the phase separation and resulting movement of methanol to the vacuum interface, was observed during deposition of upper water layers in "sandwich" experiments. In these experiments, layers of water are dosed atop methanol to isolate it from the vacuum interface, creating a layered film with a sandwich-like structure of water/methanol/water/TiO_2. When the upper layers were deposited at 80K, the methanol promptly appeared on the surface in subsequent electron stimulated desorption (ESD) experiments. When the upper layers were dosed at 50K or less, it eliminated the prompt appearance of methanol from subsequent ESD experiments, even if the film was heated to 80 K from the lower dose temperature. Heating gently to 80K and irradiating had no effect on the ESD signal structure compared to irradiation at 50 or 25K. (For details, see Chapter 2.) To eliminate the effects of such surfaction, all upper films were grown at 80K or less, depending on their position in the final film structure. Capping water layers, or layers dosed atop methanol, were grown at 50K or less to minimize the surfactant properties of methanol. Methanol films were grown at 80K or less if their final position was located at the vacuum interface (i.e., an "open-faced" sandwich structure, also referred to in this paper as a methanol-capped film), and at 50K or less if in the interior (i.e., in a "sandwich" experiment).

Radiation Conditions

To eliminate the effects of thermal mixing and focus on radiative mixing and reaction products, all irradiation was performed at 80 K or colder; changes in the ESD temperature do not change the signal structure, although it may affect the signal intensity (See Chapter 2). Any irradiation performed at 80K was done to methanol dosed at the vacuum interface, when the surfactant properties of methanol could be neglected. The electron beam was incident at 35° to the sample normal. The films were irradiated with 100 eV electrons at a current of ~2 μA for 100 scan cycles (for a total exposure of ~97 s) unless otherwise noted. A scan-averaging mode was used that samples the signal repeatedly within a single cycle, rastering across the film sample to generate "pixels." The pixels were then averaged to generate a single data point per cycle with a very high signal-to-noise ratio, as described in detail in Petrik *et al.* [14]

Results and Discussion

Capped films

Consisting of one methanol-water interface, a capped film, one layer atop the other, is the simplest case for a layered film and the logical starting point. To study the effects of CH_3OH on the formation of O_2 from water at the vacuum interface, $H_2{}^{18}O$ was capped by increasing amounts of CH_3OH and irradiated. The 36 amu signal, for $^{18}O_2$, was measured during irradiation. The addition of CH_3OH to the surface of ASW leads to a delay in the radiation-driven production of O_2 from water (Figure 4.1). For a specified threshold level of O_2 production (e.g., a signal intensity of 0.03 a.u.), this delay is

approximately linearly dependent on the amount of CH_3OH dosed on the surface (Figure 4.2). The greater the O_2 threshold, the longer the delay, indicating that O_2 production rates are slowed, and ruling out the possibility that all CH_3OH and byproducts were eliminated from the system and the remaining O_2 comes from a pure water film. Further, when the O_2 rate is measured for a given remaining amount of methanol remaining on the surface, as measured by methanol desorption, it is not constant. Dosing amounts of methanol greater than 0.5 ML also suppresses O_2 production; at amounts greater than about 0.65 ML of CH_3OH, O_2 production does not recover within 97 seconds, the length of the radiation exposure.

The suppression of O_2 was measured by integrating the O_2 ESD signal over time, and plotting its dependence on the initial methanol dose. Two integration ranges were used to capture two different behaviors. Integration over the first three seconds of irradiation exposure (i.e., the first three data points collected after the electron beam was turned on) reflects the initial suppression/retardation of early O_2 production and eliminates any radiative mixing or sputtering effects. Integration was also performed over the full radiation exposure (that is, from when the electron beam was turned on until it was turned off, or ~97 s) to reflect total O_2 suppression as a function of CH_3OH dose. Full-exposure integration includes the effects of mixing and any CH_3OH byproducts, such as CO, CH_2OH, or CH_2O, on the O_2 signal. The time-integrated O_2 signals' dependence on CH_3OH dose was fitted to an exponential decay where the 1/e constant reflects the amount of methanol needed to reduce the O_2 signal (Figure 4.3). In the initial region, O_2 production is quickly suppressed by methanol, with a 1/e constant of 0.05 ML,

indicating that CH_3OH interrupts the O_2-producing reactions even at very low concentrations. However, it may appear to be more sensitive to CH_3OH than it actually is as the signal is small even when no methanol is dosed (Figure 4.1, Inset). The full cycle is less sensitive, with 0.2-0.28 ML CH_3OH needed. This latter value reflects late stage O_2 production as methanol is removed from the vacuum interface by mixing with the film, reacting with the water, and desorbing from the surface, and as O_2 production reaches saturation. While O_2 production increases as methanol signal decreases, there does not appear to be a threshold CH_3OH surface concentration above which O_2 production is suppressed and below which it recovers. Partial isotopic labeling of the water films so that the upper 10ML are $H_2{}^{18}O$ and the bottom 70ML are $H_2{}^{16}O$ confirms that O_2 production is concentrated at the surface as it is in pure water films. In this case, the $^{18}O_2$ signal intensity was roughly 70% that seen from a pure $H_2{}^{18}O$ film.

Sandwiched films

To examine the nature of a buried water-methanol interface, as opposed to one located at the vacuum interface, "sandwich" films of *n* ML H_2O over 1 ML CH_3OH over 120-*n* ML H_2O on TiO_2 (110) were grown and irradiated at 50K. Thinner films of *n* ML H_2O over 1 ML CH_3OH over 80-*n* ML H_2O were also grown under the same conditions. In both cases, O_2 production resumed as the capping layer thickness *n* reached 10-12 ML H_2O (Fig. 4.4a). Total integrated O_2 production saturated as the capping layer reached a thickness of *n* = 30 ML (Fig 4.4b), meaning that the methanol layer was separated from the O_2 producing vacuum interface by 30 ML H_2O. Thinner capping layers, where the

methanol interface was not buried as deeply, had reduced signals as a result of delays in O_2 production and lower final production levels. However, total levels of O_2 production in these CH_3OH-containing films were about 10-20% lower than O_2 production levels in pure water, even when 80 ML of water over 1 ML CH_3OH was compared to 80 ML H_2O over TiO_2 (plotted as n=200 and labeled as "pure water" in Figure 4.4b). It is clear that the methanol is acting as an internal interface and is able to suppress O_2 production even when the interface is buried.

To determine the nature of the interface and the source of O_2 in the interface, labeled sandwiches of *n* ML $H_2{}^{18}O$ over 1 ML CH_3OH over 80-*n* ML $H_2{}^{16}O$ were grown at 25 K and irradiated at 50K. The 32, 34, and 36 amu signals were monitored to measure the $CH_3OH/{}^{16}O_2$, $^{16}O^{18}O$, and $^{18}O_2$ desorption rates respectively. In sandwich films of $H_2{}^{16}O$ and CH_3OH, the 32 amu signal is a composite of desorbing CH_3OH, which begins desorbing immediately after the electron beam is turned on, and $^{16}O_2$ that forms from $H_2{}^{16}O$. In these films, O_2 production is observed only at later times and reaches an intensity of ~0.12 units (Figure 4.4a). In contrast, the 32 amu signal from the isotopically labeled sandwich shows prompt desorption characteristic of CH_3OH desorption at low capping thicknesses, and is near zero at higher capping thicknesses (10 ML $H_2{}^{18}O$ or more, Figure 4.5). Any $^{16}O_2$ that is produced in the water layer trapped beneath the CH_3OH does not appear in the signal, even at shallow depths where the bottom layer is within the penetration depth of the electrons. The $^{16}O^{18}O$ signal shows a slow increase characteristic of O_2 production in pure water, but even at its greatest intensity (for a 30 ML $H_2{}^{18}O$ layer over 1 ML CH_3OH and 50 ML $H_2{}^{16}O$) the signal is at most 5% of the

$^{18}O_2$ signal intensity for the same film (Figure 4.6). This minor signal indicates that very little mixing of oxygen isotopes occurs between water and methanol or $H_2{}^{18}O$ and $H_2{}^{16}O$, and that there is minimal transfer of labeled water through the CH_3OH layer. Meanwhile, the $^{18}O_2$ signal grows with increasing amounts of $H_2{}^{18}O$, as expected for O_2 production, to a saturation intensity of ~0.12 units (Figure 4.7), equal to that seen in the non-isotopically labeled film (Figure 4.4a). The maximum level of O_2 production occurs when the CH_3OH layer is at about the same depth in both films, under ~20-30 ML of water. The absence of the $^{16}O_2$ and $^{16}O^{18}O$ signals, combined with the $^{18}O_2$ signal observed, indicates that all of the observed O_2 is generated in the capping water layers. Methanol is acting as an internal interface in much the same way that Pt or TiO_2 acts as one; the $^{18}O_2$ signal is similar to that seen from dosing similar quantities of water on the bare TiO_2 substrate. The combination of these signals also suggests that CH_3OH is an effective barrier at these temperatures to either the movement of O_2 produced in the bottom portion of the sandwich, or to the production of O_2 in these lower layers, possibly as a result of exciton trapping or side reactions. Experiments where the methanol/water interface was increased by growing films with greater numbers of thinner layers of methanol also suggest that the desorption products are from only the upper layer, and that lower methanol/water interfaces have little impact on O_2 production.

To determine the amount of CH_3OH needed to form this interface, O_2 production levels were measured from films of 6 ML H_2O over *n* ML CH_3OH over 80 ML H_2O on TiO_2 (110). O_2 production was dramatically suppressed by just 0.1 ML CH_3OH, and was near full suppression with the addition of 0.5 ML CH_3OH (Figure 4.8). If O_2 or excited

$H_2{}^{16}O$ produced below the CH_3OH layer is being physically blocked by the presence of CH_3OH, this effect cannot be due to a separate continuous phase of methanol acting as an opaque film, as it occurs even at very low coverages. Blocking could be the result of long-range disruptions or restructuring of the H-bonding network near the methanol/water interface to prevent excited water from moving to the vacuum interface, or of efficient electron or exciton trapping that would prevent any excited bulk $H_2{}^{16}O$ from being formed.

Pre-irradiated films

To determine if methanol was destroying existing precursors, interrupting reactions with existing precursors, or preventing new precursors from forming, a series of experiments using pre-irradiated films of water was done. In these experiments, a thick pure water layer was deposited and irradiated at 80K to build up a large O_2 precursor molecule population. Previous work by Petrik *et al.* [14] showed that such precursors are stable over time at temperatures ≤80K. When the sample was irradiated a second time after resting, O_2 production in these pure water films resumed immediately at or near the saturation level of the first irradiation cycle.

In our experiments, we added a thin (0.01 to 0.5 ML) capping layer of methanol to the processed water film as it rested, and then resumed irradiation. The addition of CH_3OH led to a significant drop in the "prompt" (observed in the first 3 s) portion of the O_2 signal that results from reactions of existing precursors (Figure 4.9), and a boost in the prompt CO signal as methanol reacts on the precursor-laden film (not shown). Fitting the

integrated prompt signals to an exponential decay indicates that only 0.1-0.2 ML CH_3OH is needed to quench the prompt response; as little as 0.01 ML CH_3OH suppresses the prompt portion of the response by 20%. The saturation coverages of the O_2 precursors H_2O_2 and HO_2 were previously estimated to be ~0.01-0.03 ML, and the OH concentrations were estimated to be lower.[14] The effectiveness of this low CH_3OH coverage on O_2 production, considered with the low concentration of O_2 precursors, suggests that the quenching effects of CH_3OH are long-range and not due to direct reaction with a precursor molecule. The effect at low coverages shows that methanol is a much more effective suppressant than additional layers of water, indicating that the quenching is not due to some sort of physical blocking.

Increasing the methanol dose primarily serves to increase the delay before O_2 production recovery, as the quenching process appears to saturate (dark and light blue traces, Figure 4.9). Prompt O_2 production levels are similar for 0.2, 0.25, and 0.5 ML CH_3OH. Preliminary results suggest that even at methanol coverages of 2 ML, prompt O_2 production is still measurable, at ~15% of O_2 production in pure water. However, at coverages greater than 0.5 ML CH_3OH, the suppression of O_2 shows a linear correlation with CH_3OH coverage, rather than an exponential one. This change in correlation suggests that we must consider two processes in the suppression of prompt O_2. The first, occurring at low coverages (less than or equal to ~0.25 ML CH_3OH), is the result of long-range effects that interrupt some part of the reaction chain. For example, CH_3OH could react with an exciton in step 7, preventing HO_2 from forming O_2. The remaining O_2 production could be explained by some HO_2 reacting with an impinging electron instead

of an exciton, suggesting that step 7 should be labeled as step 7a and 7b. Alternately, CH_3OH could interrupt the formation of H_2O^*, which would then stop production of OH and H_2O_2, leaving HO_2 to be consumed in O_2 production. However, this latter process requires that preexisting OH and H_2O_2 fully convert to HO_2 within the first second of irradiation to explain O_2 signals at this first data point. The second O_2 suppression process, which correlates linearly with CH_3OH dose, occurs at coverages greater than ~0.25 ML CH_3OH. It is less sensitive to CH_3OH dose, indicating that most of the suppression effect is caused by the long-range effects observed at very low coverages. This second process may be the result of adding more methanol to act as a physical barrier, preventing any remaining precursors from moving to the surface to react and desorb, rather than interrupting O_2-producing reactions via scavenging HO_2 or other precursors.

We also consider the recovery of O_2 production at later times in these capped pre-irradiated films. As in the capped films, increased methanol doses lead to a longer recovery time for O_2 production, indicating that the O_2 precursor population must be reestablished. However, in the preirradiated films recovery appears to take longer than in the equivalent raw film (compare 0.5 ML coverages in Figure 4.1 and Figure 4.9), suggesting that a precursor deficiency is created by the presence of methanol, perhaps through OH scavenging. Another possibility is that the increased reaction of methanol with O_2 precursors generates methanol byproducts that suppress O_2 production. The O_2 recovery in a processed film strongly depends on the surface methanol concentration and O_2 production does not resume until nearly all the methanol is gone. Fitting the O_2 signal

to the methanol signal indicates that less than 0.007 ML CH_3OH remains on the surface before O_2 production recovers (Figure 4.10).

To eliminate the possibility that methanol directly reacts with O_2 precursors such as OH and H_2O_2 in the film, three experiments using layers of water as a physical barrier were performed (Figure 4.11). In each experiment, 80 ML $H_2{}^{18}O$ were deposited and irradiated at 80K to saturate the precursor concentration. In Figure 4.11A, the processed film was then covered with *n* ML unprocessed $H_2{}^{16}O$ at 50K. In Figure 4.11B, the processed film was covered by *n* ML unprocessed $H_2{}^{16}O$ and then 0.5 ML CH_3OH at 50K, to place a physical barrier between the precursor concentration and the methanol/water interface. In Figure 4.11C, the processed film was covered first by 0.5 ML CH_3OH and then by *n* ML unprocessed $H_2{}^{16}O$ at 50K, placing the methanol in direct contact with the concentrated precursors. Each film was irradiated a second time at 50K and the $^{18}O_2$ signal measured. Film A, composed only of water, shows the expected trend that less $^{18}O_2$ desorbs from the films with thicker capping layers. There is a small reduction in prompt O_2 production as precursors must move to the vacuum interface, but recovery is quick and ultimately rises to a value greater than the initial value. Films B and C are nearly identical with each other and contrast with film A. The addition of the methanol in films B and C greatly reduces the peak O_2 production signal and delays O_2 production recovery in comparison to film A. The similarity of films B and C indicates that methanol is not reacting with the O_2 precursors at the interface, but is blocking O_2 production by other long-range means. The only difference in films B and C occurs near the end of the radiation exposure, when the recovering O_2 signal is slightly smaller in

film C, where methanol and precursors are in direct contact. The slightly reduced signal of film C compared to film B suggests that any reduction in O_2 signal due to direct reactions at the interface is of minor importance and primarily affects O_2 recovery when new precursors are forming at the CH_3OH-$H_2{}^{18}O$ interface.

Clarification of the mechanism comes from data on water desorption (Figure 4.12). The addition of methanol decreases the water desorption signal, indicating that fewer excited water molecules form. Methanol suppresses H_2O desorption less effectively than O_2 production, with a 1/e constant of ~0.5 ML CH_3OH, perhaps because of the bulk water reservoir and fewer steps required to desorb H_2O than to form O_2. The role of the bulk water reservoir may be tested in future experiments of 1-3 ML $H_2{}^{18}O$ over 80 ML $H_2{}^{16}O$. Methanol shows long-range effects on electron stimulated water desorption as well. A single monolayer of methanol in a water-methanol-water sandwich will also suppress the desorption of water, even if buried under 20-30 ML H_2O, when fewer electrons should be reaching the water/methanol interface.

Modeling

Using the simple kinetic model from Petrik *et al.* [14] as a starting point, the methanol-water system was modeled. The previous model, which we will call Model 1, included seven reactions:

$$e^- + H_2O_{bulk} \longrightarrow H_2O^+ + 2e^- \quad (1)$$

$$H_2O^+ + e^- \longrightarrow H_2O^*_{bulk} \quad (2)$$

$$H_2O^*_{bulk} \longrightarrow H_2O^*_{vac} \quad (3)$$

$$H_2O^*_{vac} \longrightarrow H_{des} + OH_{vac} \quad (4)$$

$$OH_{vac} + OH_{vac} \xleftrightarrow{k2,k3} H_2O_{2(vac)} \quad (5)$$

$$H_2O_{2(vac)} + OH_{vac} \xrightarrow{k4} HO_{2(vac)} + H_2O \quad (6)$$

$$HO_{2(vac)} + A^* \xrightarrow{k5} O_2 + \text{other products} \quad (7)$$

An additional reaction was added to account for the reaction of CH_3OH with precursors, creating Model 1A:

$$OH_{vac} + CH_3OH_{vac} \xrightarrow{k6} CH_3O_{vac} + H_2O \quad (8)$$

This reaction scheme (Model 1A) was fitted to data from the ESD of *n* ML CH_3OH on 80 ML $H_2{}^{18}O$ shown in Figure 4.1. This model is adequate up to a methanol coverage of ~0.1 ML but overestimates $^{18}O_2$ suppression by CH_3OH at higher coverages. To correct this overestimation, an additional reaction was added to reflect destruction of methanol by radiation, creating Model 2:

$$e^- + CH_3OH_{vac} \xrightarrow{k7} \text{Products (e.g. } CH_3O_{vac} + H) \quad (9)$$

Model 2 fits the data over a broader range of methanol coverages (Figure 4.13) and correctly predicts the observed methanol signals. These results suggest that methanol interferes with the formation of O_2 by reacting with OH radicals at the vacuum surface,

interrupting the latter half of the reaction chain. At the lowest coverages, less than 0.1 ML CH_3OH, reaction 8 is sufficient to predict the observed data, and the destruction of CH_3OH by impinging electrons is not significant.

The products of reaction 8, CH_3O and CH_2OH, do not appear to play a major role in subsequent reactions with OH_{vac}, especially at lower coverages where they are likely to be quickly desorbed or react to form CH_2O or CO. However, they may react at higher coverages, longer times, or with other precursors (e.g., HO_2 and H_2O_2). As can be seen in Figure 4.13, the model predicts the observed data for 0.5 ML CH_3OH well until ~80 s, when it underestimates the suppression of O_2 formation by CH_3OH, likely because later reactions are not included.

Predictions by Model 2 of O_2 suppression in pre-irradiated films yield similar results. There are two main components to the O_2 signal from these films—a prompt and a late portion. The prompt O_2 signal is the result of O_2 reacting from pre-formed precursors. The late portion reflects the recovery of O_2 production as new precursors form. The prompt portion shows a rapid decrease from the saturation signal observed in pure water films, reaching minimum O_2 production at 15-20 s. Therefore, the suppression of prompt O_2 indicates that methanol is reacting with HO_2 and including such a reaction to create Model 3 accounts for this portion of the signal.

Model 3:

$$e^- + H_2O_{bulk} \longrightarrow H_2O^+ + 2e^- \quad (1)$$

$$H_2O^+ + e^- \longrightarrow H_2O^*_{bulk} \quad (2)$$

$$H_2O^*_{bulk} \longrightarrow H_2O^*_{vac} \quad (3)$$

$$H_2O^*_{vac} \longrightarrow H_{des} + OH_{vac} \quad (4)$$

$$OH_{vac} + OH_{vac} \xleftrightarrow{k2,k3} H_2O_{2(vac)} \quad (5)$$

$$H_2O_{2(vac)} + OH_{vac} \xrightarrow{k4} HO_{2(vac)} + H_2O \quad (6)$$

$$HO_{2(vac)} + A^* \xrightarrow{k5} O_2 + \text{other products} \quad (7)$$

$$OH_{vac} + CH_3OH_{vac} \xrightarrow{k6} CH_3O_{vac} + H_2O \quad (8)$$

$$e^- + CH_3OH_{vac} \xrightarrow{k7} \text{Products (e.g. } CH_3O_{vac} + H) \quad (9)$$

$$HO_2 + CH_3OH \xrightarrow{k8} \text{Products (e.g., } CH_3O_{vac} + H_2O_2) \quad (10)$$

However, the recovery portion of the signal is more difficult to model. Model 3 adequately describes the observed results at low coverages (Figure 4.14) but underestimates the suppression of O_2 by CH_3OH in these cooked films at higher coverages and longer irradiation times, where the reaction processes are yet more complex.

Conclusions and Future Work

Methanol is an effective suppressant of O_2 production from water during irradiation. CH_3OH added to the surface of an unprocessed water film delays O_2 production by scavenging OH, with ~0.2 ML CH_3OH sufficient to reduce O_2 production by ~63%. The delay in O_2 production from capped films is not due to the destruction or desorption of methanol followed by a prompt recovery of O_2, but instead to a simultaneous recovery of O_2 as methanol is desorbed, mixed with water, and reacted, resulting in a decreased O_2 production rate compared to that of pure water. Similar results

are found in processed films, where normally prompt O_2 production is reduced as methanol reacts with HO_2 precursors. O_2 production recovery appears to be slower than in an unprocessed film as it does not resume in processed films until effectively all of the methanol is removed from the film. O_2 suppression in both types of films occurs over long ranges (30 ML) and does not appear to require contact with the precursor-rich interface in the case of processed films. This result suggests that methanol interferes with exciton production/electron capture in water, and that such capture is a key process in reaction 7 ($HO_{2(vac)} + A^* \xrightarrow{k5} O_2$ + other products). While it is clear that methanol disrupts the formation of excitons, the exact mechanism is yet to be determined and requires further study.

References:

1. Garrett, B. C.; Dixon, D. A.; Camaioni, D. M.; Chipman, D. M.; Johnson, M. A.; Jonah, C. D.; Kimmel, G. A.; Miller, J. H.; Rescigno, T. N.; Rossky, P. J.; Xantheas, S. S.; Colson, S. D.; Laufer, A. H.; Ray, D.; Barbara, P. F.; Bartels, D. M.; Becker, K. H.; Bowen, H.; Bradforth, S. E.; Carmichael, I.; Coe, J. V.; Corrales, L. R.; Cowin, J. P.; Dupuis, M.; Eisenthal, K. B.; Franz, J. A.; Gutowski, M. S.; Jordan, K. D.; Kay, B. D.; LaVerne, J. A.; Lymar, S. V.; Madey, T. E.; McCurdy, C. W.; Meisel, D.; Mukamel, S.; Nilsson, A. R.; Orlando, T. M.; Petrik, N. G.; Pimblott, S. M.; Rustad, J. R.; Schenter, G. K.; Singer, S. J.; Tokmakoff, A.; Wang, L. S.; Wittig, C.; Zwier, T. S., Role of water in electron-initiated processes and radical chemistry: Issues and scientific advances. *Chem. Rev.* **2005,** 105, (1), 355-389.
2. Angell, C. A., Amorphous water. *Annu. Rev. Phys. Chem.* **2004,** 55, 559-583.
3. Duvernay, F.; Chiavassa, T.; Borget, F.; Aycard, J. P., Experimental study of water-ice catalyzed thermal isomerization of cyanamide into carbodiimide: Implication for prebiotic chemistry. *J. Am. Chem. Soc.* **2004,** 126, (25), 7772-7773.
4. Al-Amoudi, A.; Dubochet, J.; Studer, D., Amorphous solid water produced by cryosectioning of crystalline ice at 113 K. *J. Microsc.-Oxford* **2002,** 207, 146-153.
5. Delzeit, L.; Powell, K.; Uras, N.; Devlin, J. P., Ice surface reactions with acids and bases. *J. Phys. Chem. B* **1997,** 101, (13), 2327-2332.

6. Buch, V.; Bauerecker, S.; Devlin, J. P.; Buck, U.; Kazimirski, J. K., Solid water clusters in the size range of tens-thousands of H_2O: a combined computational/spectroscopic outlook. *Int. Rev. Phys. Chem.* **2004,** 23, (3), 375-433.
7. Yue, Y. Z.; Angell, C. A., Water behaviour - Reply. *Nature* **2005,** 435, (7041), E1-E2.
8. Morishita, T., Anomalous diffusivity in supercooled liquid silicon under pressure. *Phys. Rev. E* **2005,** 72, (2).
9. Zheng, W. J.; Jewitt, D.; Kaiser, R. I., Formation of hydrogen, oxygen, and hydrogen peroxide in electron-irradiated crystalline water ice. *Astrophys. J.* **2006,** 639, (1), 534-548.
10. Baggott, S. R.; Kolasinski, K. W.; Perdigao, L. M. A.; Riedel, D.; Guo, Q. M.; Palmer, R. E., Vacuum ultraviolet surface photochemistry of water adsorbed on graphite. *J. Chem. Phys.* **2002,** 117, (14), 6667-6672.
11. Rowntree, P.; Parenteau, L.; Sanche, L., Electron-Stimulated Desorption Via Dissociative Attachment in Amorphous H_2O. *J. Chem. Phys.* **1991,** 94, (12), 8570-8576.
12. Kimmel, G. A.; Orlando, T. M.; Cloutier, P.; Sanche, L., Low-energy (5-40 eV) electron-stimulated desorption of atomic hydrogen and metastable emission from amorphous ice. *Journal of Physical Chemistry B* **1997,** 101, (32), 6301-6303.
13. Sieger, M. T.; Simpson, W. C.; Orlando, T. M., Production of O_2 on icy satellites by electronic excitation of low-temperature water ice. *Nature* **1998,** 394, (6693), 554-556.
14. Petrik, N. G.; Kavetsky, A. G.; Kimmel, G. A., Electron-stimulated production of molecular oxygen in amorphous solid water. *J. Phys. Chem. B* **2006,** 110, (6), 2723-2731.
15. Dohnalek, Z.; Kimmel, G. A.; Ayotte, P.; Smith, R. S.; Kay, B. D., The deposition angle-dependent density of amorphous solid water films. *J. Chem. Phys.* **2003,** 118, (1), 364-372.
16. Kimmel, G. A.; Stevenson, K. P.; Dohnalek, Z.; Smith, R. S.; Kay, B. D., Control of amorphous solid water morphology using molecular beams. I. Experimental results. *J. Chem. Phys.* **2001,** 114, (12), 5284-5294.
17. Henderson, M. A.; Otero-Tapia, S.; Castro, M. E., Electron-induced decomposition of methanol on the vacuum-annealed surface of TiO_2(110). *Surf. Sci.* **1998,** 413, 252-272.
18. Collignon, B.; Picaud, S., Comparison between methanol and formaldehyde adsorption on ice: a molecular dynamics study. *Chem. Phys. Lett.* **2004,** 393, (4-6), 457-463.
19. Winkler, A. K.; Holmes, N. S.; Crowley, J. N., Interaction of methanol, acetone and formaldehyde with ice surfaces between 198 and 223 K. *Phys. Chem. Chem. Phys.* **2002,** 4, (21), 5270-5275.
20. Hudson, P. K.; Zondlo, M. A.; Tolbert, M. A., The interaction of methanol, acetone, and acetaldehyde with ice and nitric acid-doped ice: Implications for cirrus clouds. *J. Phys. Chem. A* **2002,** 106, (12), 2882-2888.

Chapter 5: Closing Remarks

Summary

Water and methanol mixes are common in many environments, including various astronomical ices such as comet nuclei, interstellar dust grain mantles, asteroids, and moons/planetary bodies. Mixes of water with methanol or other simple organics are not limited to astrophysical regions; they are ubiquitous, found in every biological system, Earth's atmosphere, and nuclear power plant waste. When these systems are exposed to energetic radiation, large quantities of low-energy electrons are generated that can drive later reactions.[1] To mitigate the effects of such reactions, or to use them to our advantage, we must understand the processes involved, including the reaction mechanism, energy transport within the water, energy transport between the water and the organic molecule, and the role of the water/organic interface in promoting or retarding non-thermal reactions.

To this end, we have studied these low-energy electron-driven reactions in methanol/amorphous solid water (ASW) films at cryogenic temperatures. The use of ASW allows us to create structured films where the number and extent of water/methanol interfaces can be controlled, and processes such as mixing can be slowed and measured. These processes in layered methanol-water films were examined using ultra-high vacuum (UHV) and molecular beam techniques, electron stimulated desorption (ESD), and temperature programmed desorption (TPD). In each of the experiments described in this dissertation, a TiO_2 (110) crystal was used as the growth substrate. However, some of the

experiments reference ASW films grown on a Pt (111) crystal under the same conditions. In very thin films (40 ML or less), the substrate does play a role in determining reaction products and promoting reactions. In our work, we used thick films of 80 ML or more, rendering the nature of the substrate irrelevant, and allowing us to focus on the water/vacuum, water/methanol, and methanol/vacuum interfaces. Experiments with thick ASW films on TiO_2 (110) and Pt (111) yield very similar ESD spectra and are comparable. TPD peaks from these experiments are not compared to those using a Pt (111) substrate, although the basic shape of the water desorption peak is similar. All of the water and methanol films were grown at 80 K or less using a molecular beam at normal incidence to the substrate, conditions known to create non-porous smooth ASW films. [2, 3]

Chapter 2 comprises an overview of the results from these experiments, which we believe to be the first to examine low-energy electron-induced reactions between methanol and ASW. ESD and TPD spectra were analyzed to determine major products and consequences of irradiation. Pure methanol, methanol-capped water films (methanol / water / TiO_2 structures), and methanol-sandwiched films (water / methanol / water / TiO_2 structures) are discussed and compared.

These experiments show that methanol is quite mobile during deposition at 80 K, moving to remain at the surface, but immobile at 50 K. This mobility exists only during deposition; heating a film deposited at 25 K to 80 K does not lead to an increased concentration of methanol at the surface. We also find that the methanol-water films, even for 30 ML thick methanol layers, produce fewer product species during irradiation

than pure methanol films (also 30 ML thick). From a pure methanol film, these include H_2, CH_2O, CO, CO_2, H_2O, CH_4, C_2H_6, C_2H_4, and heavier species such as HCOOH, CH_3OCH_3, CH_3OOCH_3 , CH_3CH_2OH, and $(CH_2OH)_2$, many of which are detected during the TPD. From a layered methanol/water film, fewer products are seen, with CH_3OH and H_2O dominating TPDs. Observed products from these films included H_2, O, CH_2O, C_2H_6, CO, CO_2, CH_3CH_2OH, CH_3OCH_3 , and O_2. The variety and quantity of product species increase as the total energy deposited increases; no species besides methanol were observed when the samples were not irradiated.

The TPD data indicate that methanol and water co-desorb over a broad temperature range, and are mixed by radiative processing during the ESD. The kinetics of desorption from the layered films are not discussed, as up to four peaks overlap during desorption. Surface area measurements suggest that water-dominated surfaces are marginally rougher than methanol-dominated surfaces. Confirmation of these products by spectroscopic methods (e.g., infrared spectroscopy), improved surface area measurements, and the effects of extended irradiation exposures will be included in future work.

Extra attention was given to the generation and destruction of the main radiolytic water products, molecular hydrogen and molecular oxygen, due to the importance of these species in major environments of interest: nuclear waste tanks, nuclear reactors, and astronomical ices. For example, the presence of H_2 in waste tanks poses a serious hazard to attempts to clean up contaminated sites, and increases the risks associated with long-term storage of nuclear waste. Previous studies have found greater quantities of H_2

present in these tanks than predicted by theory.[1] Our research shows that this excess H_2 could be due to the presence of small quantities of organic compounds, a factor that must be included in future models of nuclear waste storage and treatment. The formation of O_2 from water present in these tanks increases the combustion and containment hazards posed by H_2 build up, and consequently must be considered. O_2 production and the associated radicals also increase corrosion rates in water-cooled nuclear reactors. [1] The production and destruction in ASW of both O_2 and H_2 are also important for astrophysical models that explain the evolution of stars and planets, and for interpreting spectroscopic signals.

Chapter 3 discusses how methanol changes electron-driven H_2 production from water films, focusing on the role played by the new methanol/water interface. The addition of a methanol layer to an ASW film increases the total electron-driven hydrogen production during ESD. Part of this increase is due to contributions from the H-rich methanol, and supports the hypothesis that excess H_2 in waste storage results from the presence of organic compounds. However, at low methanol coverages, part of the increase also appears to be the result of increased H contributions from water. Isotopic labeling showed that coverages of less than 0.6 ML methanol on ASW at the vacuum interface increase D_2 production occurring strictly in the amorphous D_2O film (that is, both D atoms come from a water source). At these sub-monolayer doses, methanol increases the ability of water to generate D_2 by increasing D_2 production later. This increase appears to be due to the creation of an extended methanol/water/vacuum

interface. This effect is lost as methanol capping layer thickness increases, blocking the D_2-forming water/vacuum interface.

Similar results were seen with buried methanol/water interfaces, where the H contribution from water was observed to increase by as much as 40%. This increase is due to the creation of a reactive methanol/water interface in regions of the bulk water that are typically unreactive, and to interfacial reactions between methanol and water. When the effect of mixing between the water and methanol layers is considered, i.e., at longer irradiation exposures, the increase is greatest. We propose that these new interfaces increase the number of dangling bonds, more easily trapping the excitons that drive the reaction. Mixing during the ESD, leading to the observed increase at later times, would enhance this effect. The disruption of ASW's H-bonding network by methanol may also increase the mobility of water molecules near the interface and aid H_2 production.

The reactivity of the buried methanol-water interface was confirmed by growing $H_2O/D_2O/CH_3OH/H_2O/TiO_2$ "sandwich" films. In thick films of pure water, H_2 is produced only in the 10 ML closest to the vacuum interface. In constructing these sandwich films, a methanol layer was placed in this non-reactive region, creating a D_2O/CH_3OH interface. The D_2 signal was found to be 20% larger when this interface was placed 12 ML away from the vacuum interface than when it was only 8 ML distant, despite receiving a lower electron flux. The increase was again due to D_2 production at later times, which is associated with production at a buried interface where D_2 must diffuse to the vacuum surface. However, thick layers of methanol were found to effectively block D_2 production in $H_2O/CH_3OH/D_2O/H_2O/TiO_2$, so the methanol layer is

semi-opaque to either diffusing D_2, or more likely, to excitons. Therefore, the methanol-water interface is opaque and reactive, somewhat similar to a buried Pt-water or TiO_2-water interface.

Chapter 4 covers the suppression of electron-driven O_2 production from water and explores the mechanisms by which methanol interrupts this multi-step reaction process. In water, O_2 is known to form at the vacuum interface during irradiation.[4] We find that placing methanol at this interface efficiently suppresses O_2 production, even at very low (0.05 ML) coverages. Unlike H_2 production, in which hydrogen formed at the methanol/water interface could come from either source, the O_2 that was observed to form is almost exclusively (more than 95%) from water.

Kinetic modeling shows that CH_3OH added to the surface of an unprocessed water film delays O_2 production by scavenging OH as it is produced, with ~0.2 ML CH_3OH sufficient to reduce O_2 production by ~63%. O_2 production does eventually recover as methanol is removed from the surface by desorption, mixing with water, and reacting to form other (non-OH-scavenging) species. While O_2 suppression is most easily observed when methanol is placed at the vacuum interface, a monolayer of methanol buried in the upper 30 ML of a water film also suppresses O_2 production. In these sandwich films, we found that methanol was opaque to O_2 produced below the methanol layer, with nearly all of the detected O_2 resulting from water capping layers. Greater suppression is observed as the methanol is placed closer to the vacuum interface, and fewer capping layers of water are available to produce O_2. No O_2 was produced during the 97 s radiation cycle when the methanol layer was placed in the most reactive

uppermost 10 ML of H_2O. Clearly, scavenging OH at the vacuum interface is not the only mechanism by which methanol interrupts the O_2-forming process.

Similar results are seen in pre-processed films, where an ASW film has be pre-irradiated to saturate the O_2-precursor population. Normally immediate O_2 production is quickly reduced as methanol reacts with HO_2 precursors, and O_2 production recovery does not resume until effectively all methanol is removed from the film. Again, the scavenging of the O_2 precursor HO_2 by CH_3OH, although it fits the kinetic model very well, is not the only mechanism causing O_2 reduction. O_2 suppression in both types of films occurs over long ranges (30 ML) and does not appear to require contact with the precursor-rich interface in the case of pre-processed films. This result suggests that methanol also interferes with exciton production/electron capture in water, and that such capture is a key process in the final O_2-forming reaction step ($HO_{2(vac)} + A^* \xrightarrow{k5} O_2 +$ other products).

Future Work

A number of important questions remain, including fundamental ones about mobility at low temperatures and energy transport within the ASW film. To better describe the water/methanol system, future studies will better characterize methanol surfaction and confirm the products identified so far. We will also examine the effects of longer radiation exposures on mixing and reactions in the layered methanol/water films.

More study is needed to confirm the observed increases in H_2 production in these layered films, and the mechanisms responsible. For example, the role of H-exchange

between CH_3OH and H_2O at the interface, and any effect it might have on the apparent increases in H_2, was not examined in this dissertation. The data suggest that other factors, such as increased exposure time and increased mixing, will positively affect H_2 production. However, we did not study the effects of long irradiation times, pre-processing, or co-dosed (truly mixed, as opposed to layered) films on H_2 production. It is possible that this increase may not be observed at greater exposures, as the sample can undergo radiative annealing that could reduce the reactivity of the water/vacuum interface.

Related experiments should study the nature of the methanol/water interface. The methanol layer appears to be opaque and to increase H_2 production when buried. However, previous experiments with H_2 production from ASW on Pt (111) showed that H_2 production at the Pt interface was significant only when the Pt interface was within 50 ML of the vacuum interface.[5] Future experiments must determine the mechanism responsible for the observed increase in D_2 production from a D_2O layer at the methanol interface (ASW H-bonding network disruption, exciton trapping and transfer by CH_3OH, or H-D exchange between the D_2O and CH_3OH), and find if there is a depth that maximizes this increase. Finding the "length" of the water/methanol interface, or how close the water must be to the methanol to be affected by its presence, will inform us about some of the mechanisms involved.[a]

[a] Films of m ML H_2O / 2 ML D_2O / n-m ML H_2O / 1 ML CH_3OH / 50 ML H_2O / TiO_2 can help answer both questions about H-D exchange between CH_3OH and D_2O, and the length of the interface.

The most pressing and interesting questions remaining are in regard to the observed long-range effects of methanol. While our expanded kinetic model accounts for the observed data on O_2 production very well, especially at low methanol coverages, it does not describe the observed long-range interruption caused by CH_3OH shown in Figure 4.11. The mechanism of this long-range effect is unknown, although we posit that it is the result of electron or exciton trapping by methanol. We expect that determining this mechanism will reveal basic information about how energy and matter are transferred between molecules in the condensed phase, to interfaces, and through interfaces. We will continue to use methanol/water interfaces to probe this question.

References

1. Garrett, B. C.; Dixon, D. A.; Camaioni, D. M.; Chipman, D. M.; Johnson, M. A.; Jonah, C. D.; Kimmel, G. A.; Miller, J. H.; Rescigno, T. N.; Rossky, P. J.; Xantheas, S. S.; Colson, S. D.; Laufer, A. H.; Ray, D.; Barbara, P. F.; Bartels, D. M.; Becker, K. H.; Bowen, H.; Bradforth, S. E.; Carmichael, I.; Coe, J. V.; Corrales, L. R.; Cowin, J. P.; Dupuis, M.; Eisenthal, K. B.; Franz, J. A.; Gutowski, M. S.; Jordan, K. D.; Kay, B. D.; LaVerne, J. A.; Lymar, S. V.; Madey, T. E.; McCurdy, C. W.; Meisel, D.; Mukamel, S.; Nilsson, A. R.; Orlando, T. M.; Petrik, N. G.; Pimblott, S. M.; Rustad, J. R.; Schenter, G. K.; Singer, S. J.; Tokmakoff, A.; Wang, L. S.; Wittig, C.; Zwier, T. S., Role of water in electron-initiated processes and radical chemistry: Issues and scientific advances. *Chem. Rev.* **2005,** 105, (1), 355-389.
2. Dohnalek, Z.; Kimmel, G. A.; Ayotte, P.; Smith, R. S.; Kay, B. D., The deposition angle-dependent density of amorphous solid water films. *J. Chem. Phys.* **2003,** 118, (1), 364-372.
3. Kimmel, G. A.; Stevenson, K. P.; Dohnalek, Z.; Smith, R. S.; Kay, B. D., Control of amorphous solid water morphology using molecular beams. I. Experimental results. *J. Chem. Phys.* **2001,** 114, (12), 5284-5294.
4. Petrik, N. G.; Kavetsky, A. G.; Kimmel, G. A., Electron-stimulated production of molecular oxygen in amorphous solid water. *J. Phys. Chem. B* **2006,** 110, (6), 2723-2731.

5. Petrik, N. G.; Kimmel, G. A., Electron-stimulated production of molecular hydrogen at the interfaces of amorphous solid water films on Pt(111). *J. Chem. Phys.* **2004,** 121, (8), 3736-3744.
6. Petrik, N. G.; Kavetsky, A. G.; Kimmel, G. A., Electron-stimulated production of molecular oxygen in amorphous solid water on Pt(111): Precursor transport through the hydrogen bonding network. *J. Chem. Phys.* **2006,** 125, (12).

Tables and Figures

Table 2.1: Experimental cracking fractions for CH_3OH.

M/Z	Relative intensity, Isothermal measurements	Relative Intensity, During TPD
2	.056	
12	.032	
13	.040	
14	.093	
15	.451	.317
16	.039	.018
17	.028	
18	.064	.026
27		.002
28	.396	.176
29	.744	.679
30	.158	.103
31	1	1
32	.691	.591
33	.023	.016
44	.003	.001

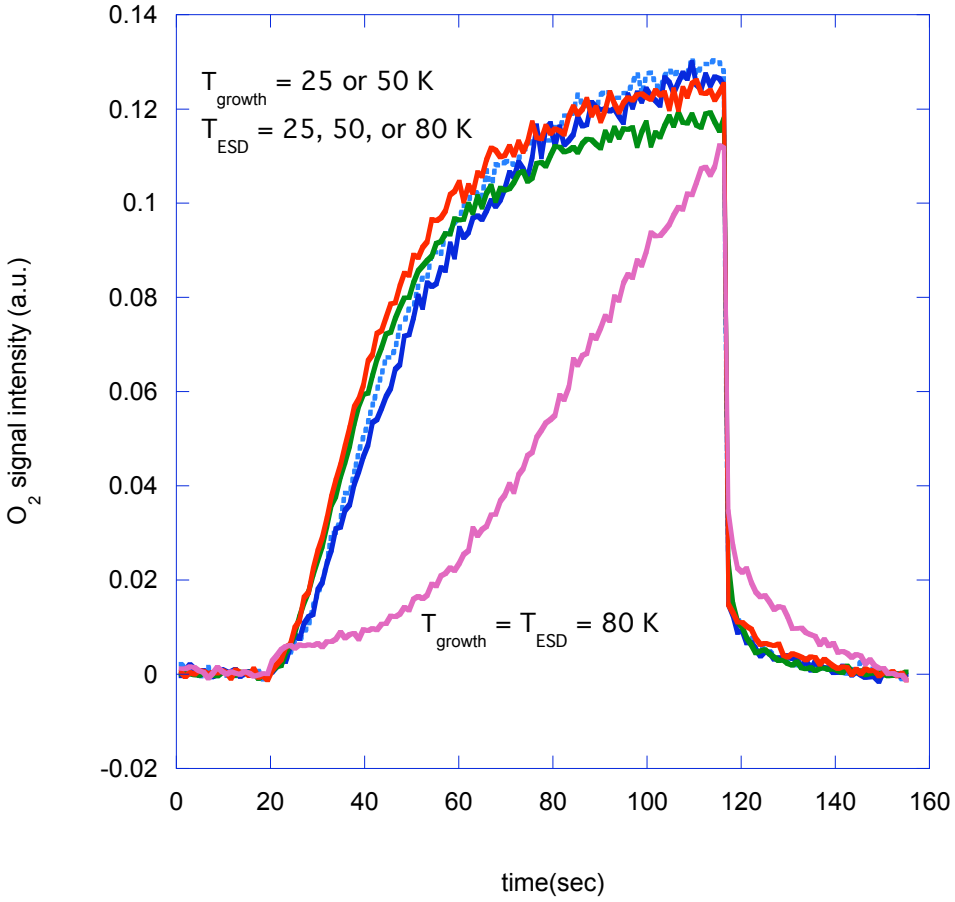

Figure 2.1: Deposition of ASW over CH_3OH at T=80K leads to an increased concentration of CH_3OH at the sample surface. Films of 30 ML H_2O over 1 ML CH_3OH over 50 ML H_2O / TiO_2 (110) were grown at various temperatures. The sandwich film was then irradiated at various temperatures and the 32amu ESD was measured. The different irradiation temperatures (T_{ESD}) lead to slightly different signal intensities. To compensate, all data were scaled to ~0.12 units for easier comparison. The appearance of methanol at the surface leads to a delay in the onset of O_2 production as seen when the deposition temperature (T_{growth}) = 80K, which determines the degree of surfaction. No such delay is observed when the film is grown at 25 or 50 K, regardless of the irradiation temperature.

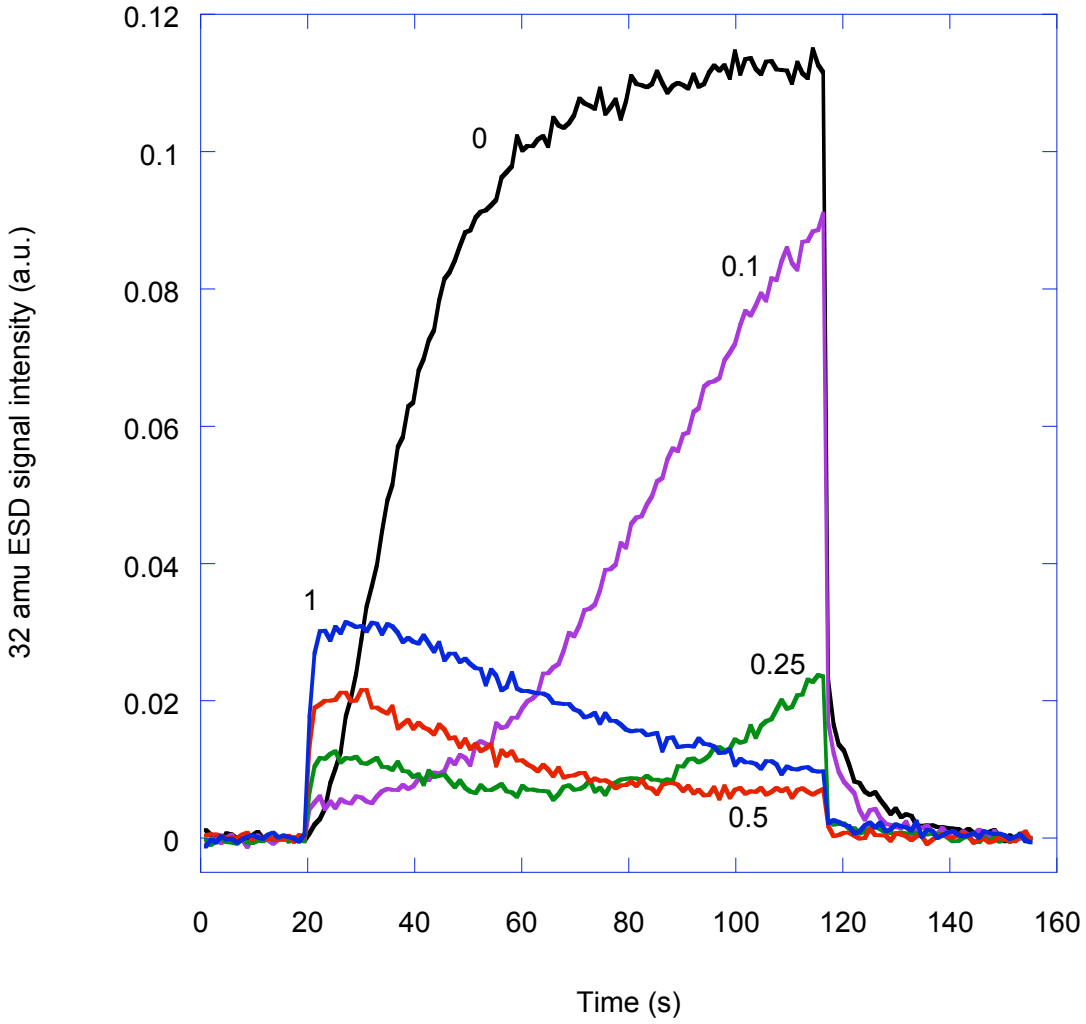

Figure 2.2: O_2 production from a methanol-capped water film deposited at 50 K and irradiated at 80K. n ML CH_3OH were deposited at 50 K on 80 ML H_2O. The film was irradiated beginning at 20 s and continuing until 117 s using 100 eV electrons at ~2 μA current. Mass 32 was monitored, measuring the CH_3OH and O_2 signals. The rapid rise at 20 s (observed for all coverages except 0 ML CH_3OH) is the result of desorbing CH_3OH. The O_2 signal is only observed at later times when CH_3OH is deposited; in the case of 0.5 ML CH_3OH and 1 ML CH_3OH, the O_2 signal is not observed.

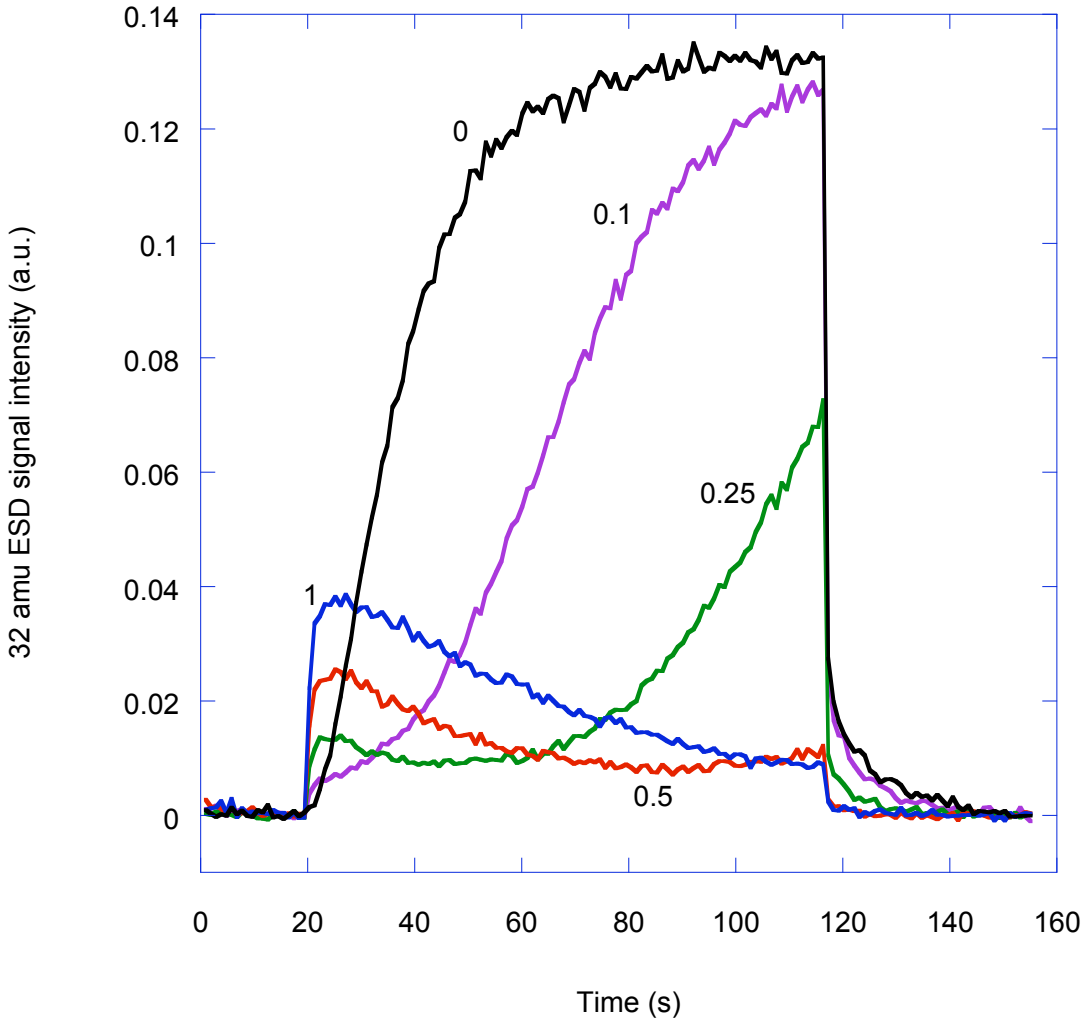

Figure 2.3: O_2 production from a methanol-capped water film deposited and irradiated at 80K. n ML CH_3OH were deposited at 80 K on 80 ML H_2O. The film was irradiated beginning at 20 s and continuing until 117 s using 100 eV electrons at ~2 μA current. Mass 32 was monitored, measuring the CH_3OH and O_2 signals. The rapid rise at 20 s (observed for all coverages except 0 ML CH_3OH) is the result of desorbing CH_3OH. The O_2 signal is only observed at later times when CH_3OH is deposited; in the case of 1 ML CH_3OH, the O_2 signal is not observed. In comparison to Figure 2.2, the O_2 signal recovers sooner. Both films were irradiated at 80 K, so this result is not due to higher desorption rates. Instead, it is likely due to greater mobility of CH_3OH during deposition at 80 K than at 50 K.

Table 2.2: Major desorption peaks during TPD from 30 ML unprocessed CH_3OH.

M/Z	Temperature at peak (K)	Peak Intensity (a.u.)	notes
44	173	.045	
45	173	.005	
46	173	.003	
30	557	.039	On tail
32	315	.124	On tail
32	~170	Saturated; estimate ~54	
33	172	5.417	
33	172	.831	
18	275	.01	Convoluted with tail of 172K peak
15	317	.02	Convoluted with tail of 172K peak

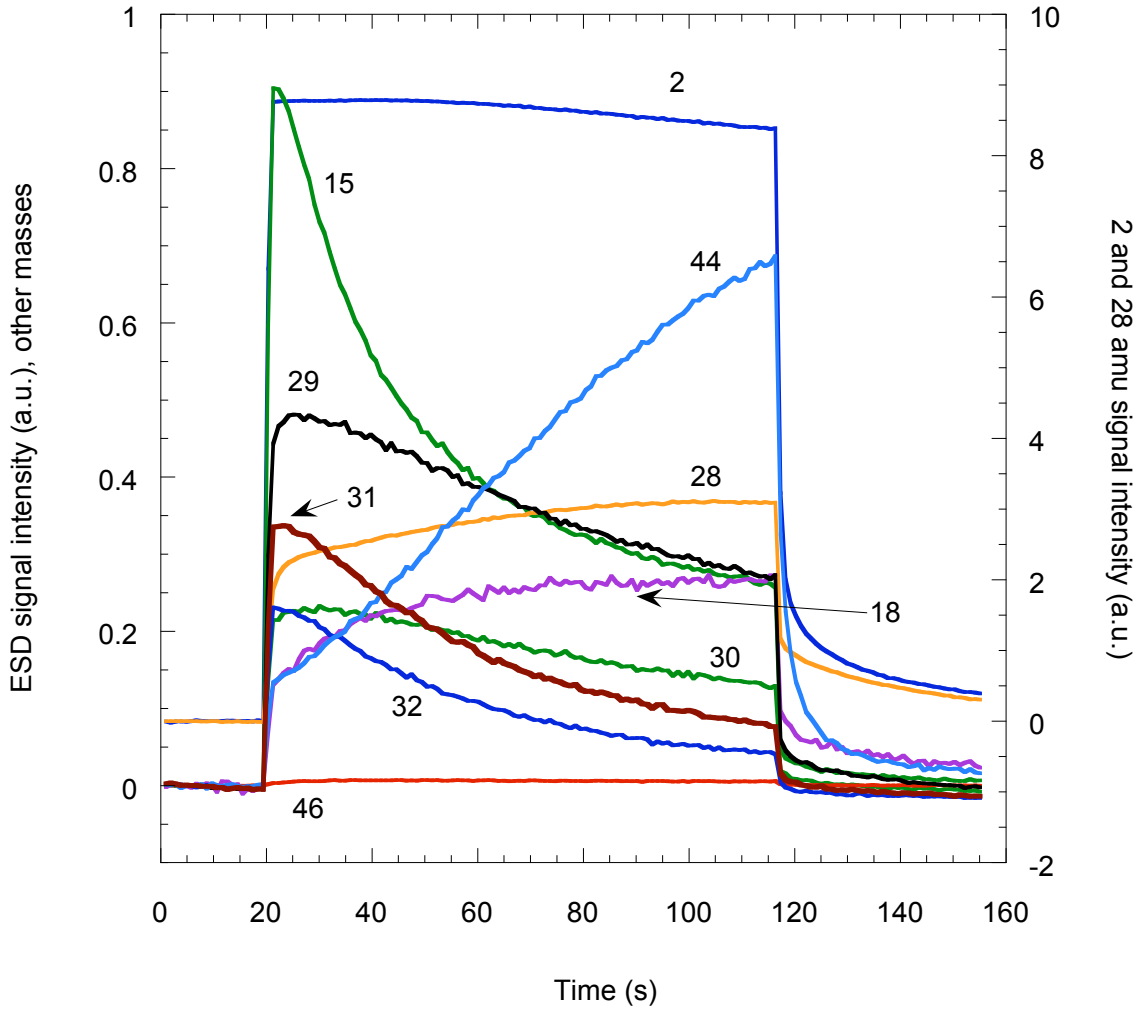

Figure 2.4: ESD products of 30 ML CH_3OH. 30 ML CH_3OH were deposited and irradiated at 80 K, beginning at 20 s and continuing until 117 s. 100 eV electrons were used at a current of ~5μA. ESD products are shown above; major products include H_2 and CO, plotted on the right-hand axis.

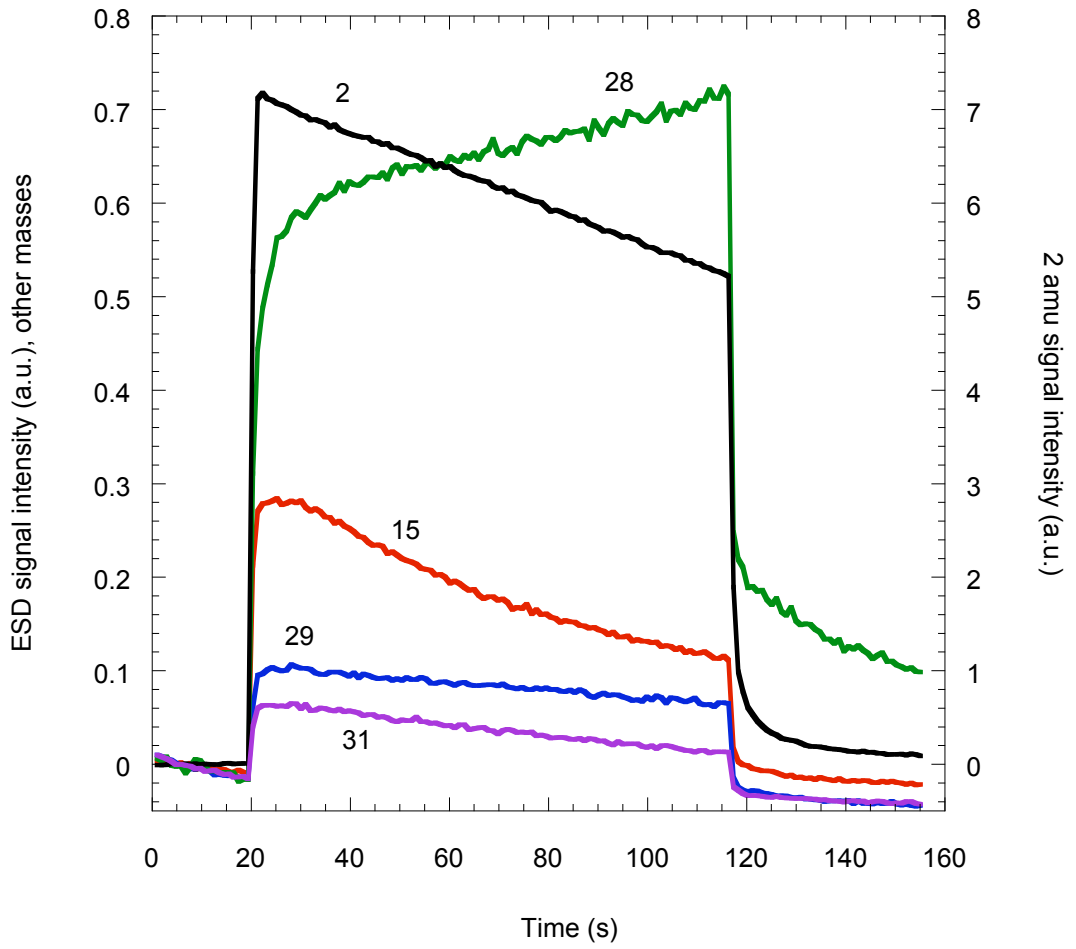

Figure 2.5: Selected ESD products of 30 ML CH_3OH, 2μA. 30 ML CH_3OH were deposited and irradiated at 80 K, beginning at 20 s and continuing until 117 s. 100 eV electrons were used at a current of ~2μA. Selected ESD products are shown above; major products include H_2, plotted on the right-hand axis. The reduced electron current leads to a reduced overall signal.

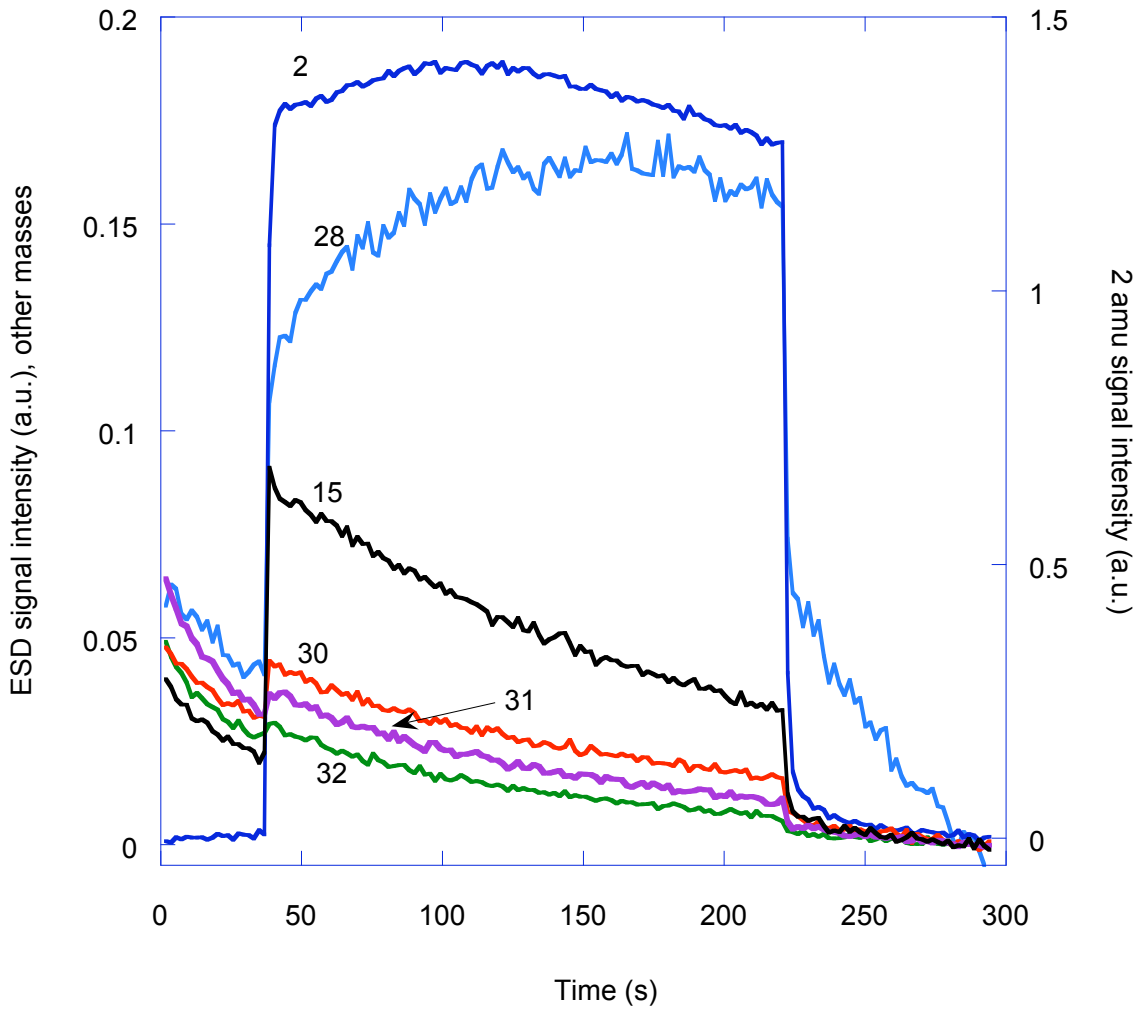

Figure 2.6: ESD products of 30 ML CH_3OH, 20eV. 30 ML CH_3OH were deposited and irradiated at 80 K, beginning at 20 s and continuing until 117 s. 20 eV electrons were used at a current of ~2μA. Selected ESD products are shown above; major products include H_2, plotted on the right-hand axis. The reduced electron energy leads to a greatly reduced overall signal; almost no CH_3OH is observed to desorb.

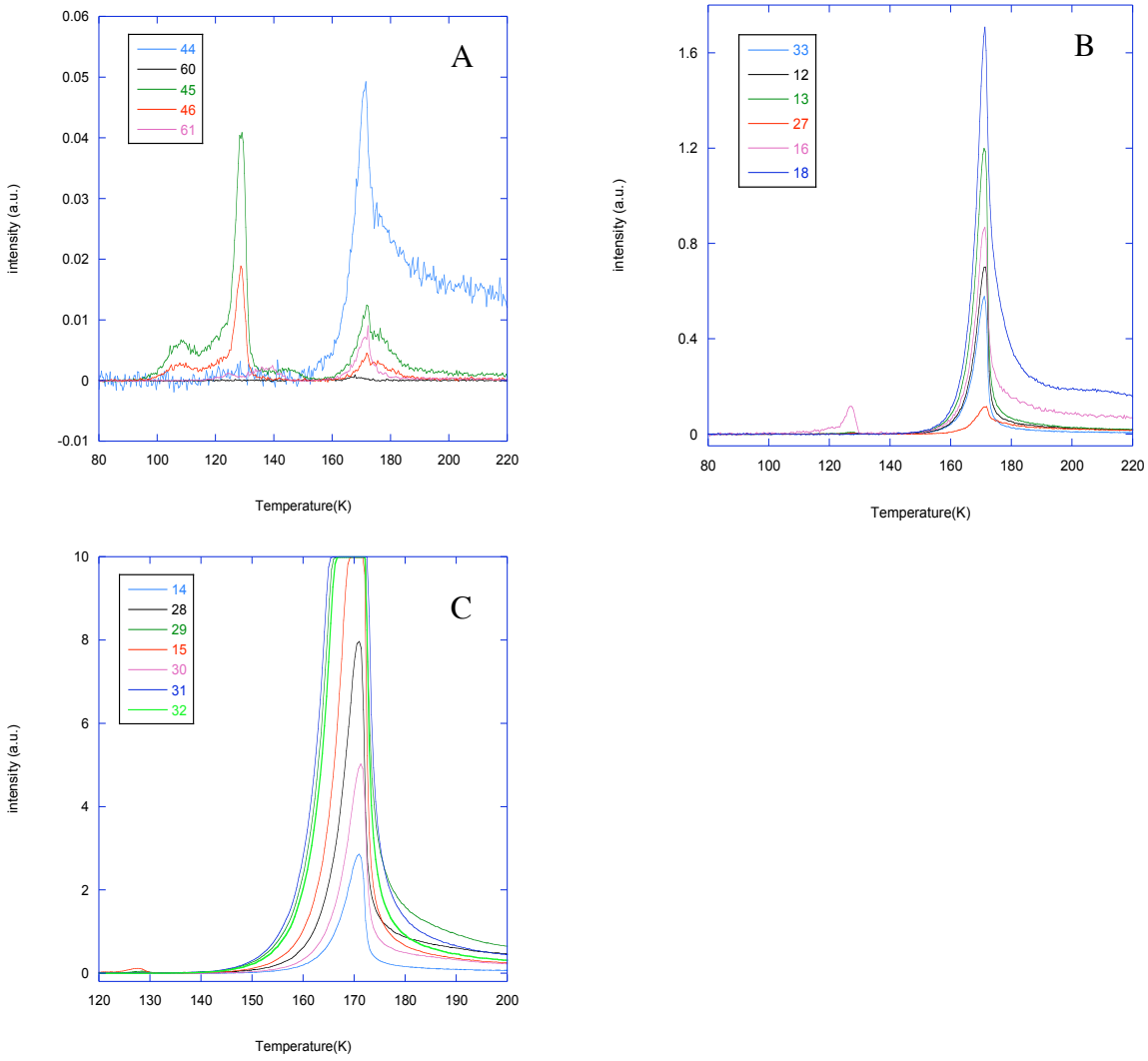

Figure 2.7: TPD products after irradiation of 30 ML CH_3OH using 20eV electrons. 30 ML CH_3OH were deposited and irradiated at 80 K for 97 s. 20 eV electrons were used at a current of ~2μA. TPD products are shown above. Minor peaks are shown in panel A. Moderate peaks are shown in panel B. The major CH_3OH desorption peak occurs at ~170 K (panel C).

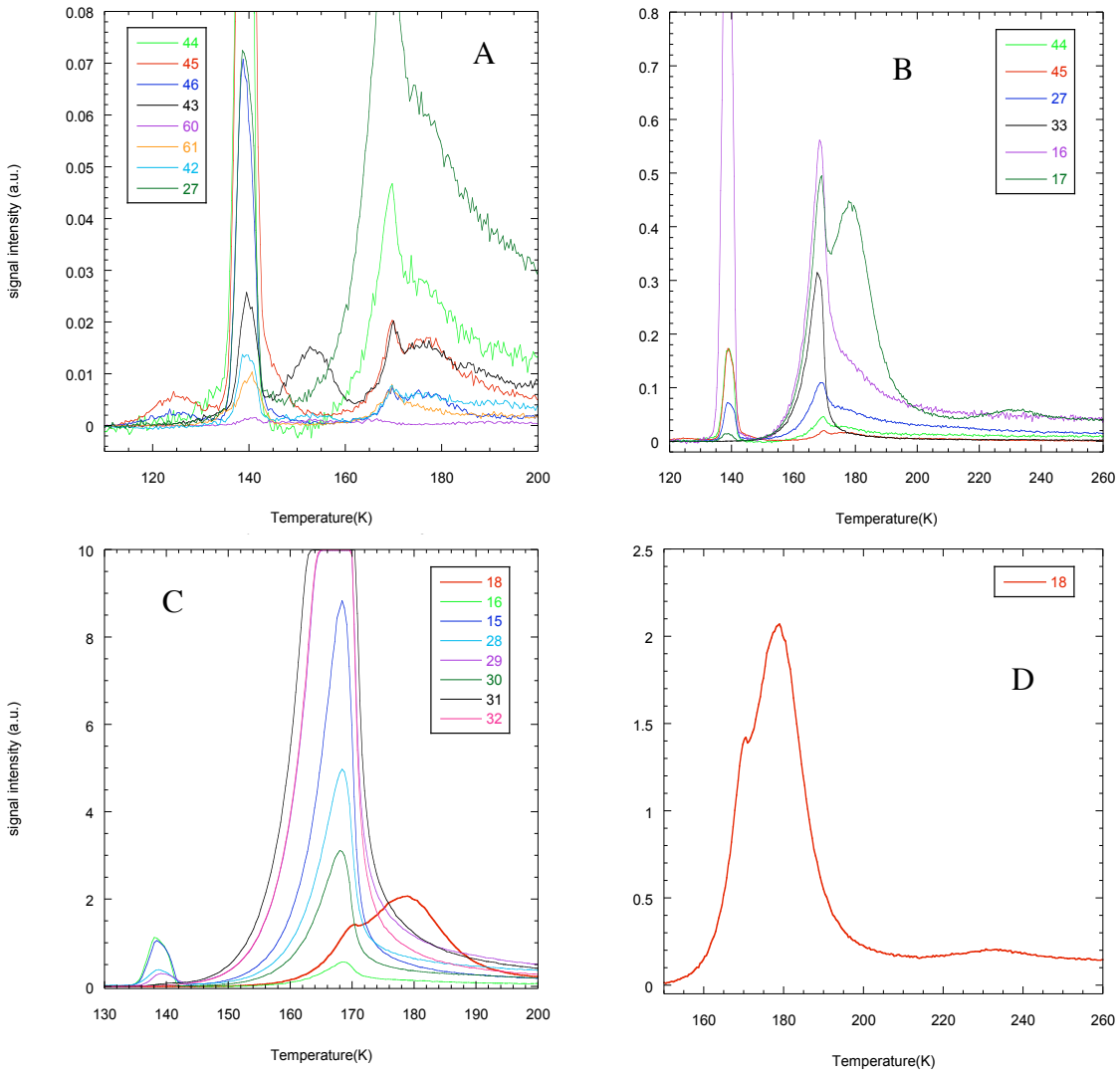

Figure 2.8: TPD spectra of 30 ML CH_3OH following irradiation with 100 eV electrons. 30 ML CH_3OH were deposited and irradiated at 80 K for 97 s. 100 eV electrons were used at a current of ~5μA. TPD products are shown above. Minor peaks are shown in panel A, moderate peaks in panel B. The major CH_3OH desorption peak occurs at ~170 K (panel C). Panel D highlights the effect of increasing the energy deposited on the production of H_2O.

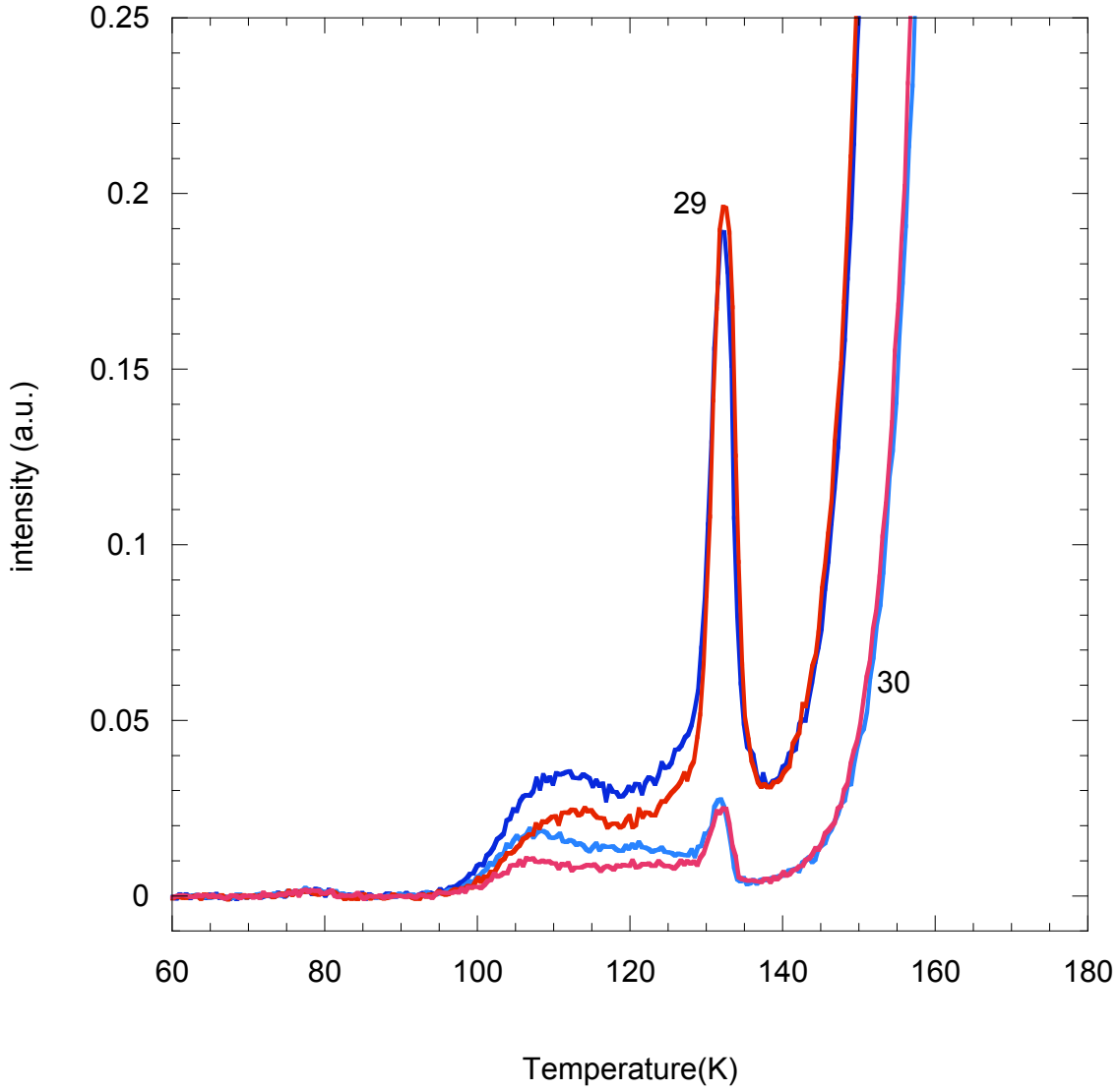

Figure 2.9: TPD products after irradiation of 30 ML CH_3OH at different temperatures. 30 ML CH_3OH were deposited and irradiated at either 25 K (blue) or 50 K (red) for 97 s. 100 eV electrons were used at a current of ~2μA. Little difference is observed in these signals (due to CH_2O; the CH_3OH signal is negligible at T < 40 K) due to their different growth and irradiation temperatures. The 29 and 30 amu peaks at ~135 K are also present when MeOH is irradiated at 80 K, but the peak present here at 110 K is absent.

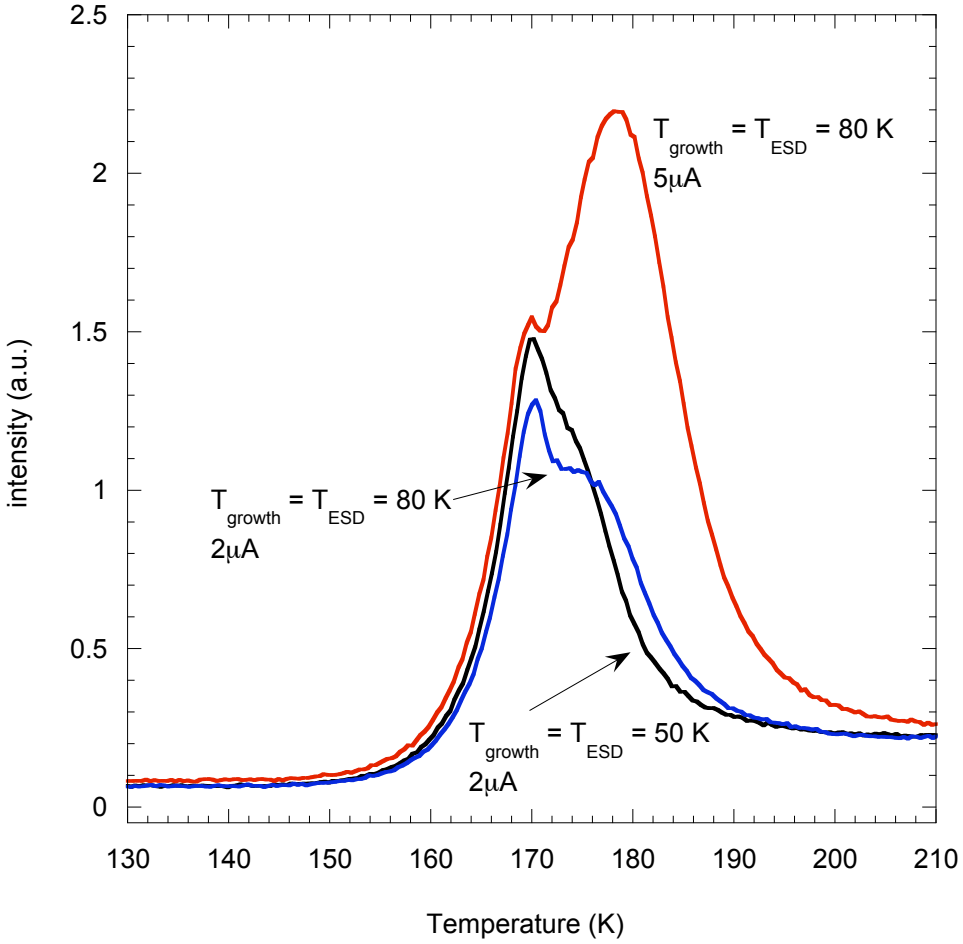

Figure 2.10: Increasing the irradiation temperature to 80K increases the pure water signal. 30 ML CH_3OH were deposited and irradiated at either 25 K (not shown), 50 K, or 80 K for 97 s. Little difference was observed in TPDs following irradiation at 25 and 50 K, so the 25 K signal is not included to increase clarity. Irradiations used 100 eV electrons at a current of either ~2μA or ~5μA, as indicated. Increasing the irradiation temperature from 50 K (black) to 80 K (blue), while holding the current constant, increased the high-temperature shoulder of the water signal associated with major water desorption. However, a much greater increase is seen when the electron current is raised (red). Increasing the current, and total energy deposited in the film, led to a large increase in the water signal, primarily at 180 K. Methanol desorbs at ~170 K while water in a pure water film and in later mixed films desorbs at higher temperatures. The growth in the 180 K peak suggests the formation of large quantities of H_2O during ESD.

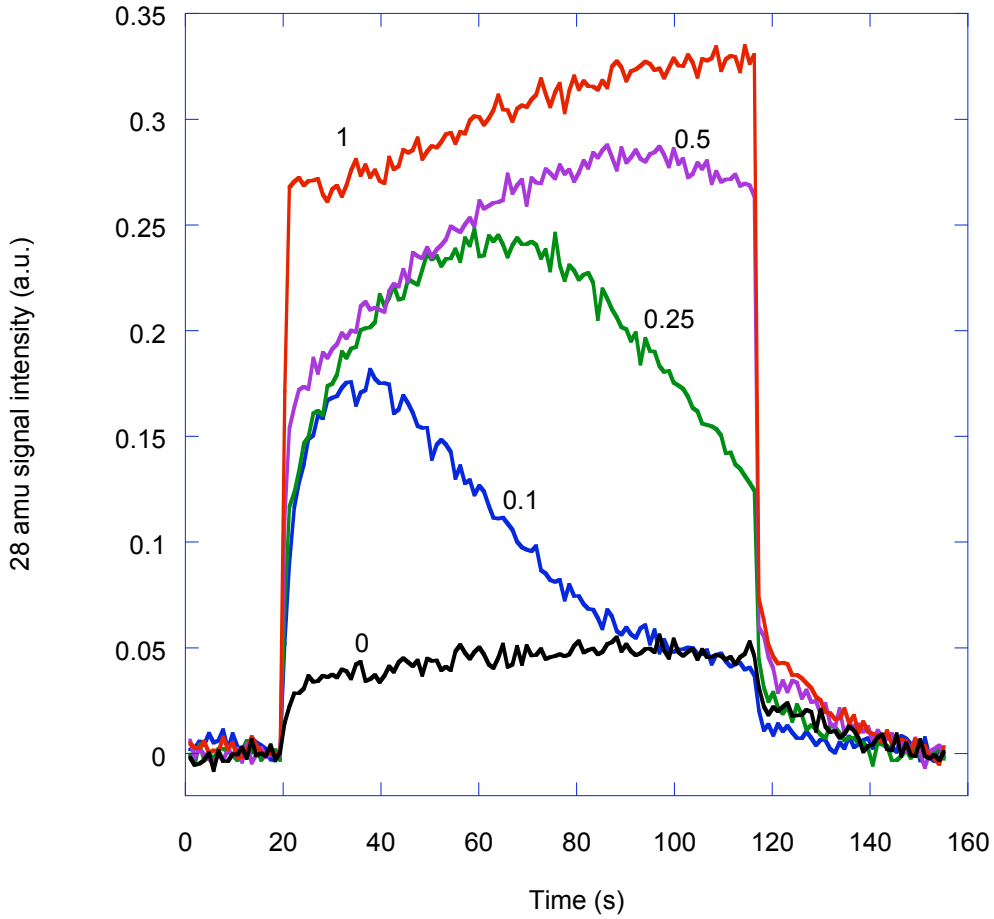

Figure 2.11: CO desorption during ESD from n ML CH_3OH on 80 ML H_2O. n ML CH_3OH were deposited at 80 K on 80 ML H_2O. The film was then irradiated beginning at 20 s and continuing until 117 s using 100 eV electrons at ~2μA current. Mass 28 was monitored to measure CO desorption. As more CH_3OH is deposited, the CO signal increases. At low coverages the CO signal rises and then drops off as the CH_3OH is consumed (for comparison, an examination of the O_2 signals from this film show that O_2 signals increase as the CO signals fall for coverages less than 0.5 ML CH_3OH). At coverages greater than 0.5 ML CH_3OH, the CO continues to rise with time as more CO is generated from the thicker CH_3OH layer (O_2 signals are not detected during the 97 s ESD in these films).

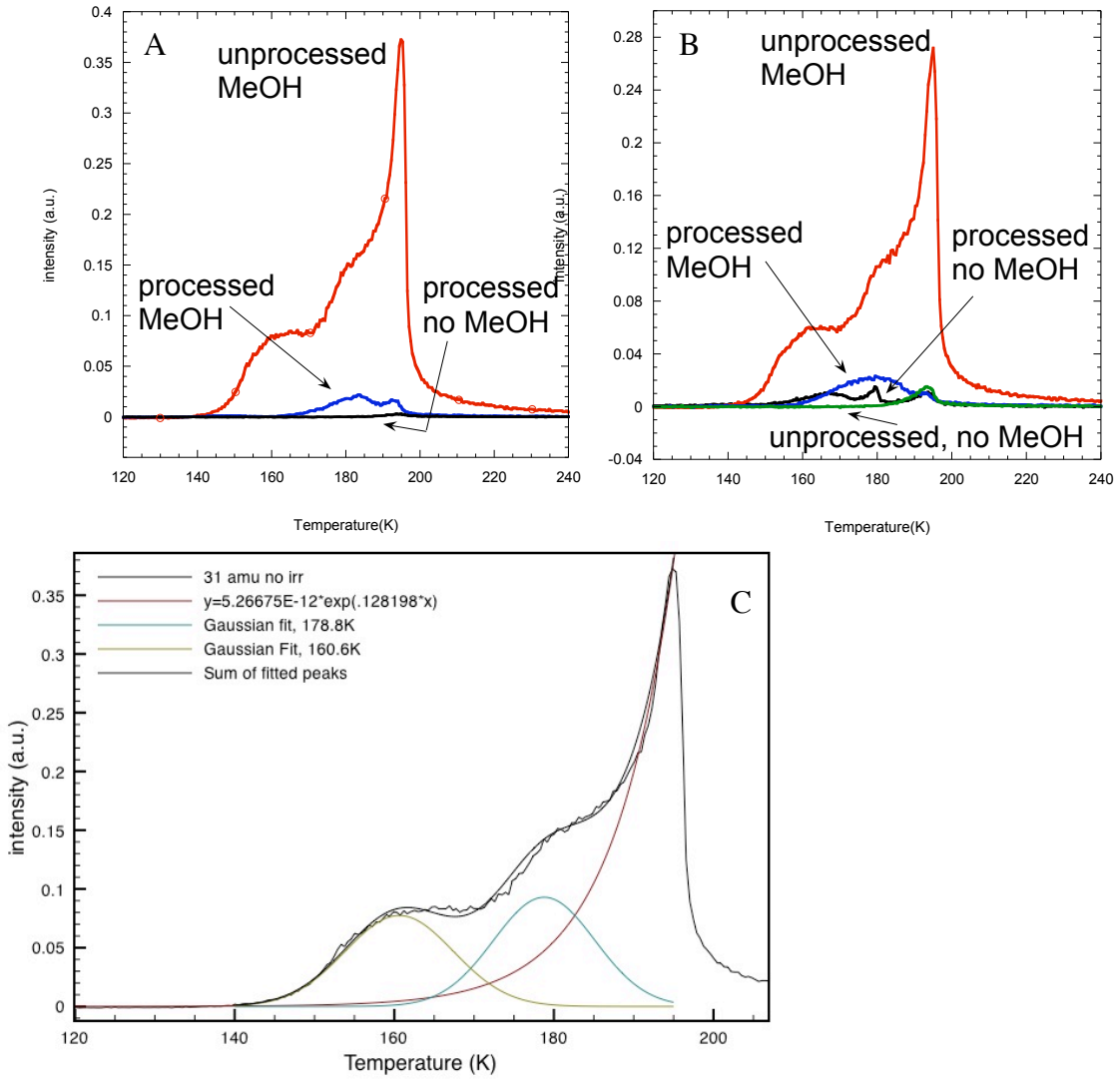

Figure 2.12: Methanol desorption from a water film before and after irradiation, compared to 31 amu (methanol, panel A) and 32 amu (methanol + O_2, panel B) signals from a pure water film. Films of 80 ML ASW ("no MeOH") and 1 ML CH_3OH on 80 ML ASW ("MeOH") were grown at 80 K. "Unprocessed" films were not irradiated; "processed" films were irradiated for 97 s using 100 eV electrons at ~2 μA current at 80 K. In pure water films, the 31 amu signal is negligible, but the 32 amu signal has a small peak in both processed and unprocessed films at ~193 K. Upon irradiation, two additional peaks appear in the pure water film at ~165K and 180K, the result of O_2 formation. In CH_3OH-capped films, the main effect of processing is the removal of methanol by desorption. Panel B shows that the addition of CH_3OH to the film eliminates the O_2 signal seen in processed pure water films. Panel C shows the deconvolution of the three peaks composing the methanol signal from an unprocessed 1 ML CH_3OH/80 ML ASW film.

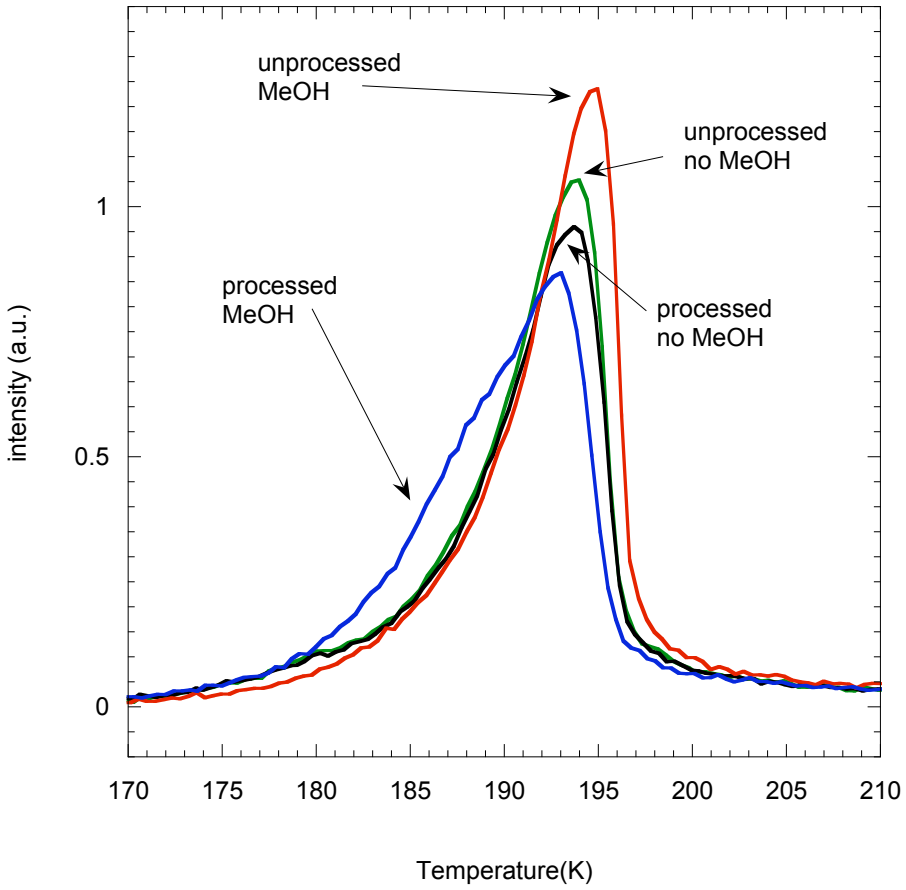

Figure 2.13: The addition of methanol to a water film creates additional atomic oxygen, detected in the TPD. Films of 80 ML ASW ("no MeOH") and 1 ML CH_3OH on 80 ML ASW ("MeOH") were grown at 80 K. "Unprocessed" films were not irradiated; "processed" films were irradiated for 97 s using 100 eV electrons at ~2 μA current at 80 K. The 16 amu signal shown above indicates that processed and unprocessed pure water films and unprocessed CH_3OH/H_2O films produce similar quantities of O. Processed CH_3OH-capped films produce additional O (not CH_4, as the 15 amu signal is very small) at ~185 K.

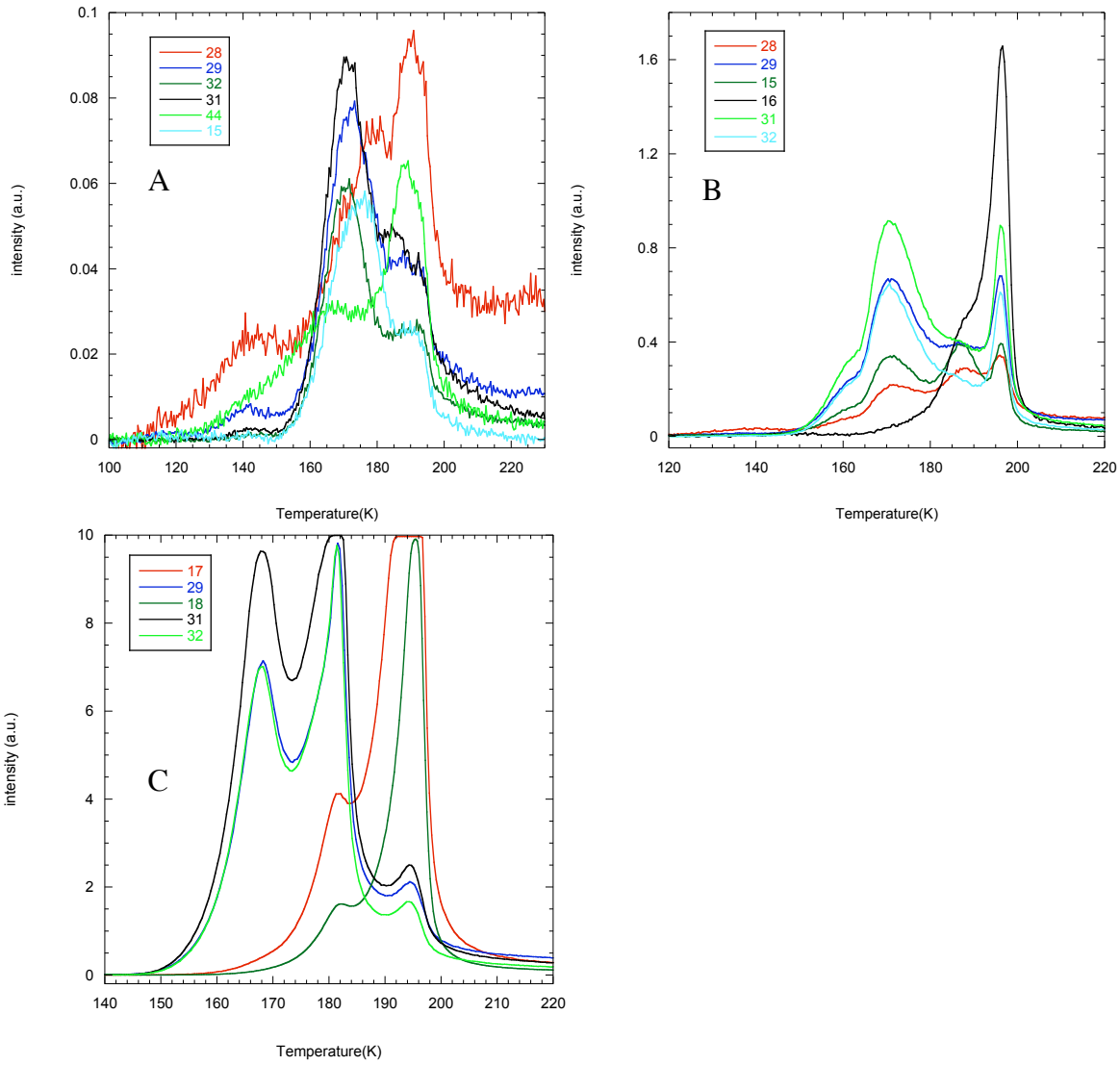

Figure 2.14: Major TPD peaks of a) 4 ML b) 10 ML and c) 30 ML CH_3OH on 80 ML ASW after irradiation. Films of a)4 ML CH_3OH b)10 ML CH_3OH and c) 30 ML CH_3OH were grown atop 80 ML H_2O at 80 K. The films were irradiated at 80 K using 100 eV electrons at a current of ~5μA for 97 s. Major TPD peaks of each film are shown above and discussed in the text.

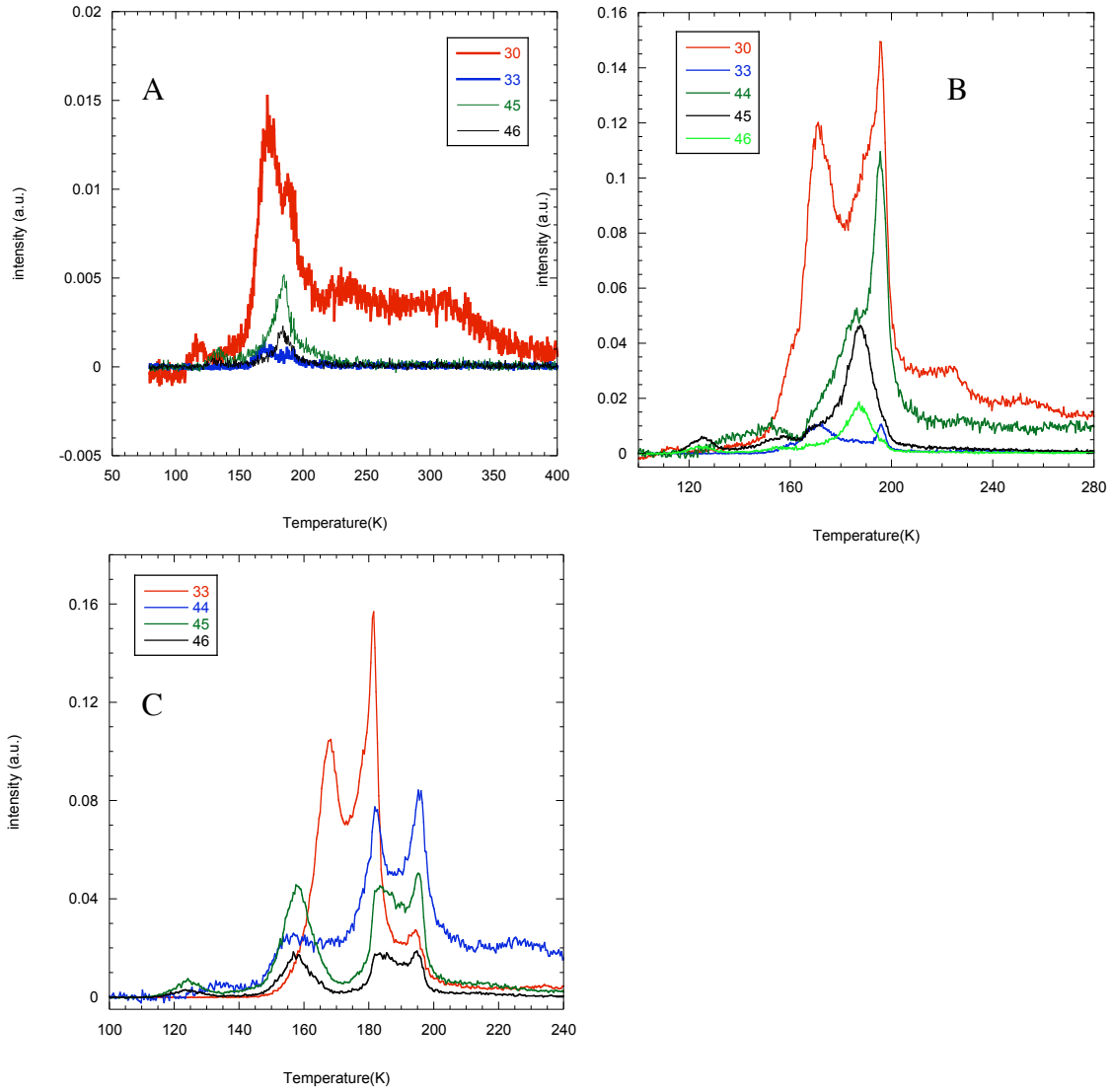

Figure 2.15: Minor TPDs of a) 4 ML b) 10 ML and c) 30 ML CH_3OH on 80 ML ASW after irradiation. Films of a) 4 ML CH_3OH b) 10 ML CH_3OH and c) 30 ML CH_3OH were grown atop 80 ML H_2O at 80 K. The films were irradiated at 80 K using 100 eV electrons at a current of ~5μA for 97 s.

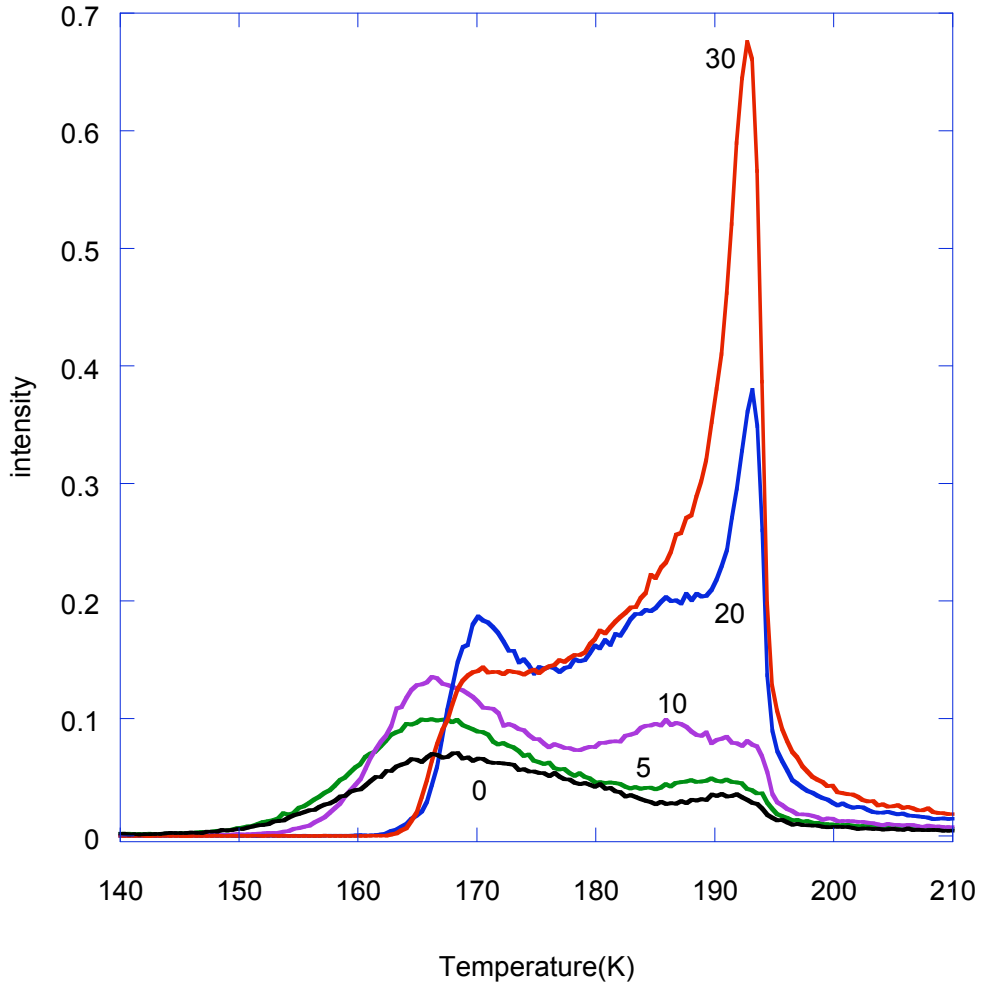

Figure 2.16: 31 amu TPD from selected sandwich films. *n* ML H_2O were deposited atop 1 ML CH_3OH on 80-*n* ML H_2O at 25 K. The film was then irradiated at 25 K for 97 s using 100 eV electrons at ~2μA before the TPD shown above was collected. As the capping water layer thickens, methanol desorption is delayed. No change in methanol desorption is observed for $n \leq 2$ ML H_2O.

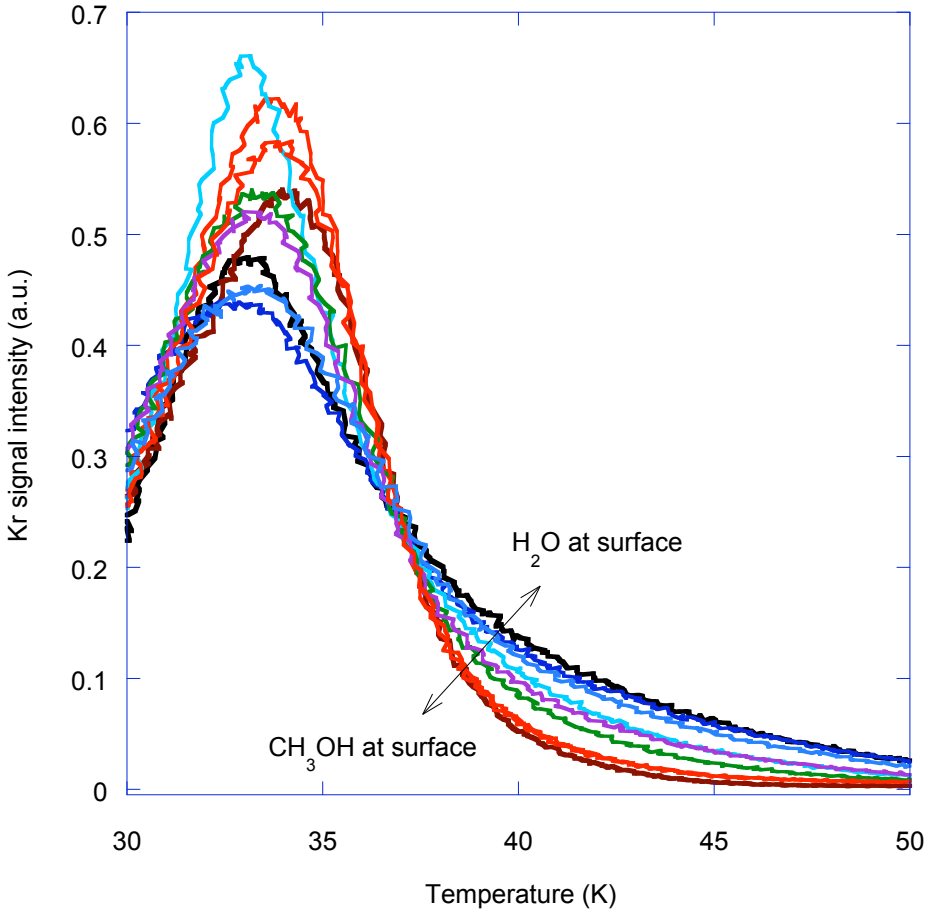

Figure 2.17: Surface area measurements using Kr. Various films were prepared at 80 K prior to being dosed with Kr at T less than 30 K. While there is no clear trend in the Kr desorption signals at T less than 37 K, at T greater than 37 K an increased surface concentration of water correlates to a longer retention of Kr. Pure water (black) and pure methanol (maroon) films show the greatest difference at T greater than 37 K. Methanol capped films are shown in red (1 ML CH_3OH cap) and purple (0.5 ML CH_3OH cap). *n* ML H_2O/ 1 ML CH_3OH/ 80-*n* ML H_2O sandwich films were also grown at 80 K, where the effects of surfaction should leave decreasing amounts of CH_3OH at the surface as *n* increases; these films are shown in blue, with a darker color blue corresponding to a thicker capping water film (10, 6, and 4 ML H_2O). An additional sandwich film of 2 ML H_2O/ 1 ML CH_3OH/ 78 ML H_2O was grown under the same conditions and is shown in green. Note that the 0.5 ML CH_3OH/H_2O capped film (purple) shows very similar desorption characteristics at T greater than 37 K to the $n = 2$ and $n = 4$ sandwich films.

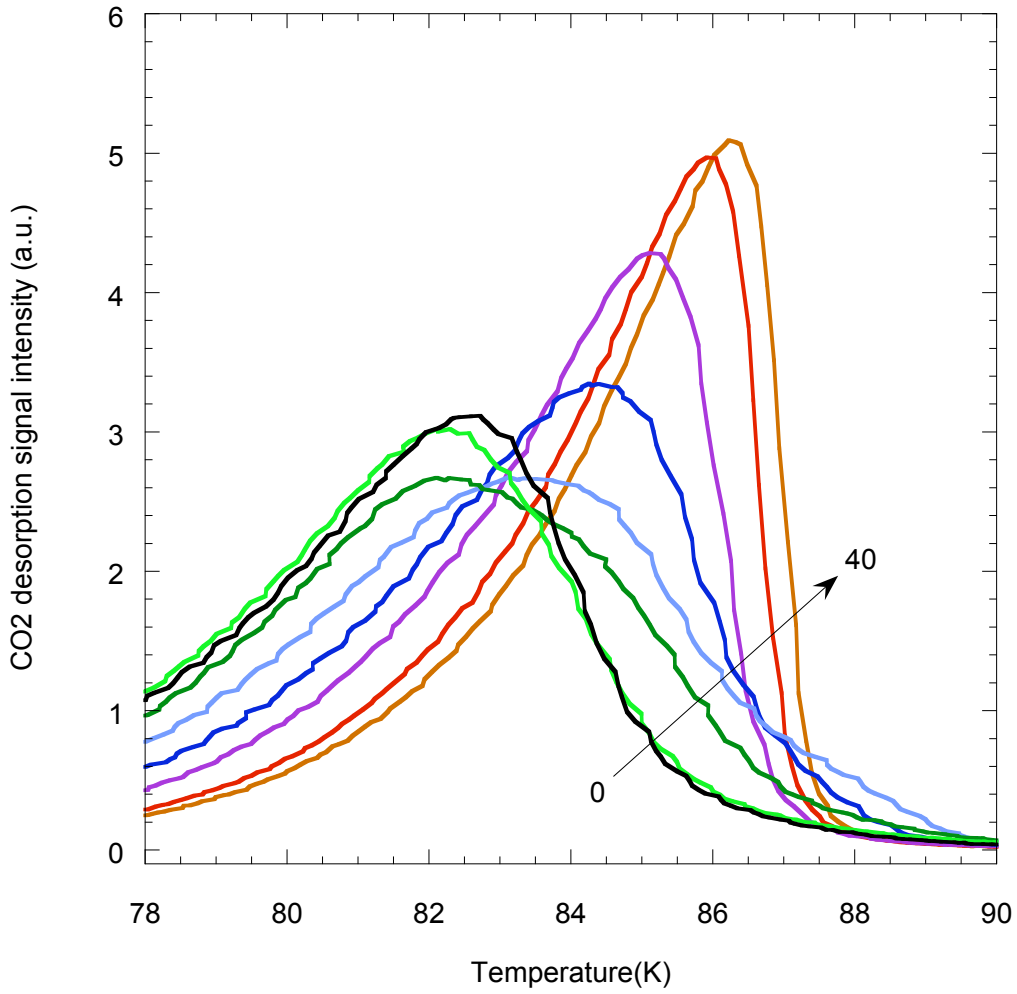

Figure 2.18: CO_2 surface area measurements. Sandwich films of *n* ML H_2O / 1 ML CH_3OH/80-*n* ML H_2O were grown at 80 K and then exposed to 120 torr s of CO_2 at 21 K. The desorption signal of CO_2 was then measured. Values of *n* shown above include [0, 1, 5, 10, 15, 20, 30, and 40]. Because of surfaction, sandwiches with thinner water capping layers have increased surface concentrations of methanol. These films do not retain CO_2 as long as the water-rich surfaces, similar to the Kr desorption completion seen in Figure 2.17.

Table 2.3: Pure methanol TPD products

Pure methanol, unprocessed:

Peak Temperature (K)	Species
172	CH_3OH
315	unassigned
550	CH_2O

Pure methanol, processed, 20eV, 2μA:

Peak Temperature (K)	Species
170	CH_3OH, CH_2O
109,128	CH_4, CH_3OCH_3
550	H_2CO
650	C_2H_4

Pure methanol, processed, 100eV, 5μA:

Peak Temperature (K)	Species
170	CH_3OH, CH_2O
125	CH_3OCH_3
139	CH_4, CO, CO_2, CH_3OOCH_3, plus CH_3CH_2OH *
153	$(CH_2OH)_2$
180, 232, 480	H_2O
585	Unassigned
610	unassigned

*Ethanol is the presumed fifth source. On the basis of cracking patterns alone, a combination of C_2H_6 + HCOOH + $(CH_2OH)_2$ or C_2H_6+ CH_3OCH_3 + $(CH_2OH)_2$ fits as well as ethanol, but is treated as less likely since three species must form instead of one.

Table 2.4: TPD products, methanol-capped films:

1 ML Methanol –capped water films, unprocessed:

Peak Temperature (K)	Species
195	H_2O + entrained CH_3OH
161	CH_3OH
179	$CH_3OH + H_2O$
340	CH_3OH

1 ML Methanol-capped water films, processed, 100eV, ~2μA:

Peak Temperature (K)	Species
193	H_2O + residual CH_3OH
180	$CH_3OH + H_2O$
187	O
265	CH_2O
315	$CH_3OH + CH_2O$
625	C_2H_6

4, 10, and 30 ML Methanol-capped water films, processed, 100eV, ~5μA:

Peak Temperature (K)	Species
195	H_2O + residual CH_3OH, CO, CO_2
170[A]	CH_3OH, H_2O, CO, CO_2
160[A]	CH_3OH, CO, CO_2
187[B]	$CH_3OH + H_2O$, CH_3CH_2OH, CH_3OCH_3
125[C]	CH_3OCH_3
158[D]	unassigned
265	CH_2O
315	$CH_3OH + CH_2O$
625	C_2H_6

[A] This peak shifts to higher temperatures by ~10K with increasing CH_3OH dose.
[B] Not present at 4 ML CH_3OH dose, this peak appears to be the result of methanol radiatively mixed with water plus trace amounts of either ethanol or dimethyl ether.
[C] Not present at 4 ML CH_3OH dose.
[D] Present at 30 ML CH_3OH dose. Likely due to either ethanol or dimethyl ether.

Table 2.5: TPD products, sandwich films:

Sandwich films: n ML H_2O/1 ML CH_3OH/80-n ML H_2O/TiO_2 (110), processed, 100eV, ~2μA:

Peak Temperature (K)	Species
193	Water + CH_3OH
170[E]	CH_3OH, H2O
270	CH_2O
550	O_2
90[F]	Unassigned
130[F]	Unassigned
160[F]	Unassigned

[E] As the water capping layer increases in thickness, this peak shifts from 165 to 170 K.
[F] trace quantities.

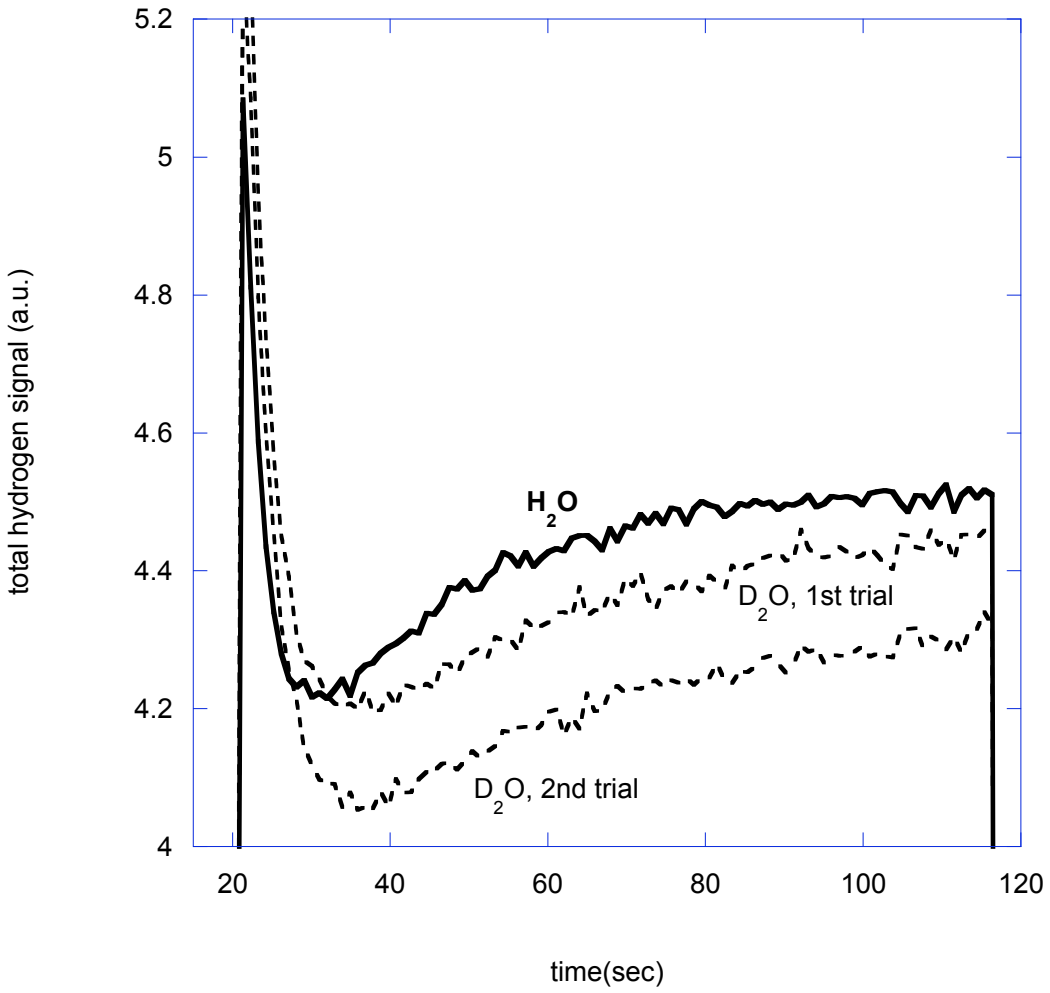

Figure 3.1: Hydrogen production from H_2O and D_2O is similar. 100 ML H_2O and D_2O films were irradiated beginning at 20 s and continuing until 117 s. Irradiation was performed at 80 K using 100 eV electrons at ~2μA current. Masses 2, 3, and 4 were measured. Using the relative sensitivities of $S_{H2} = 1$, $S_{HD} = 1.52$, and $S_{D2} = 2.04$, the total hydrogen produced from the films was calculated (as described in the text). The total hydrogen signal from D_2O and H_2O are shown above for comparison. There is a 5-10% difference between the summed D_2O signals and the H_2O signal. The difference seen in the two D_2O signals is largly due to changes in the background H_2 level during the two experiments, and is the same size as the differences seen between trials for the same reason.

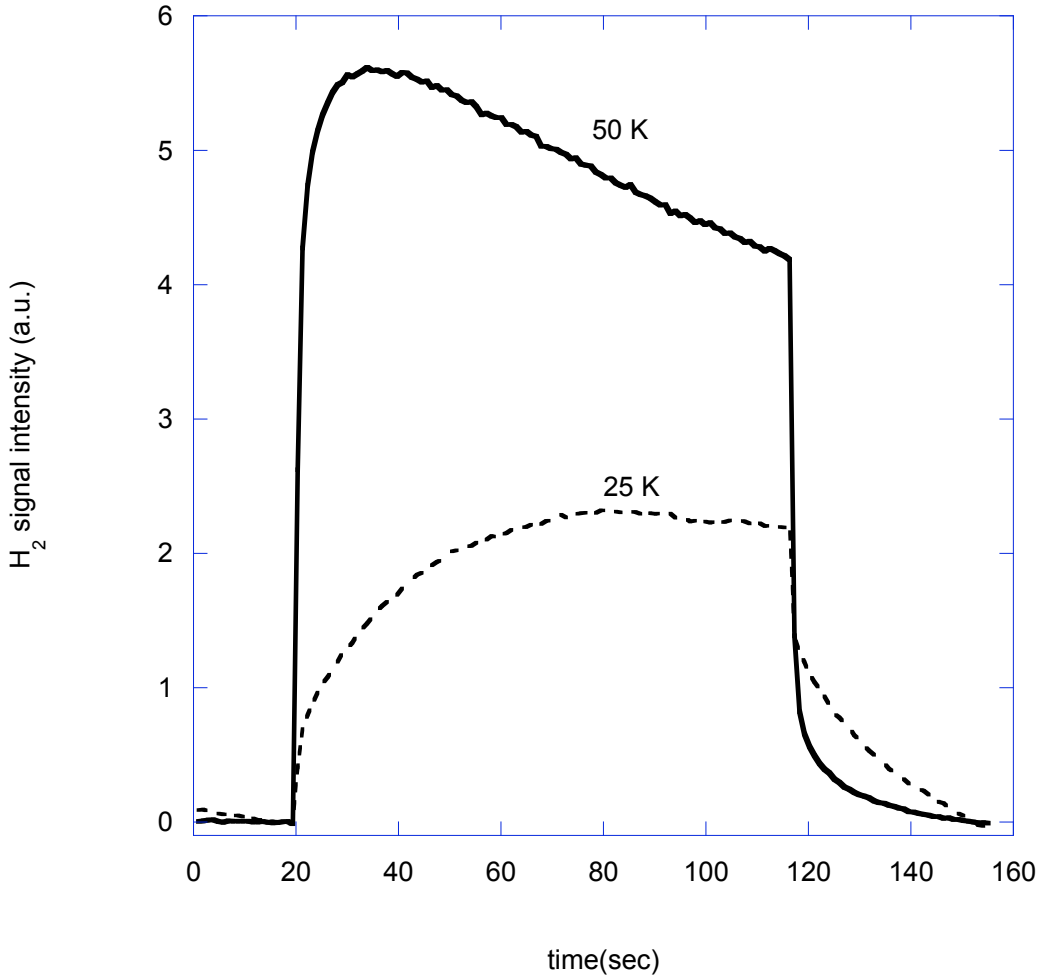

Figure 3.2: Temperature affects H_2 formation and desorption from CH_3OH. 30 ML CH_3OH were dosed and irradiated ($T_{dose} = T_{irr}$) at 25 K and 50 K to determine the effects of temperature upon the H_2 ESD signal. The films were irradiated beginning at 20 s and continuing until 117 s using 100 eV electrons at a current of ~2μA. Significantly more H_2 is produced during ESD at higher temperatures.

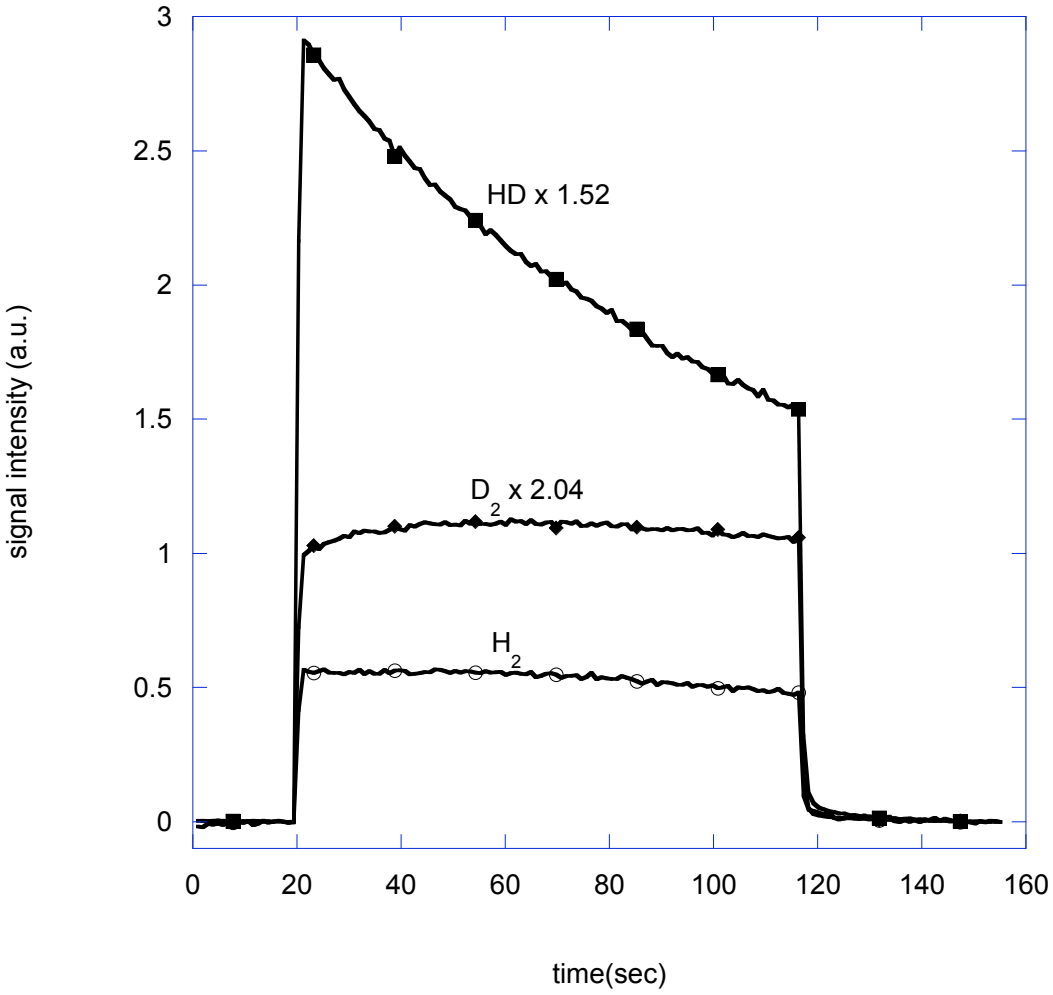

Figure 3.3: Molecular hydrogen isotopologues desorbing from CD_3OH. 10 ML CD_3OH were deposited and irradiated at 80 K. Irradiation began at 20 s and continued until 117 s, using 100 eV electrons at a current of ~2 μA. Signal intensities for H_2, HD, and D_2 were measured during irradiation. HD and D_2 signals are corrected for decreased QMS sensitivity by scaling using sensitivity factors of 1.52 and 2.04 respectively.

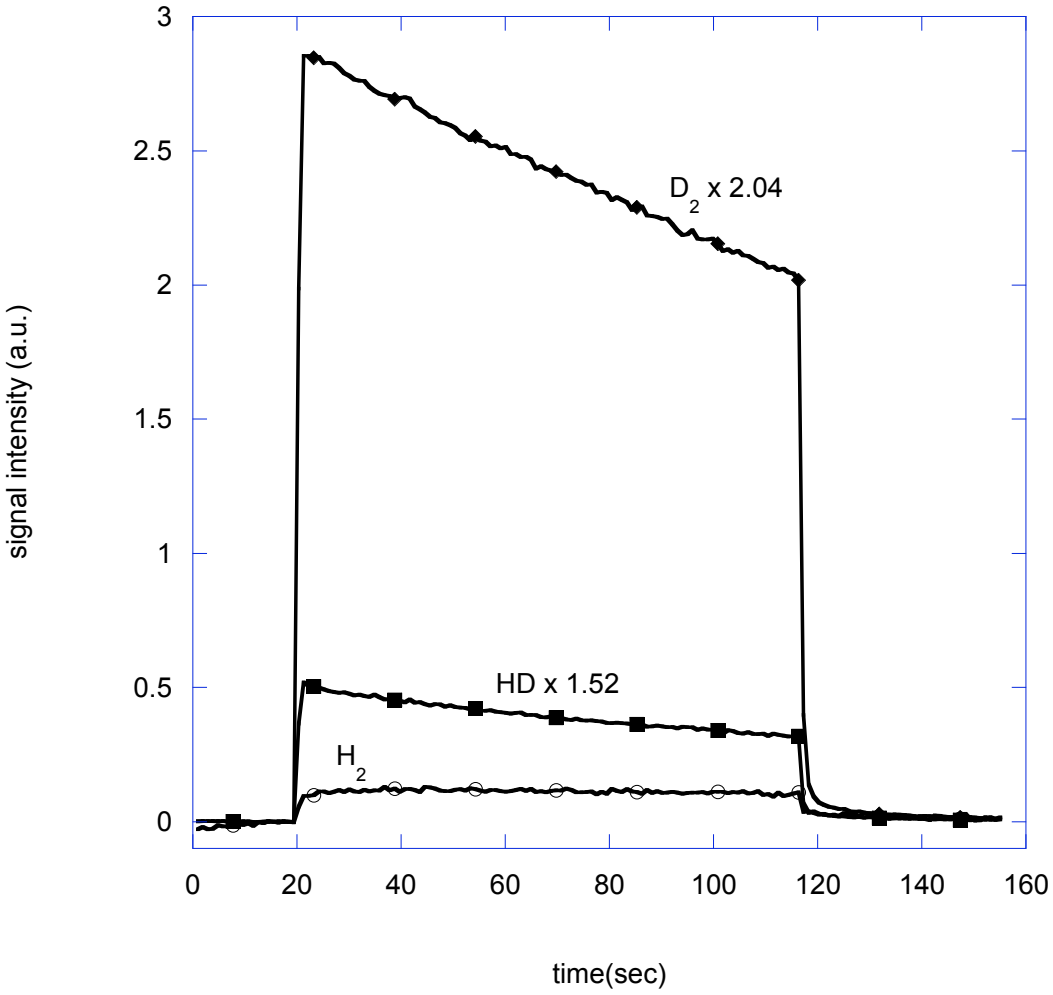

Figure 3.4: Molecular hydrogen isotopologues desorbing from CD_3OD. 10 ML CD_3OD were deposited and irradiated at 80 K. Irradiation began at 20 s and continued until 117 s, using 100 eV electrons at a current of ~2 μA. Signal intensities for H_2, HD, and D_2 were measured during irradiation. HD and D_2 signals are corrected for decreased QMS sensitivity by scaling using sensitivity factors of 1.52 and 2.04 respectively.

Table 3.1: Sources of hydrogen species from each isotopologue of methanol

	CH_3OH	CD_3OH	CD_3OD
H_2	$^{m}H_2$, $^{a}H_2$, $^{m}H^{a}H$, $^{m}H^{c}H$, $^{a}H^{c}H$, background	$^{a}H_2$,$^{a}H^{c}H$, background	background
HD	Background (minimal)	$^{m}D^{a}H$, $^{m}D^{c}H$	$^{m}D^{c}H$, $^{a}D^{c}H$
D_2	none	$^{m}D_2$	$^{m}D_2$, $^{a}D_2$, $^{m}D^{a}D$

^{m}H = methyl hydrogen

^{a}H = alcoholic hydrogen

^{c}H = hydrogen adsorbed to chamber walls

^{m}D = methyl deuterium

^{a}D = alcoholic deuterium

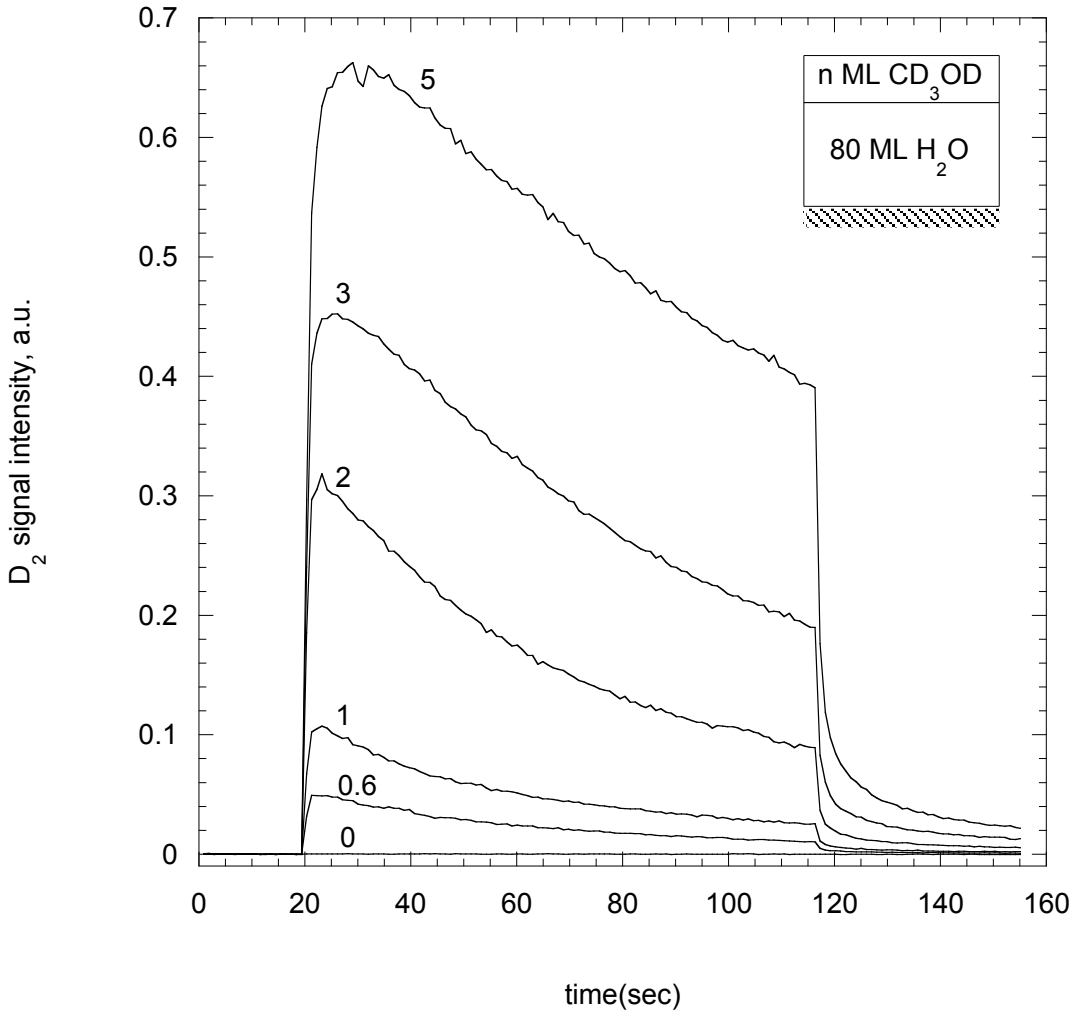

Figure 3.5: D_2 produced in methanol (CD_3OD) layer. *n* ML CD_3OD were deposited on 80 ML H_2O at 50 K. The film was irradiated at 50 K and the D_2 signal monitored, beginning at 20 s and continuing until 117 s, using 100 eV electrons at a current of ~2 μA. D_2 appears promptly with the onset of the impinging electrons. Selected doses are shown above; as CD_3OD dose increased, the D_2 signal also rose. Note: as these are all D_2 signals with equal sensitivities, they have not been corrected for decreased QMS sensitivity to D_2 .

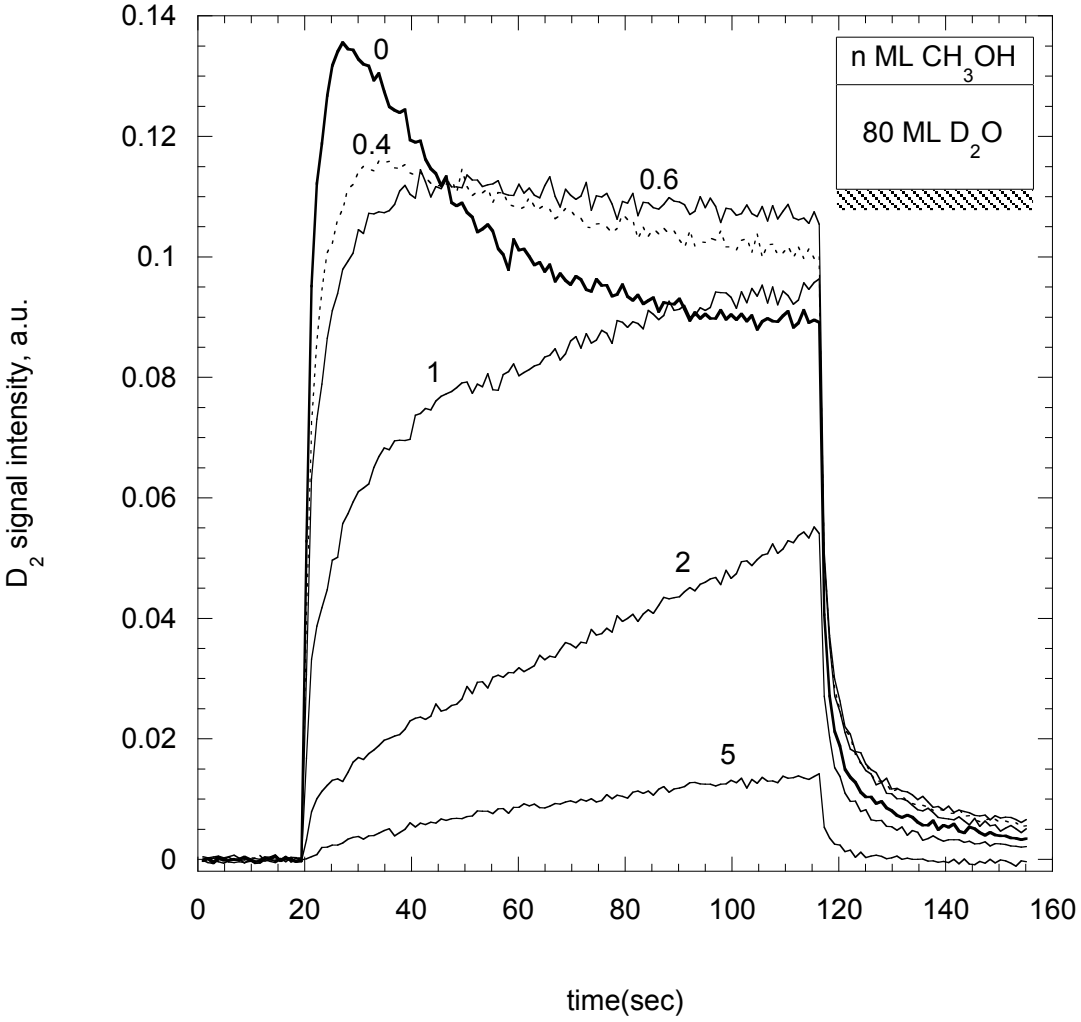

Figure 3.6: D_2 produced from water beneath a methanol cap. *n* ML CH_3OH were deposited on 80 ML D_2O at 50 K. The film was irradiated at 50 K and the D_2 signal monitored, beginning at 20 s and continuing until 117 s, using 100 eV electrons at a current of ~2 μA. Selected doses are shown above. D_2 appears promptly with the onset of the impinging electrons in the pure D_2O film. As CD_3OD coverage increased, the prompt D_2 signal decreased. While the late D_2 signal increased at low coverages of CH_3OH, at coverages greater than 0.6 ML it is reduced. Note: as these are all D_2 signals with equal sensitivities, they have not been corrected for decreased QMS sensitivity to D_2.

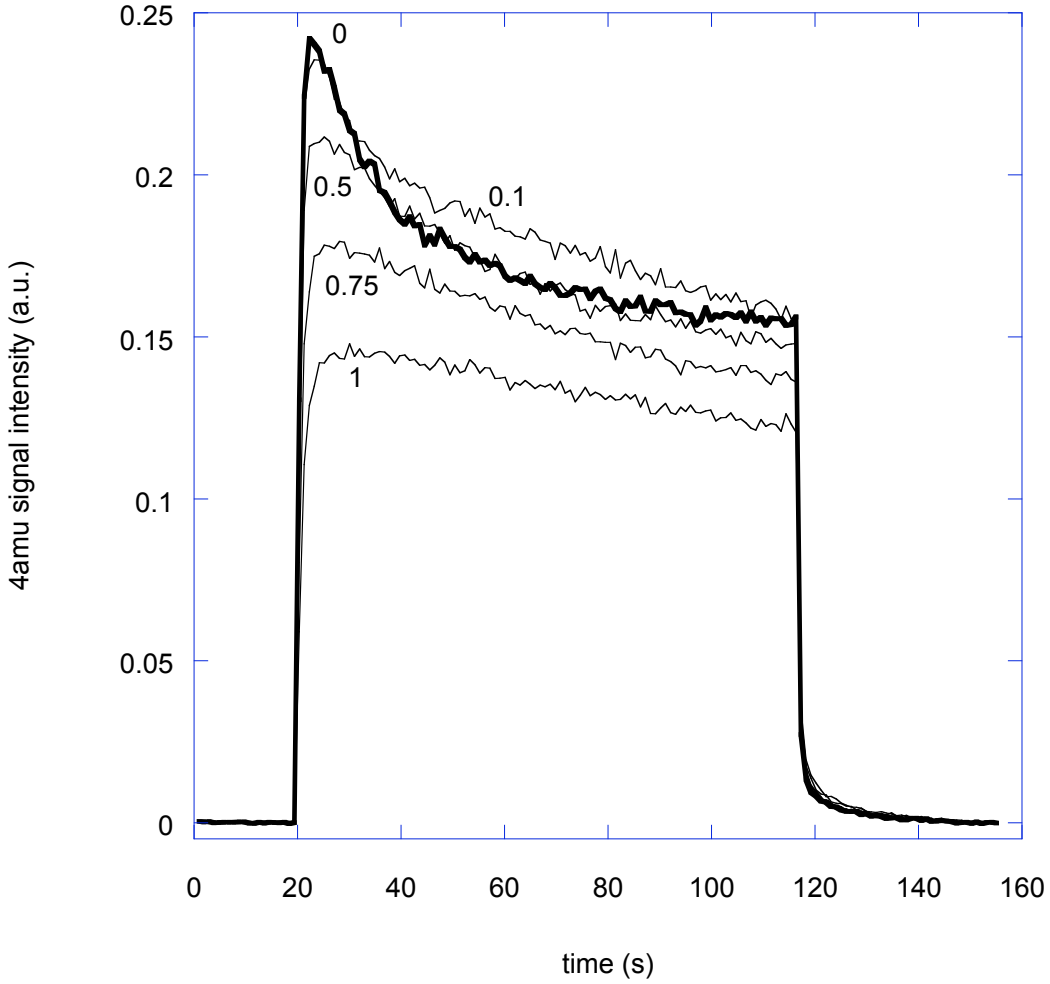

Figure 3.7: The addition of CH_3OH to the surface of D_2O inhibits D_2 formation. *n* ML CH_3OH were deposited at 50 K on 20 ML D_2O over 60 ML H_2O. The film was irradiated at 80 K and the D_2 signal monitored, beginning at 20 s and continuing until 117 s, using 100 eV electrons at a current of ~2 μA. D_2 appears promptly with the onset of the impinging electrons in the pure D_2O film. As CD_3OD coverage increased, the D_2 signal decreased, in agreement with CH_3OH blocking D_2O desorption and/or excitation. Note: as these are all D_2 signals with equal sensitivities, they have not been corrected for decreased QMS sensitivity to D_2.

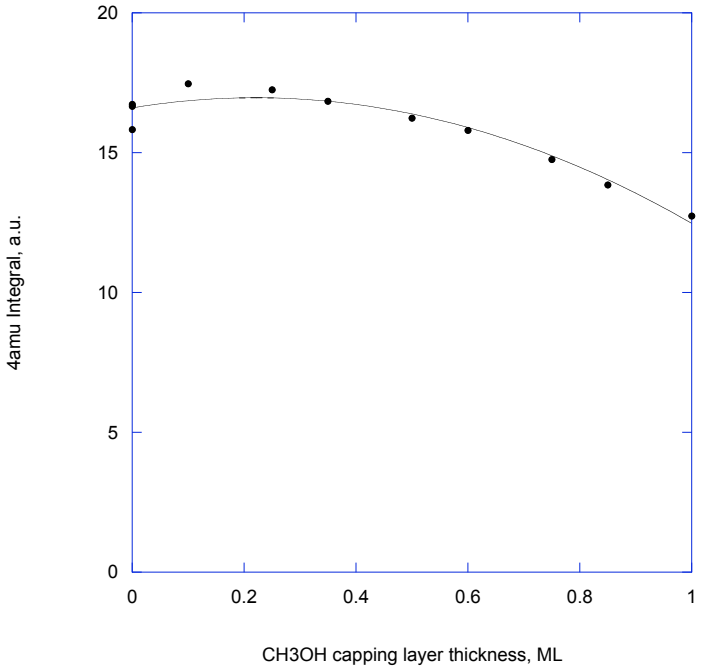

Figure 3.8: Integral of D_2 signal showing reduction of D_2 production by CH_3OH. *n* ML CH_3OH were deposited at 50 K on 20 ML D_2O over 60 ML H_2O. The film was irradiated for 97 s at 80 K using 100 eV electrons at a current of ~2 μA, and the D_2 signal monitored. The D_2 signal was integrated over the 97 s irradiation exposure to determine total D_2 produced. While very small quantities of CH_3OH (0.1 to 0.35 ML) appear to slightly increase the amount of D_2 produced compared to a methanol-free film, larger doses steadily decrease the D_2 produced, with the addition of 1 ML CH_3OH reducing the signal by ~24%.

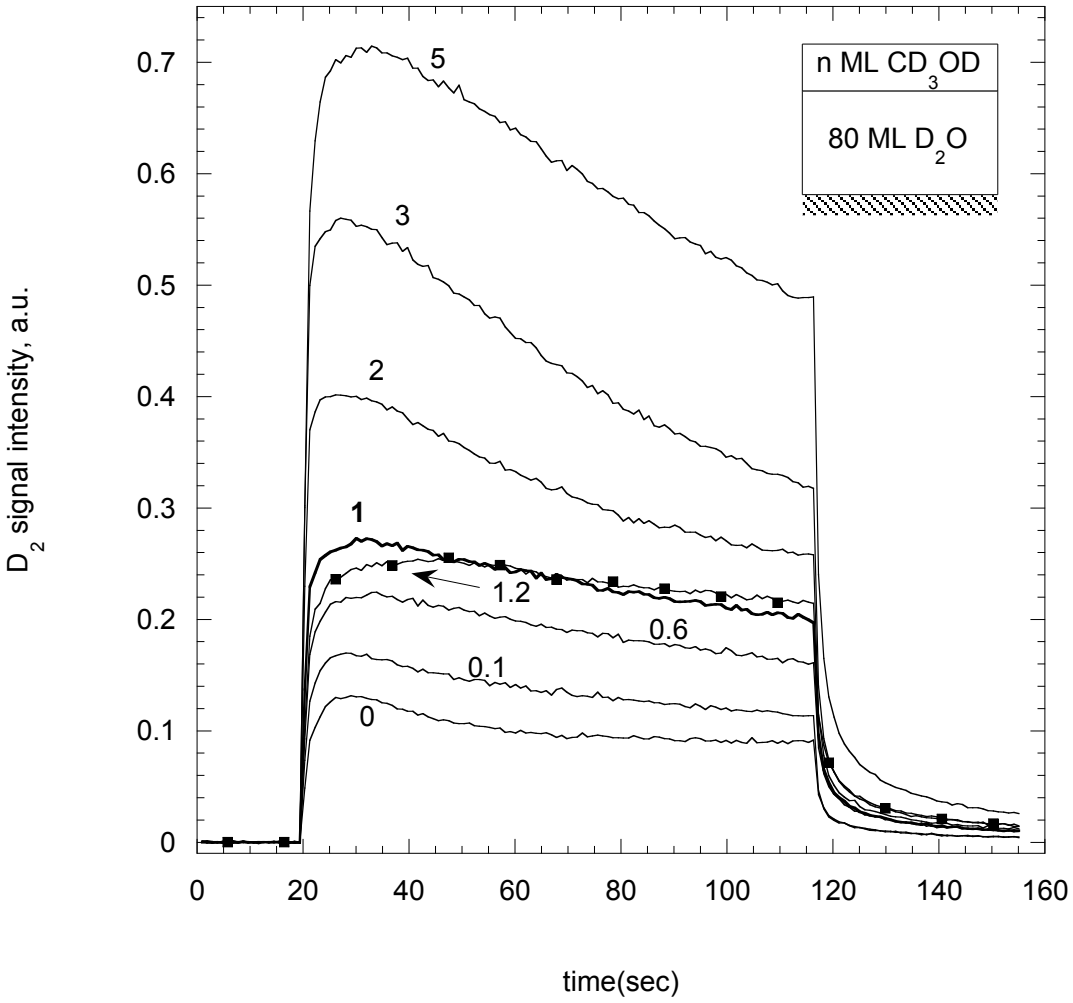

Figure 3.9: D_2 produced during ESD of CD_3OD on D_2O. *n* ML CD_3OD were deposited at 50 K on 80 ML D_2O. The film was irradiated at 80 K using 100 eV electrons at a current of ~2 μA, beginning at 20 s and continuing until 117 s, and the D_2 signal monitored. Selected doses are shown above. As the CD_3OD coverage increased, the total D_2 signal also increased. Note that because these are all D_2 signals, they have not been corrected for QMS sensitivity.

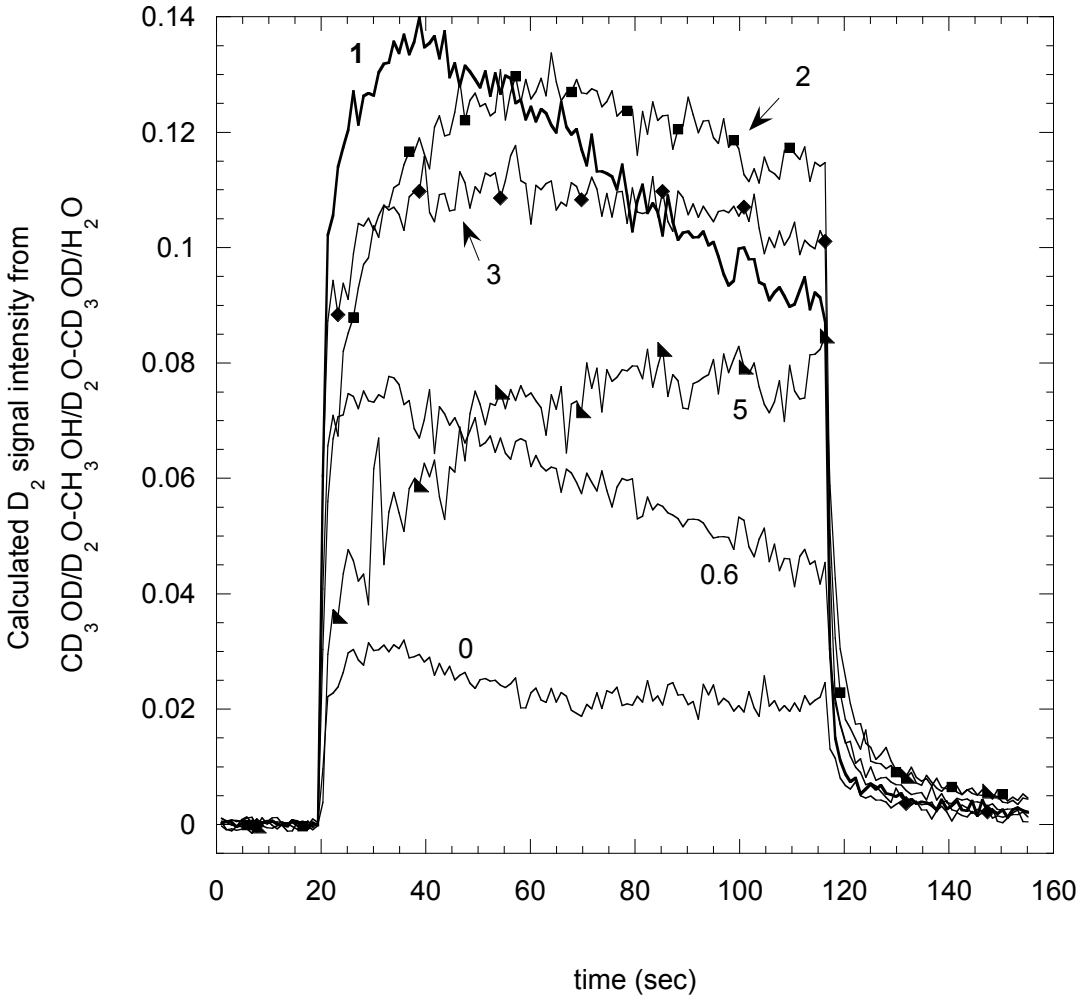

Figure 3.10: D_2 produced at the methanol/water interface. *n* ML methanol were deposited at 50 K on 80 ML water using different isotopologues: CD_3OD/H_2O, CH_3OH/D_2O, and CD_3OD/D_2O. The films were irradiated at 50 K using 100 eV electrons at a current of ~2 μA, beginning at 20 s and continuing until 117 s, and the D_2 signal monitored in each case. The D_2 signals from CH_3OH/D_2O and CD_3OD/H_2O were subtracted from the D_2 signal from CD_3OD/D_2O to determine the D_2 produced at the methanol/water interface. Selected coverages are shown above. This interfacially produced D_2 appears to peak when there is ~1 ML methanol at the water surface, where the water/methanol interface is maximized and receives a high electron flux. Note that because these are all D_2 signals, they have not been corrected for QMS sensitivity.

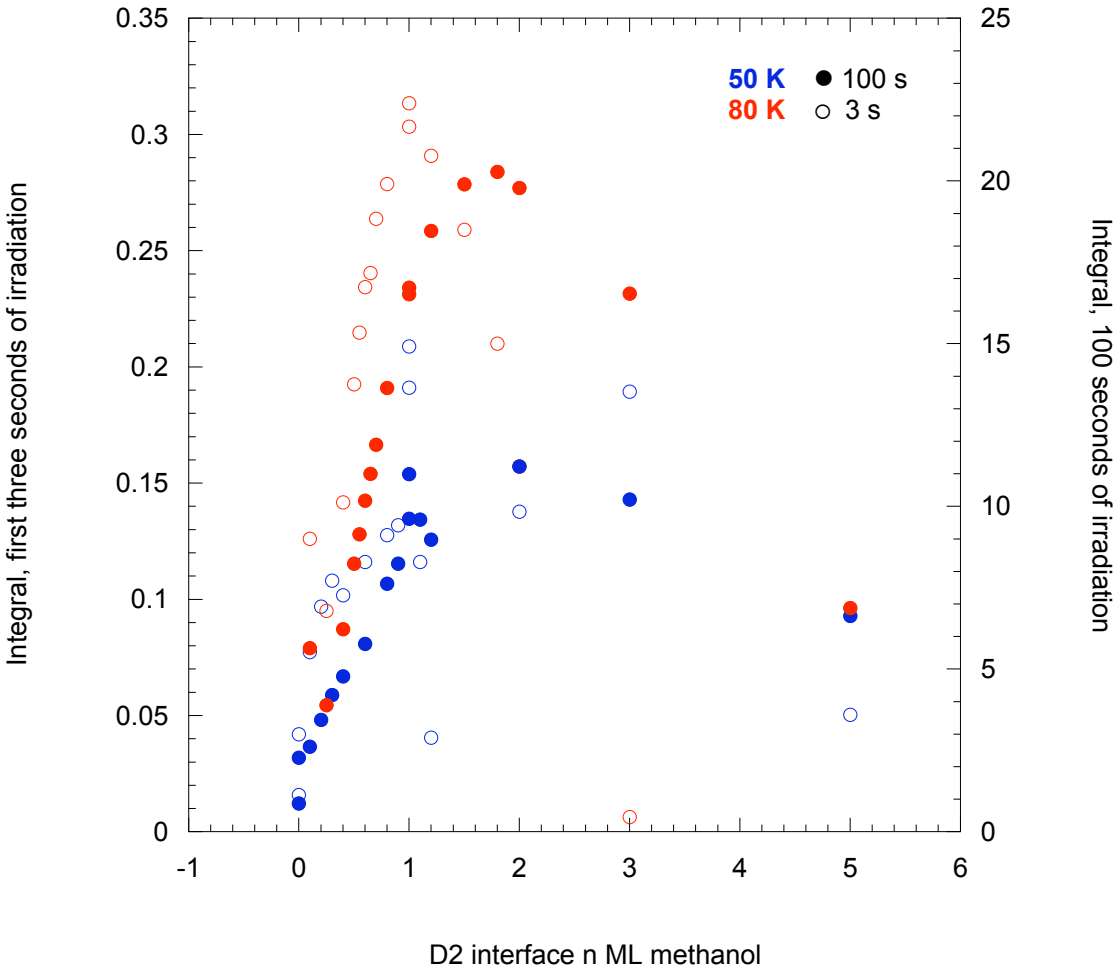

Figure 3.11: Integrals of D_2 produced at methanol/water interface, peaking at ~1 ML methanol coverage. *n* ML methanol were deposited and irradiated at either 50 K (blue) or 80 K (red) on 80 ML water using different isotopologues: CD_3OD/H_2O, CH_3OH/D_2O, and CD_3OD/D_2O. The films were irradiated at both temperatures for 97 s with 100 eV electrons at a current of ~2 μA, and the D_2 signal monitored in each case. The D_2 signals from CH_3OH/D_2O and CD_3OD/H_2O were subtracted from the D_2 signal from CD_3OD/D_2O to determine the D_2 produced at the methanol/water interface. This interfacially produced D_2 signal was integrated over two time ranges: the first 3 s of irradiation, to determine initial production dependencies, and the full 97 s exposure, to determine how additional processes such as mixing affect the yield. In the non-mixed regime, interfacial D_2 yield peaks at 1 ML methanol coverage. When longer integration ranges are used to include mixing effects, the peak occurs at ~2 ML methanol, indicating that as the second monolayer is mixed it continues to react. At the highest coverages (5 ML) little interfacial D_2 is produced, as methanolic hydrogen production dominates over these time scales and the methanol/water interface receives less energy. However, if the exposure time was extended, the effects of mixing at the increasingly buried methanol/water interface (under thicker methanol capping layers) could be studied.

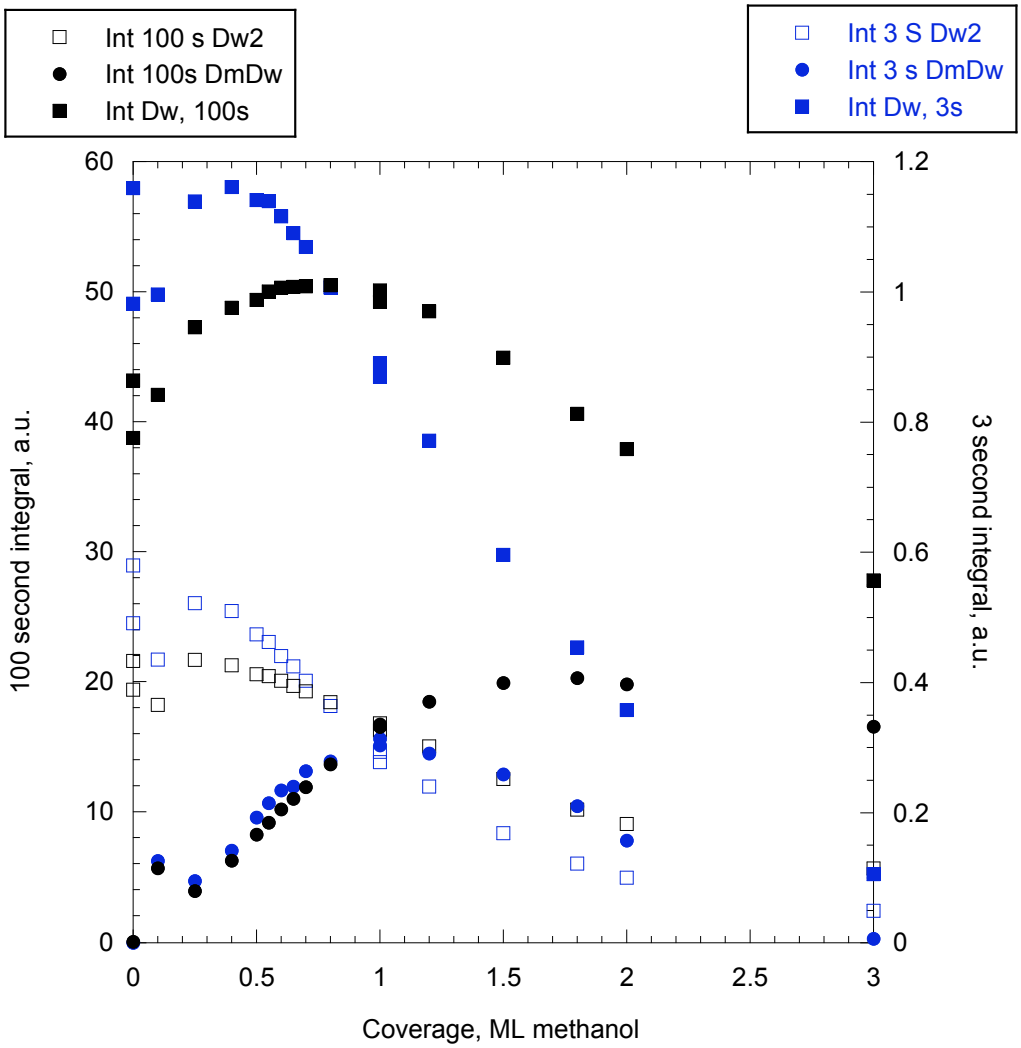

Figure 3.12: The addition of methanol can increase the availability of D in water to form D_2. *n* ML methanol were deposited and irradiated at 80 K on 80 ML water using different isotopologues: CD_3OD/H_2O, CH_3OH/D_2O, and CD_3OD/D_2O. The films were irradiated at 80 K for 97 s with 100 eV electrons at a current of ~2 μA. The contribution of D from water (D_w) was calculated by adding twice the D_2 signal from CH_3OH/D_2O to the interfacial D_2 signal (D_mD_w) discussed in the previous two figures. The total D_w contribution is compared to that from a pure D_2O signal over two integration ranges: the first 3 s of irradiation (initial reactions, and no mixing effects), and 97 s (which includes some mixing effects). Although the peak D_w contribution occurs at different methanol coverages due to mixing during the 97 s integration, in both cases the addition of small quantities of methanol increases the D_w contribution. Similar results were seen when the experiment was repeated at 50 K.

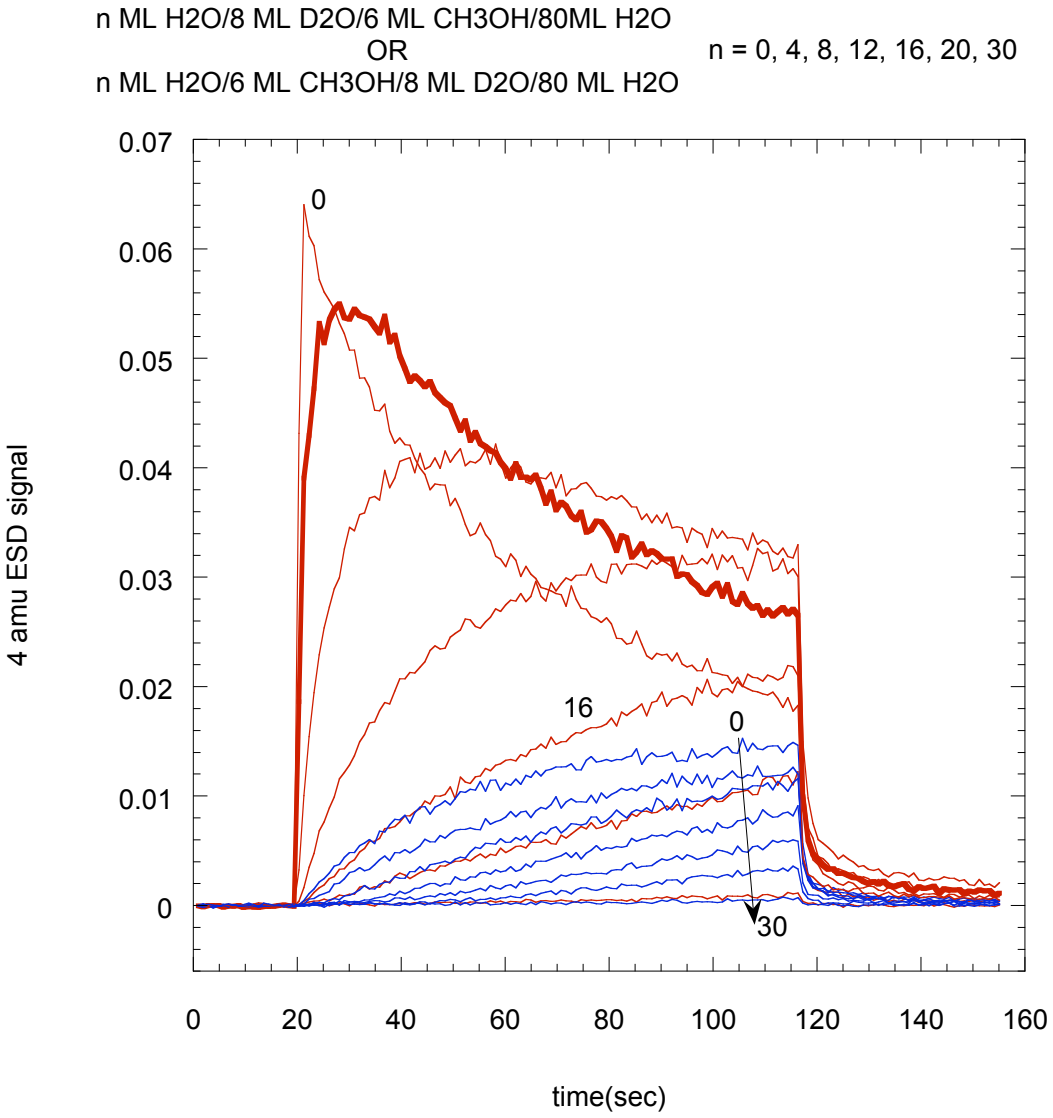

Figure 3.13: Methanol is a more efficient suppressant than H_2O of D_2 production from D_2O. Two sandwich structured films were grown at 50 K: *n* ML H_2O / 6 M CH_3OH / 8 ML D_2O / 80 ML H_2O/ TiO_2 (blue) and *n* ML H_2O / 8 ML D_2O / 6 M CH_3OH / 80 ML H_2O / TiO_2 (red). The films were irradiated at 50 K beginning at 20 s and continuing until 117 s using 100 eV electrons at a current of ~2μA. The D_2 signal was measured during the ESD. While the addition of any methanol delays and decreases D_2 production, placing the methanol between the D_2O and the water/vacuum interface is much more effective, as seen by the greater suppression of D_2O by 6 ML CH_3OH than by 16 ML H_2O. The difference in blocking of D_2 by CH_3OH and H_2O is less prominent as the capping layer thickness increases and the D_2 signal approaches zero.

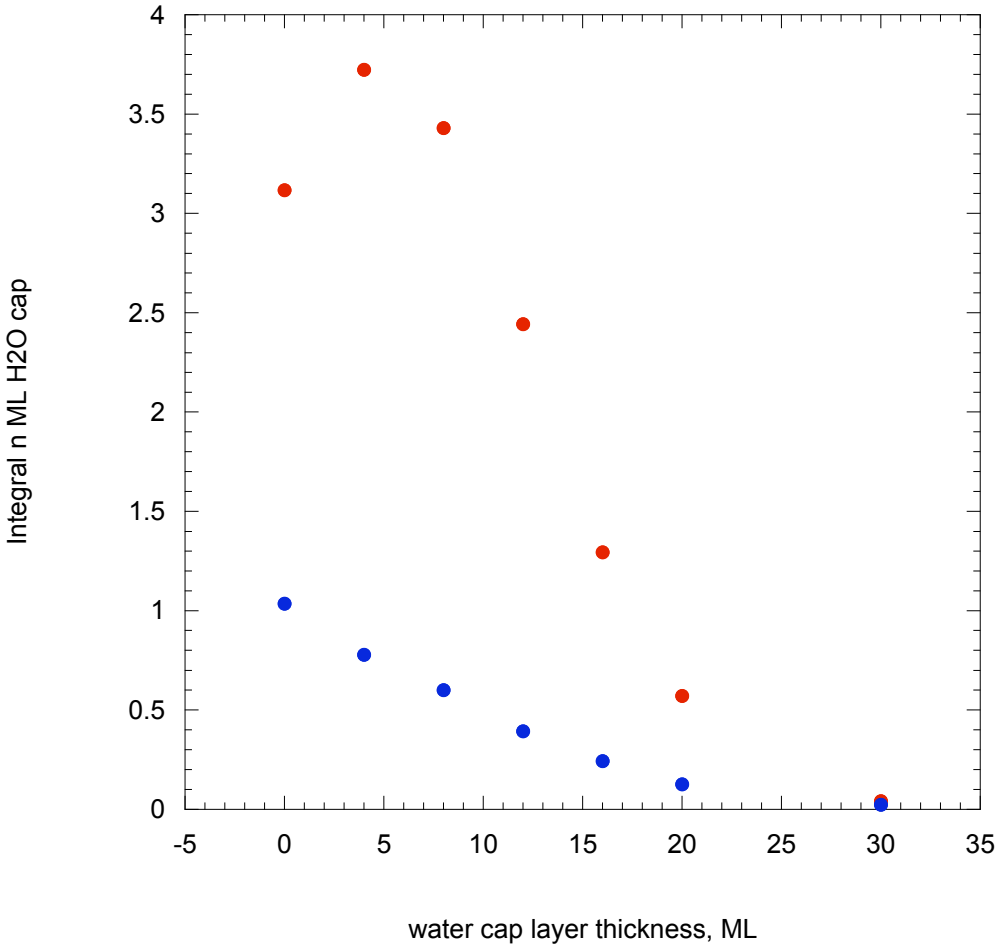

Figure 3.14: Total D_2 production from D_2O decreases greatly when the capping layer includes CH_3OH. Two sandwich structured films were grown at 50 K: *n* ML H_2O / 6 M CH_3OH / 8 ML D_2O / 80 ML H_2O/ TiO_2 (blue) and *n* ML H_2O / 8 ML D_2O / 6 M CH_3OH / 80 ML H_2O / TiO_2 (red). The films were irradiated at 50 K beginning at 20 s and continuing until 117 s using 100 eV electrons at a current of ~2μA. The D_2 signal was measured during the ESD. The integrals of the D_2 produced from each film during irradiation are shown above. If any D_2 is produced beneath the methanol layer, very little of it is able to escape through the methanol to be detected.

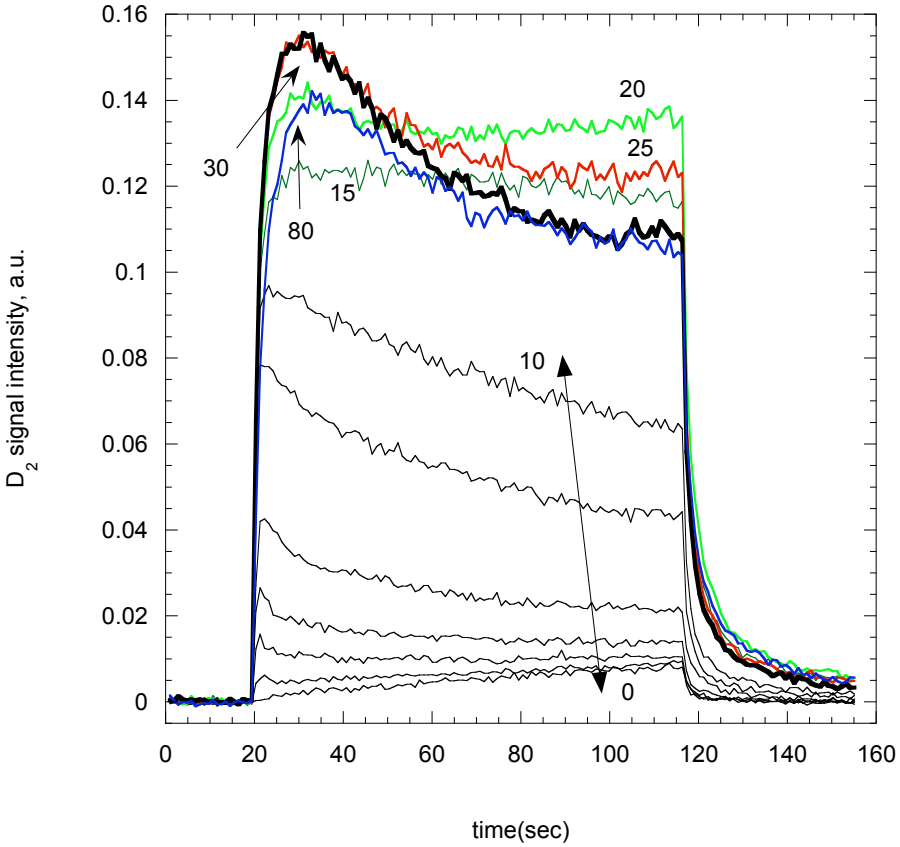

Figure 3.15: Methanol may act as an internal interface. Sandwich structures of *n* ML D_2O / 6 ML CH_3OH / 80-*n* ML D_2O were grown and irradiated at 50 K. Irradiation began at 20 s and continued until 117 s using 100 eV electrons at a current of ~2μA. The D_2 signal was measured during the ESD. In the $n = 0$ case, the D_2 signal rises with time as the CH_3OH desorbs. Increasing the capping thickness of D_2O up to 30 ML increases the prompt D_2 signal (due to D_2 produced at the vacuum interface), with the prompt signal beginning to saturate at $n = 17$ ML and decreasing once *n* is greater than 30 ML. A similar pattern is seen in the late D_2 signal, which results from D_2 produced deeper in the film and peaks around $n = 20$. Methanol capped by more than ~30 ML D_2O appears to have little effect on the D_2 yield.

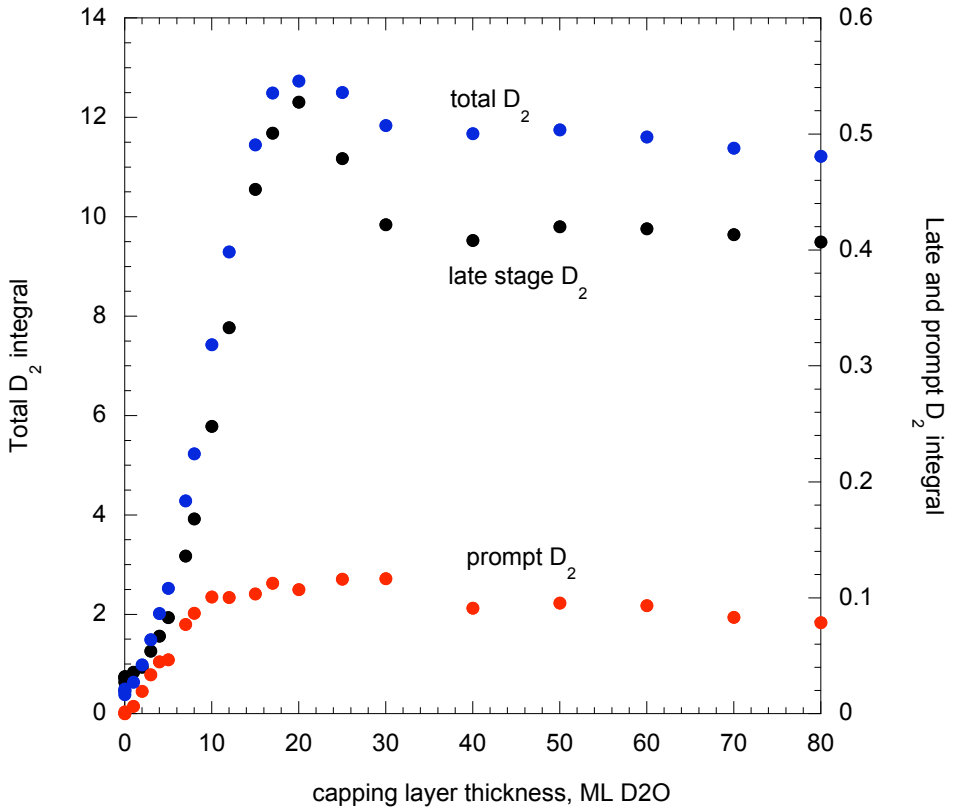

Figure 3.16: Saturation of D_2 production. Sandwich structures of *n* ML D_2O / 6 ML CH_3OH / 80-*n* ML D_2O were grown and irradiated at 50 K. Irradiation exposure was 97 s using 100 eV electrons at a current of ~2μA. The D_2 signal was measured during the ESD and integrated over three ranges: the first 3 s of exposure, representing prompt D_2 production, which occurs at the vacuum interface; the last 5 s of exposure, representing D_2 production saturation and D_2 produced deeper in the film, which includes mixing effects; and the full irradiation cycle (97 s) to consider total D_2 production. Prompt D_2 production quickly saturates at *n* = 10 ML. Late and total production both peak at *n* = 20 ML and decrease to *n* = 30 ML after which they saturate.

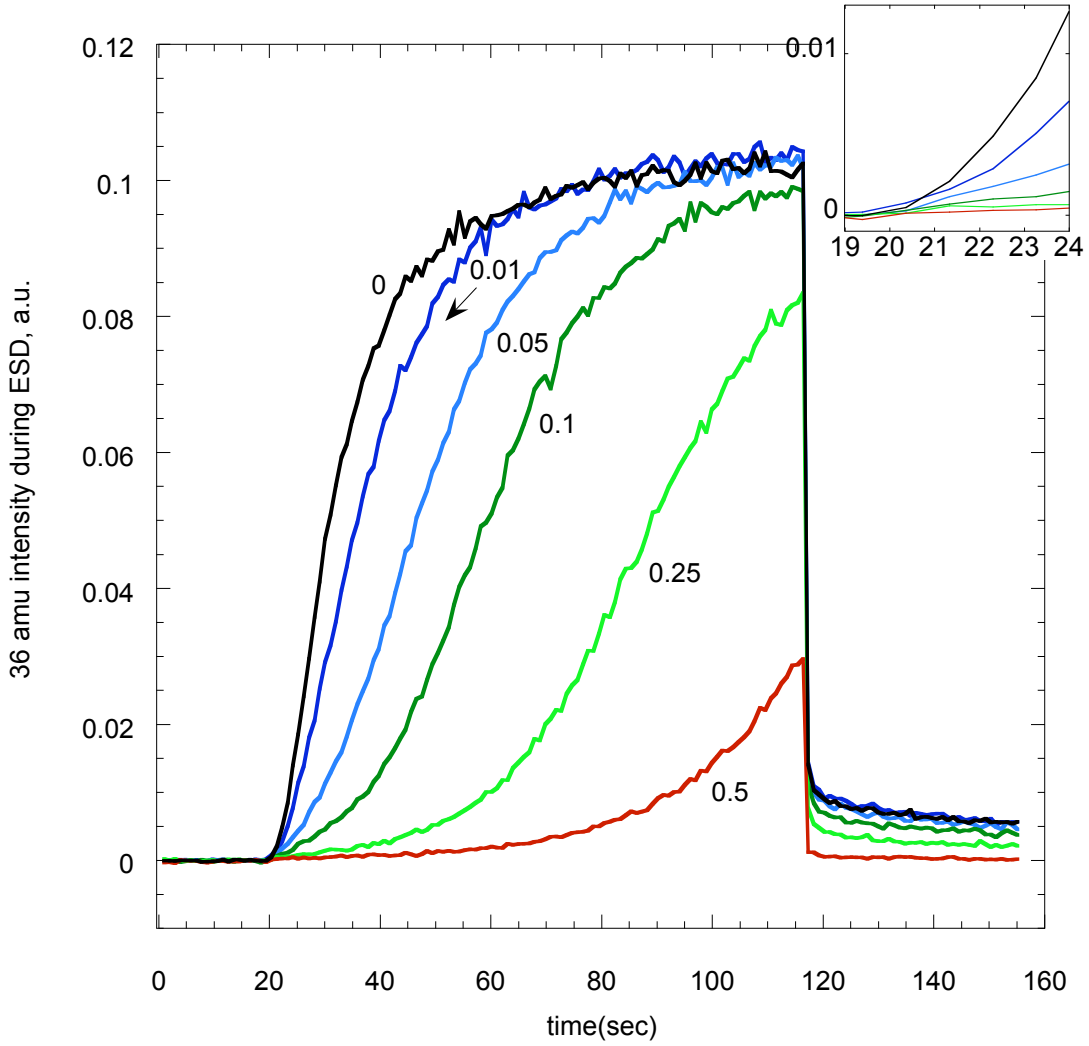

Figure 4.1: Suppression of O_2 production by CH_3OH capping layer. n ML of CH_3OH were deposited on 80 ML unprocessed $H_2{}^{18}O$ in the structure shown below. The film was grown and irradiated at 80 K, with irradiation beginning at 20s and ending at 117s. The $^{18}O_2$ signal was monitored during ESD. The addition of small quantities of methanol reduces the O_2 signal from water. **Inset:** An expanded view of the $^{18}O_2$ signals during the first four seconds of irradiation.

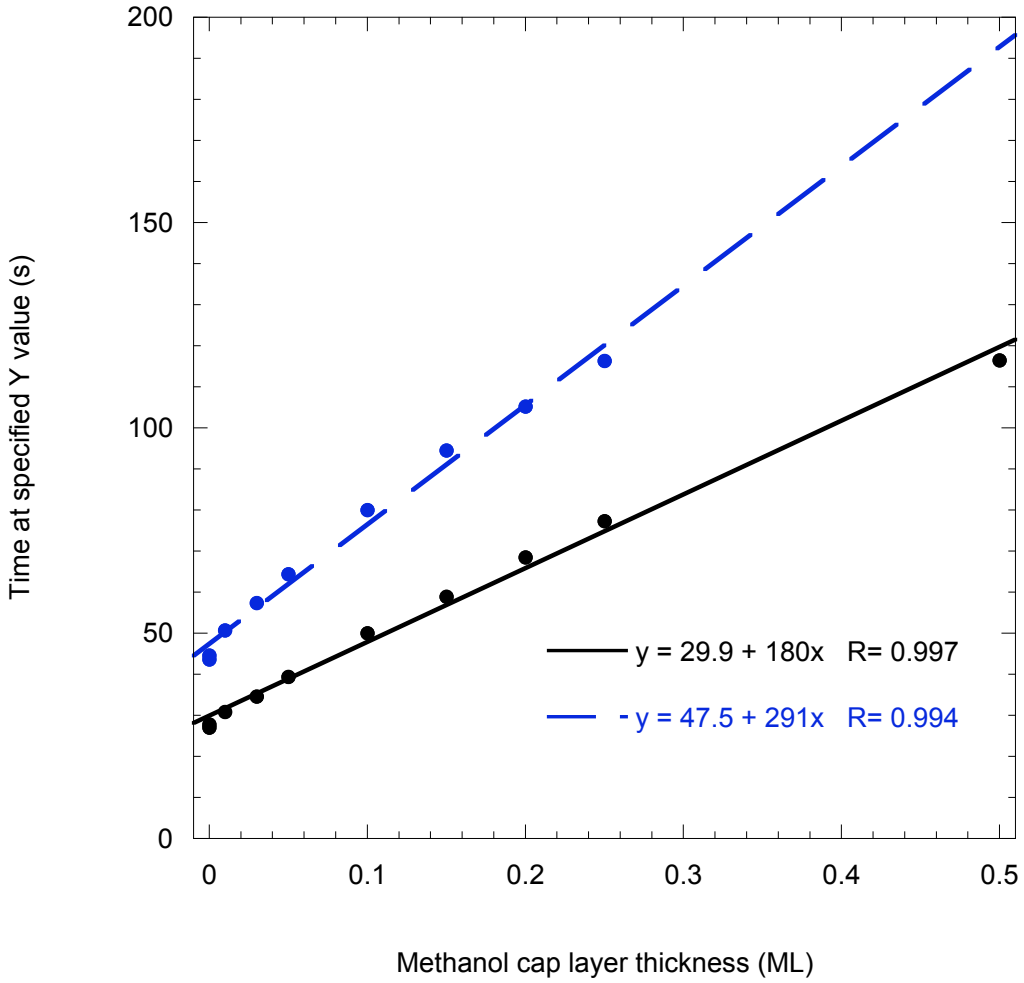

Figure 4.2: Time delay in O_2 production caused by methanol. n ML of CH_3OH were deposited on 80 ML unprocessed $H_2{}^{18}O$ in the structure shown in Figure 1. The film was grown and irradiated at 80 K for 97s. The $^{18}O_2$ signal was monitored during ESD. The length of time that it takes for the O_2 signal to reach a specified level was measured from the data given in Figure 1 to find how much the addition of methanol delayed O_2 production. The specified signal levels were determined by the intensity of the 0.5 and 0.25 ML CH_3OH-capped ASW film just before the beam was turned off. The final intensity of the 0.5 ML CH_3OH/80 ML ASW film is 0.0296 (shown in black), while the final intensity of the 0.25 ML CH_3OH/80 ML ASW film is 0.0834 (shown in blue). The delay caused by the addition of methanol for a specified signal intensity increases linearly with methanol dose.

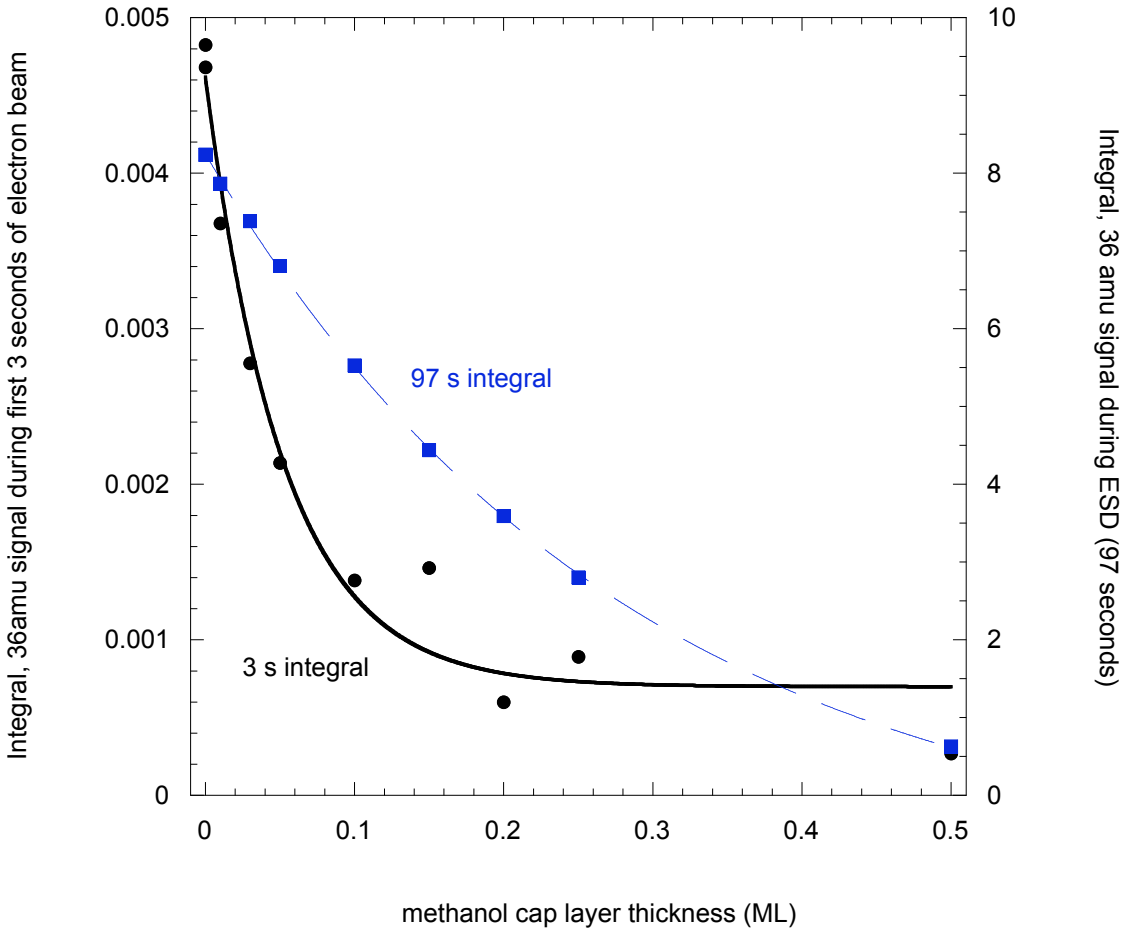

Figure 4.3: $^{18}O_2$ Suppression kinetics. n ML of CH_3OH were deposited on 80 ML unprocessed $H_2{}^{18}O$ in the structure shown in Figure 1. The film was grown and irradiated at 80 K for 97s. The $^{18}O_2$ signal was monitored during ESD. The resulting desorption signals (shown in Figure 1) were integrated over two ranges: 3 s and 97 s. The 3 s integral includes the first three seconds of irradiation, reflecting the initial suppression of O_2 prior to any induced mixing. The 97 s integral includes the full irradiation cycle and reflects total O_2 suppression as a function of deposited CH_3OH; the total signal is affected by mixing and CH_3OH desorption, and does not show as strong a suppression effect as O_2 begins to recover at later exposure times. The integrals were found to exponentially decay with increasing methanol dose, with 1/e constants of 0.05 ML CH_3OH and 0.29 ML CH_3OH for the 3 s and 97 s integrals, respectively.

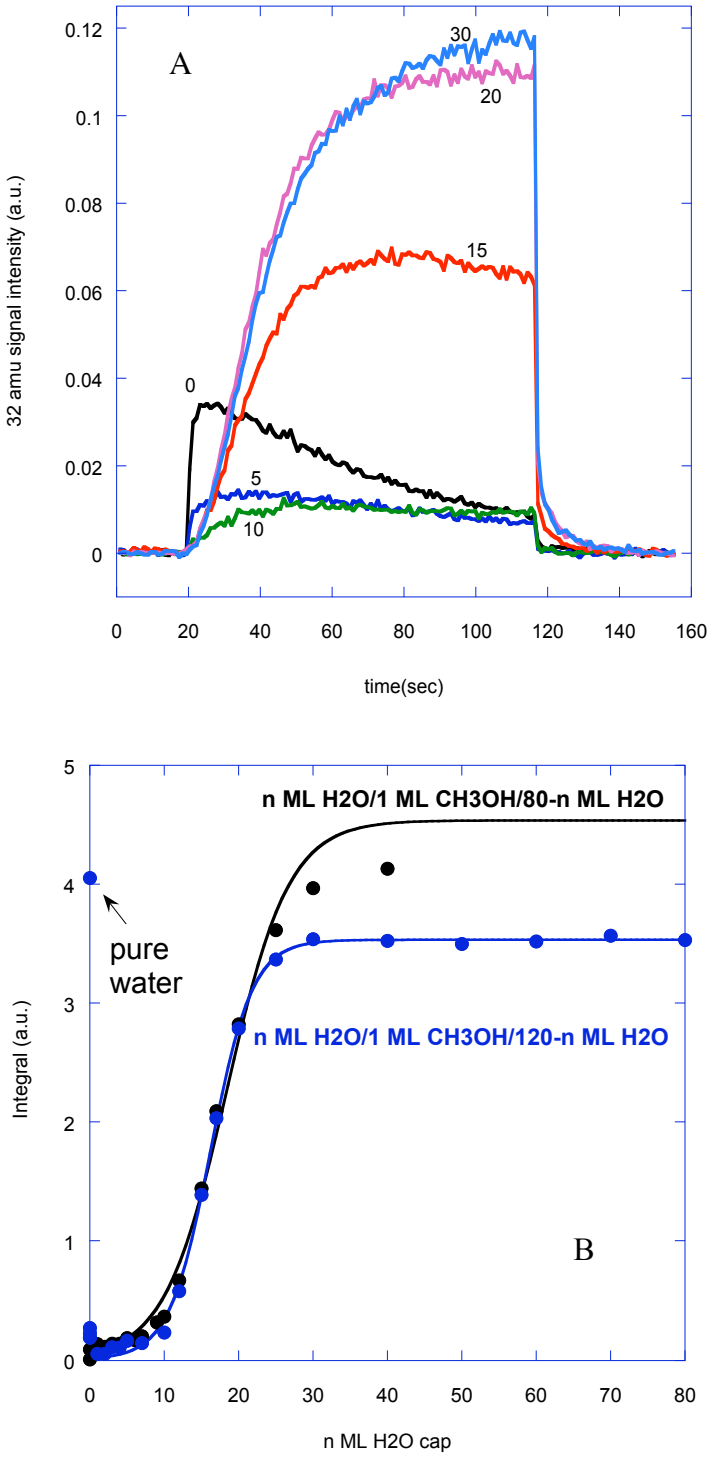

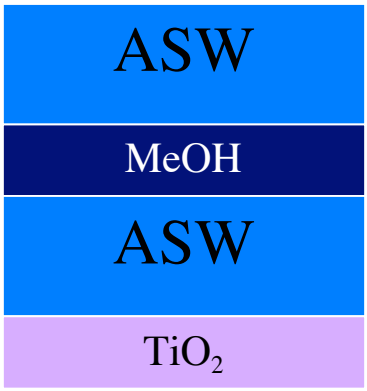

Figure 4.4: Sandwich films of water and 1 ML CH_3OH.

4.4A, top: 32amu signal during ESD. The initial rise in 32 amu signal is due to desorption of CH_3OH; the later slow rise of 32amu signal is due to O_2 production. Note that O_2 production does not resume until the capping layer is ~10 ML thick.

4.4B, bottom: The O_2 production signal was integrated over the 97 s scan and plotted with respect to capping layer thickness for two total film thicknesses: 80 ML ASW + 1 ML CH_3OH, and 120 ML ASW + 1 ML CH_3OH. Note that even in the 80 ML ASW / 1 ML CH_3OH / 40 ML ASW case, the production level is about 15% lower than in a 120 ML film of pure water.

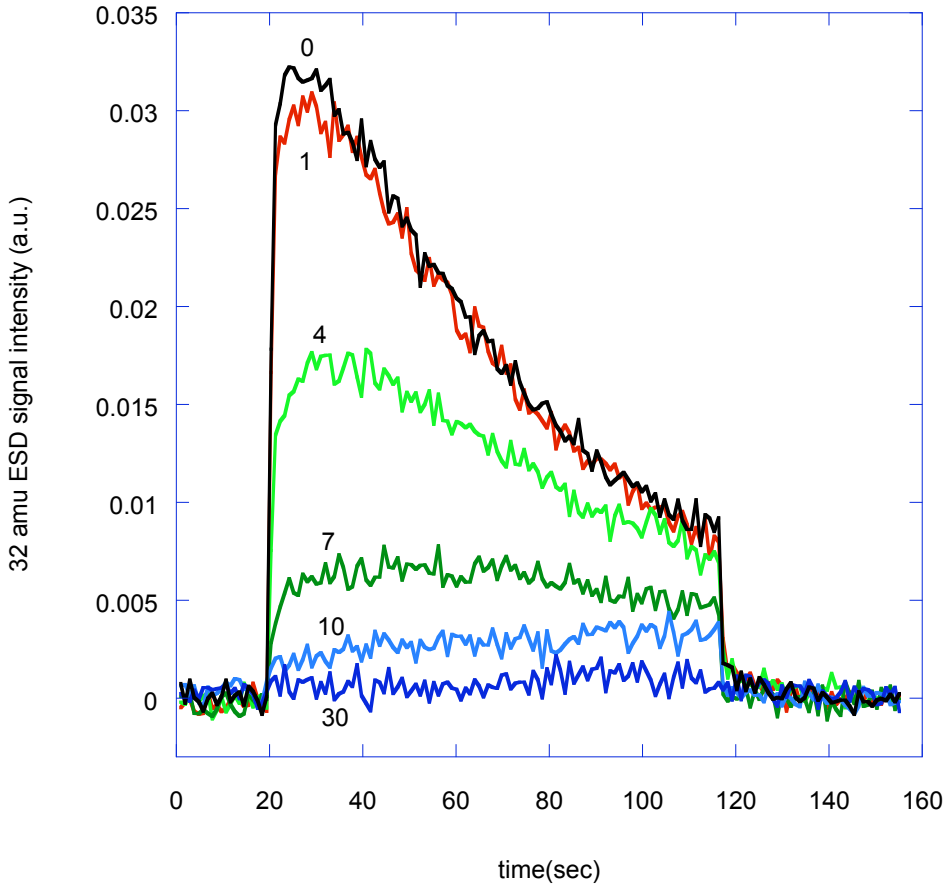

Figure 4.5: $^{16}O_2$ production during ESD from isotopically labeled sandwich films. Films of n ML $H_2{}^{18}O$/1 ML CH_3OH /80-n ML $H_2{}^{16}O$ were deposited at 25 K, and then irradiated at 80 K. The electron beam was turned on at 20 seconds and turned off at 117 seconds. Mass 32, due to the CH_3OH and O_2 signals, was monitored during desorption. CH_3OH is generally seen in the prompt portion of the signal immediately after the beam is turned on, while O_2 forming from $H_2{}^{16}O$ in the presence of CH_3OH is seen later. This graph shows the desorption of CH_3OH clearly, but no appreciable O_2 signal is observed. This absence, in combination with the late 36 amu ($^{18}O_2$) signal seen in this film, suggests that CH_3OH blocks the formation/desorption of O_2 formed from the bottom, $H_2{}^{16}O$, layer. In this way, CH_3OH is acting as an internal interface in much the same way that Pt or TiO_2 acts as an interface: the upper layers can interact with the CH_3OH but the lower layers appear to be totally blocked. These results suggest that MeOH is an effective barrier to O2 production from the lower layers, possibly as the result of efficient exciton trapping or side reactions.

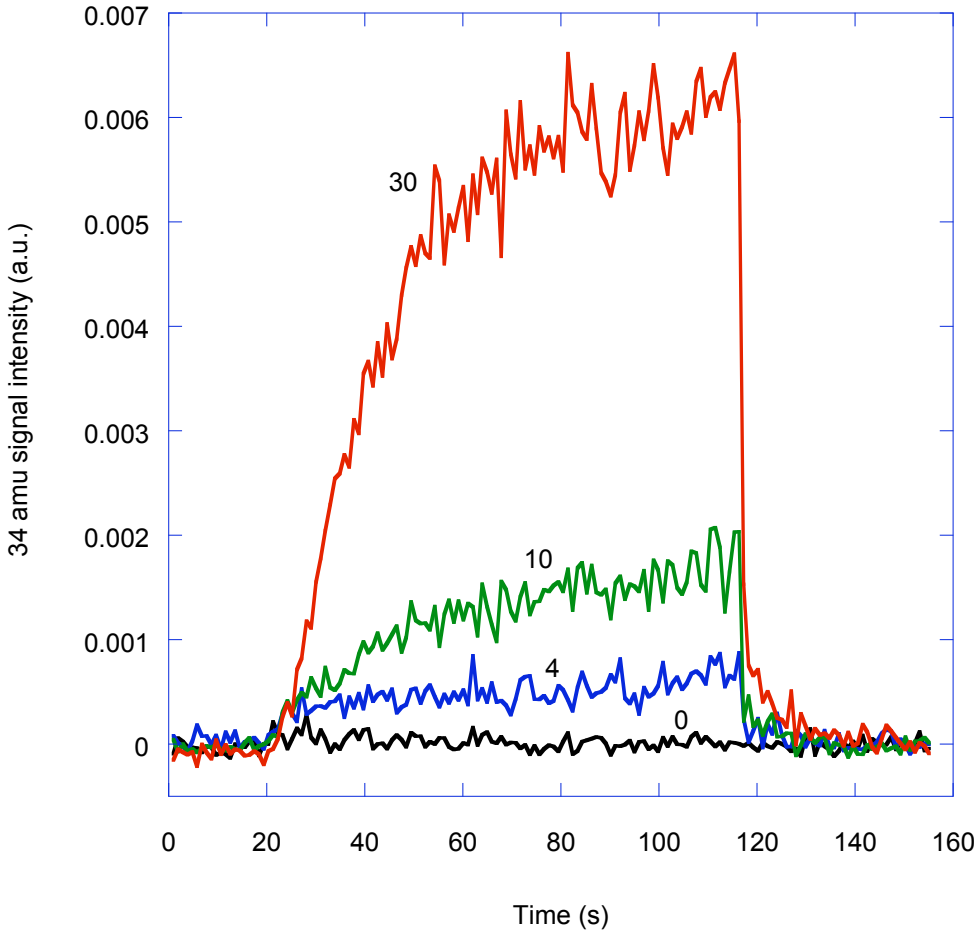

Figure 4.6: $^{16}O^{18}O$ production during ESD from isotopically labeled sandwich films. Films of n ML $H_2{}^{18}O$/1 ML CH_3OH/80-n ML $H_2{}^{16}O$ were grown at 25 K and irradiated at 80 K. The electron beam was turned on at 20 seconds and continued until 117 seconds. The 34 amu signal for $^{16}O^{18}O$ was measured to determine the amount of mixing between the upper $H_2{}^{18}O$ layer and the CH_3OH and $H_2{}^{16}O$ layers. Although the $^{16}O^{18}O$ signal increases with thicker $H_2{}^{18}O$ films as expected, the total signal is minimal for all thicknesses, indicating that mixing between the layers is not a major process.

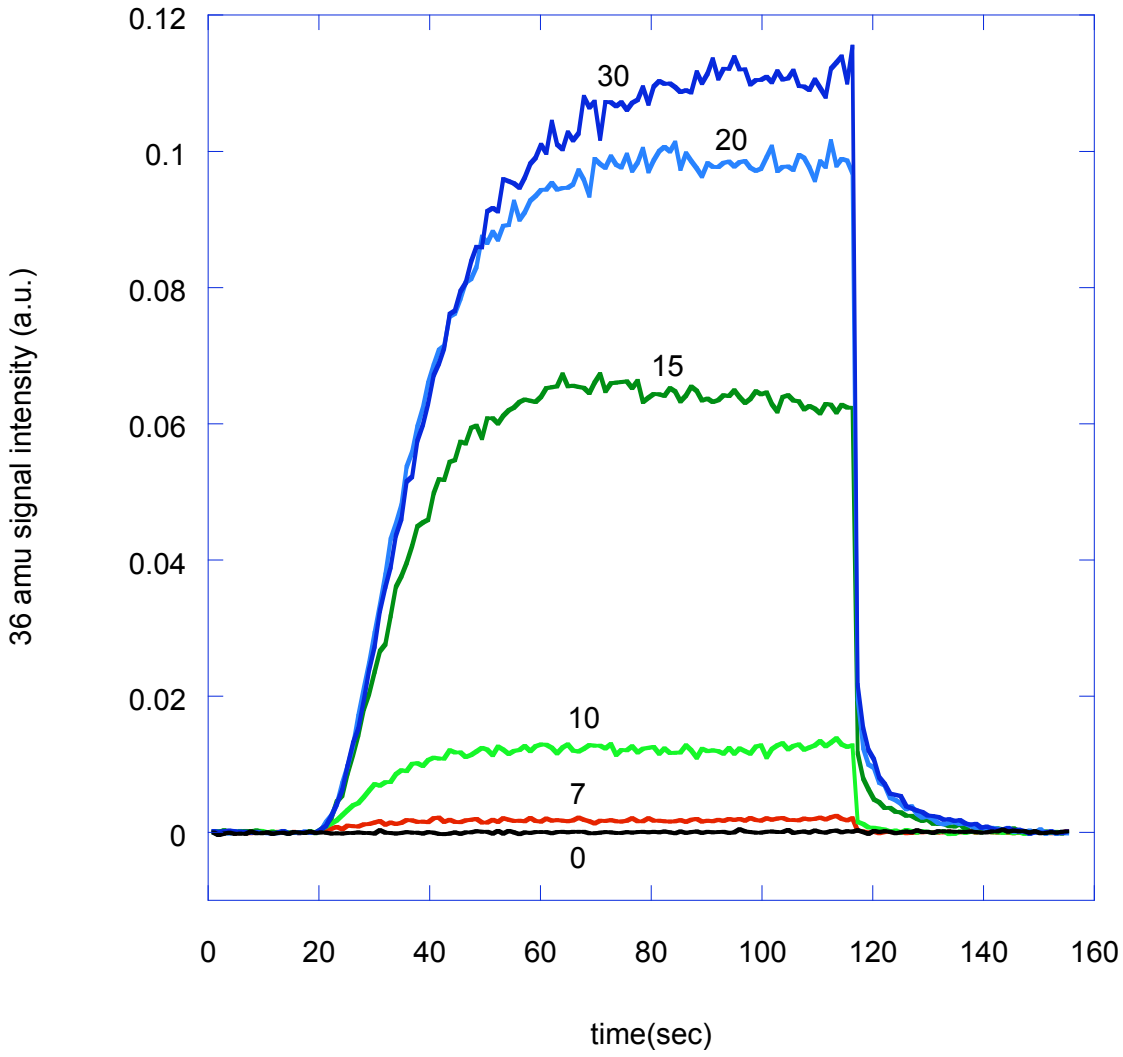

Figure 4.7: $^{18}O_2$ production during ESD from isotopically labeled sandwich films. Films of n ML $H_2{}^{18}O$/1 ML CH_3OH/80-n ML $H_2{}^{16}O$ were grown at 25 K and irradiated at 80 K. The electron beam was turned on at 20 seconds and continued until 117 seconds. The 36 amu signal for $^{18}O_2$ was measured to determine the O_2 produced in the upper $H_2{}^{18}O$ layer. Although the $^{18}O_2$ signal increases with thicker $H_2{}^{18}O$ layers, it does not return to a signal intensity comparable to that from a methanol-free film until the $H_2{}^{18}O$ layer is thicker than 20 ML. For comparison, in an isotopically labeled pure water film, a 10 ML thick $H_2{}^{18}O$ capping layer on 70 ML $H_2{}^{16}O$ produces nearly as much $^{18}O_2$ (70%) as an 80 ML $H_2{}^{18}O$ film. Total $^{18}O_2$ signal from the 10 ML $H_2{}^{18}O$/1 ML CH_3OH/70 ML $H_2{}^{16}O$ film is only 12% of the total $^{18}O_2$ signal from the 30 ML $H_2{}^{18}O$/1 ML CH_3OH/50 ML $H_2{}^{16}O$ film, making it clear that a buried methanol interface can suppress O_2 production over long ranges.

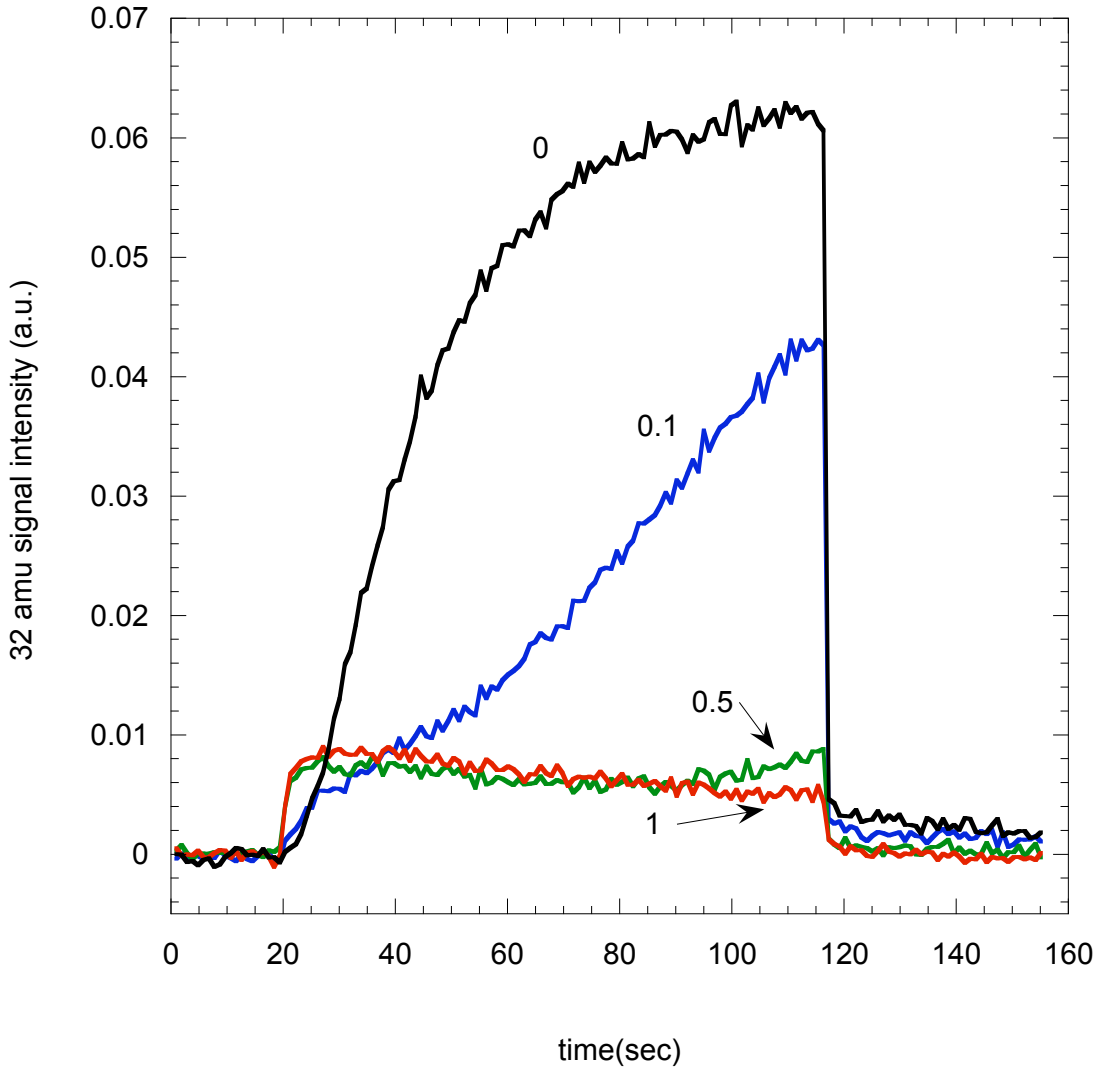

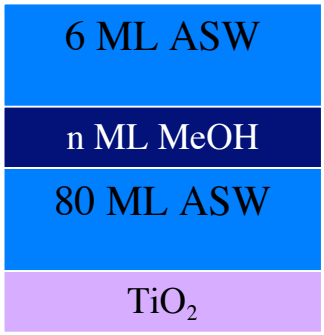

Figure 4.8: Dose dependence of oxygen suppression by buried methanol. 6 ML H_2O/n ML CH_3OH/80 ML H_2O films were grown and irradiated at 50 K. The electron beam was turned on at 20 seconds and continued for 97 seconds. Values of n ranging from 0 to 10 ML were dosed. However, methanol layers greater than 1 ML CH_3OH are not shown here as the 32 amu signals from these films are indistinguishable from the 6 ML H_2O/1 ML CH_3OH/80 ML H_2O films. Note that O_2 suppression is apparent before the methanol layer is complete; the signal from a film with 0.1 ML CH_3OH is roughly half that of the O_2 signal from a pure water film. As higher coverages of methanol (0.5 ML or more) are buried in the film, the initial O_2 signal is replaced by a prompt CH_3OH signal and the O_2 signal is increasingly eliminated.

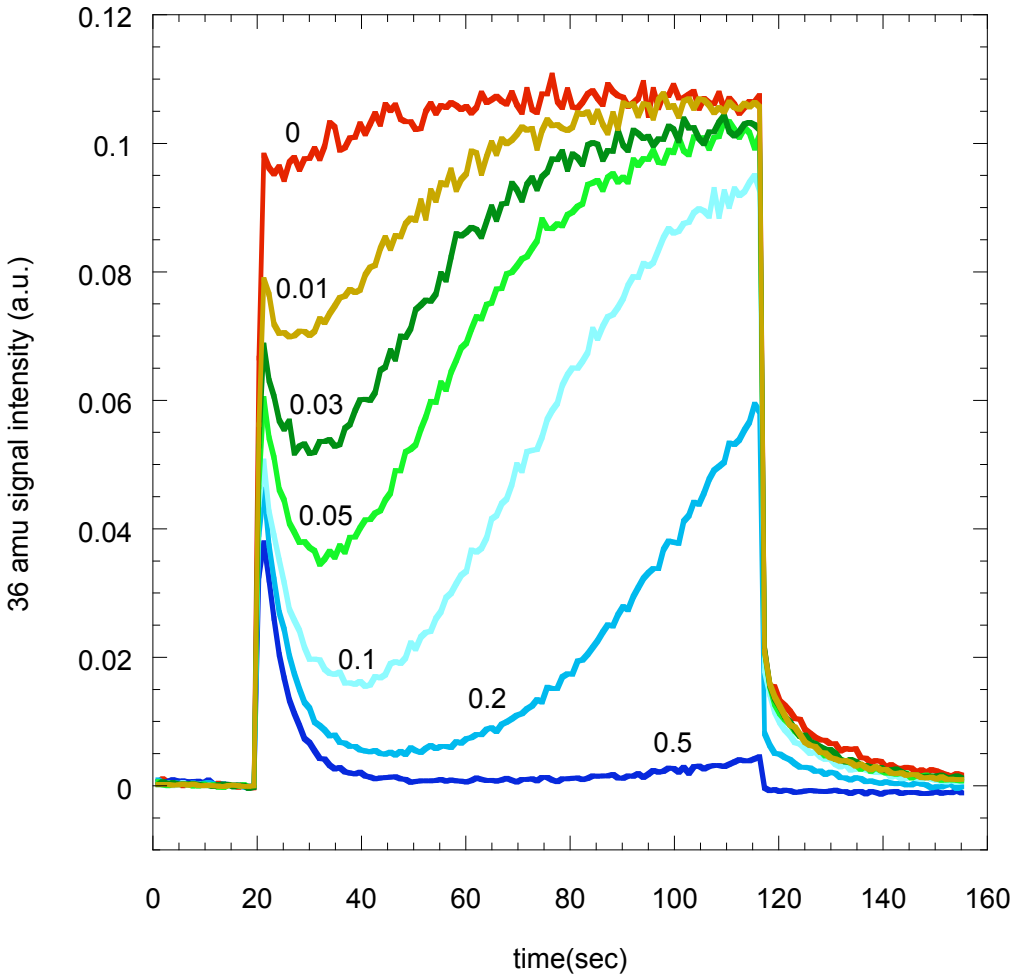

Figure 4.9: O_2 production from capped pre-irradiated $H_2{}^{18}O$ films. 80 ML $H_2{}^{18}O$ were dosed and irradiated at 80 K for 97 s. The preirradiated film was then capped with n ML CH_3OH and irradiated a second time at 80 K, beginning at 20 s above. In the graph above, the labels indicate the value of n. In the absence of CH_3OH, the $^{18}O_2$ signal returns promptly to it steady state value, as illustrated by the red trace labeled "0." The addition of CH_3OH suppresses the prompt production of O_2, and slows the recovery of O_2 production.

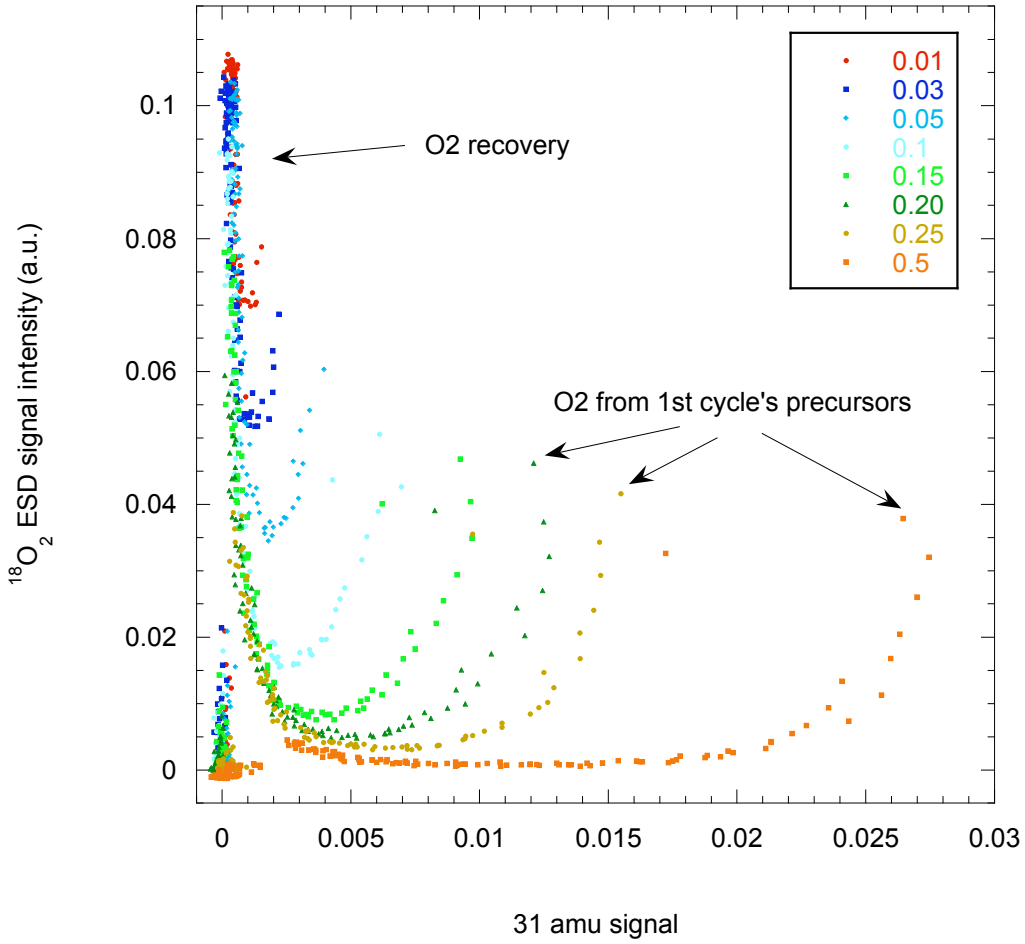

Figure 4.10: O_2 production dependence on surface MeOH concentration. 80 ML $H_2{}^{18}O$ were irradiated at 80 K to saturate the precursor population. Then, n ML CH_3OH were dosed on the processed film at 80 K and irradiated a second time for 97 s. The $^{18}O_2$ (36 amu) and the CH_3OH (31 amu) signals were measured in a series of ESDs. The dependency of the $^{18}O_2$ signal on the CH_3OH signal (which reflects the amount of CH_3OH remaining at the vacuum interface) is plotted above. Early in the cycle, when large quantities of methanol remain at the surface, the precursors formed in the first irradiation scan are scavenged, leading to a rapid decrease in prompt O_2 production. As methanol is removed from the film surface by mixing, reacting, and sputtering, O_2 production recovers. There is a strong correlation between the amount of CH_3OH remaining on the film, and the onset of O_2 recovery, with the recovery signals converging as the methanol signal falls below 0.003 units. Fitting the convergent recovery signals shows that less than 0.007 ML CH_3OH remains on the surface when recovery begins.

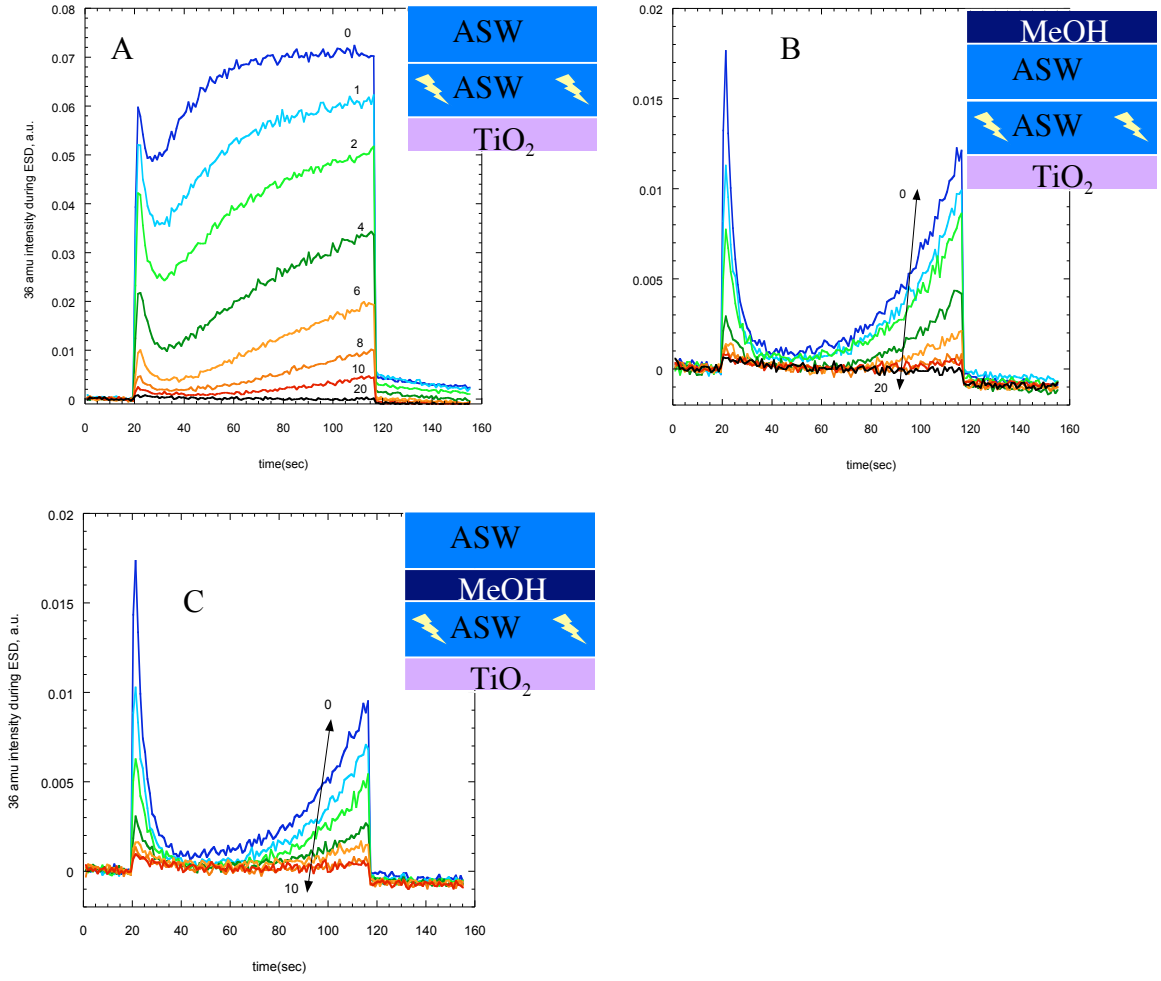

Figure 4.11: Effect of a $H_2{}^{16}O$ spacer layer on O_2 suppression by methanol. 80 ML $H_2{}^{18}O$ were irradiated for 97 s at 80 K to saturate the precursor population. This preprocessed film was then capped at 50 K by A) *n* ML unprocessed $H_2{}^{16}O$, B) *n* ML unprocessed $H_2{}^{16}O$, followed by 0.5 ML CH_3OH, or C) 0.5 ML CH_3OH followed by *n* ML unprocessed $H_2{}^{16}O$. The films were then irradiated at second time at 50 K, beginning at 20 s and continuing until 117 s, monitoring the $^{18}O_2$ signal from the pre-processed layer. Both irradiation cycles used 100 eV electrons at a current of ~2μA. The addition of CH_3OH reduced the $18O_2$ signal, regardless of whether it was in direct contact with the precursor-rich $H_2{}^{18}O$ layer. The placement of an $H_2{}^{16}O$ spacer layer between the methanol and the preprocessed film made no difference in the prompt portion of the ESD signal, which reflects O_2 forming from pre-existing precursors, and only very little difference in the recovery of the $^{18}O_2$ signal. This result suggests that the suppression effect caused by CH_3OH is due to some long-range process.

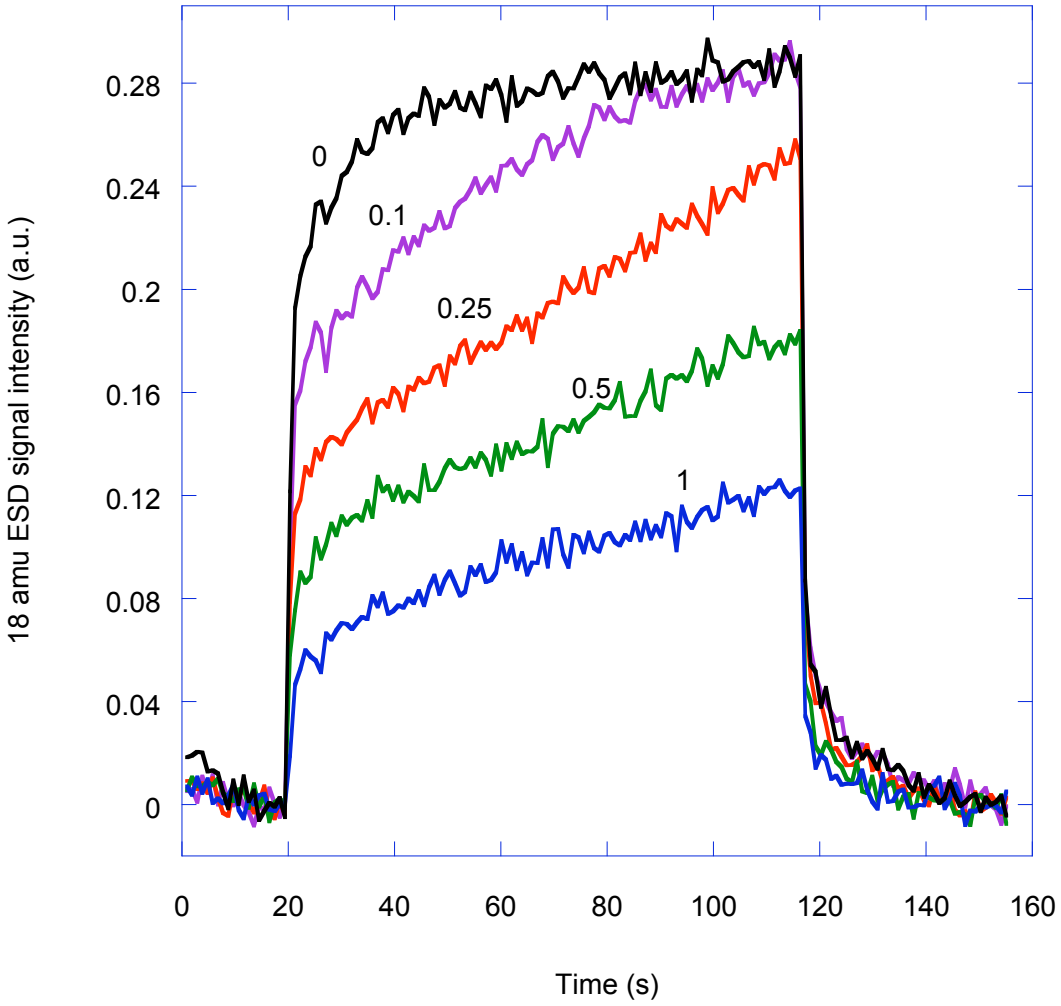

Figure 4.12: Suppression of water by CH_3OH. *n* ML CH_3OH were deposited atop an 80 ML H_2O film at 80 K. The film was irradiated beginning at 20 s and continuing until 117 s using 100 eV electrons at ~2μA current at 80 K. The H_2O signal was measured during ESD to determine how the addition of CH_3OH suppresses water desorption. Increasing quantities of methanol decrease the amount of water observed during ESD.

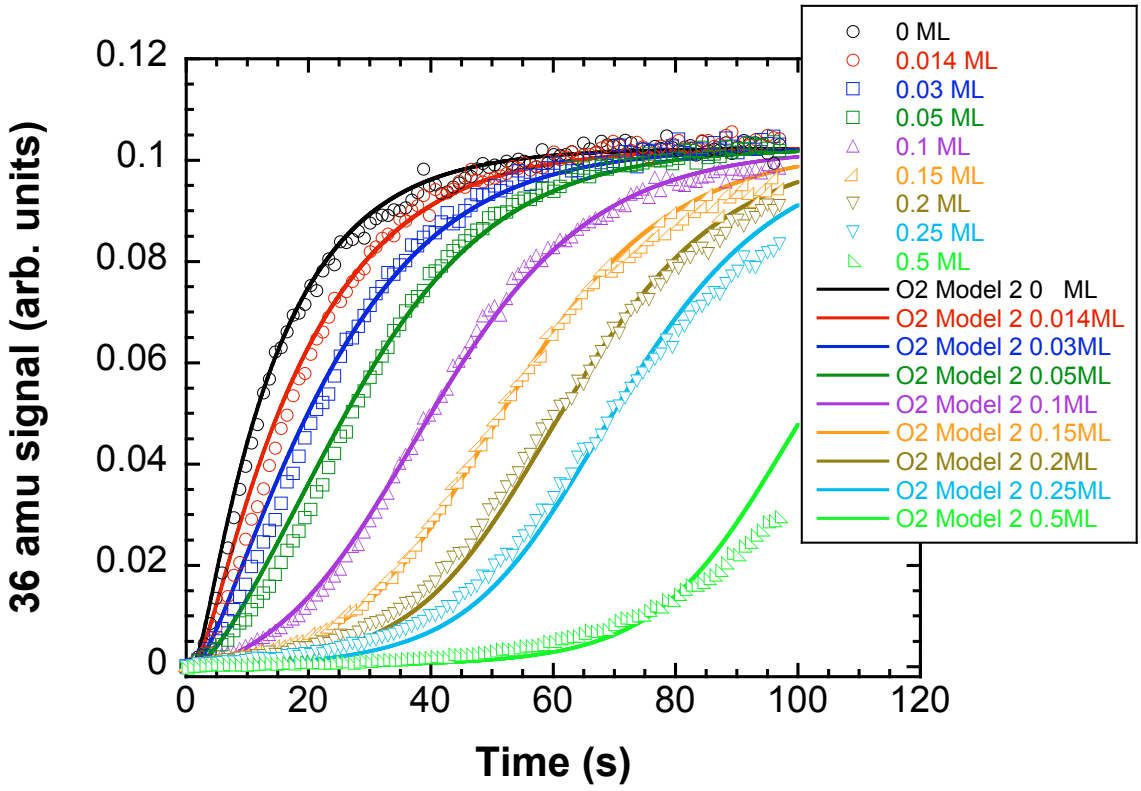

Figure 4.13: Model 2 predictions compared to data from Figure 4.1. The addition of reactions modeling scavenging of OH by CH_3OH and destruction of CH_3OH by electrons yields a good fit to the data.

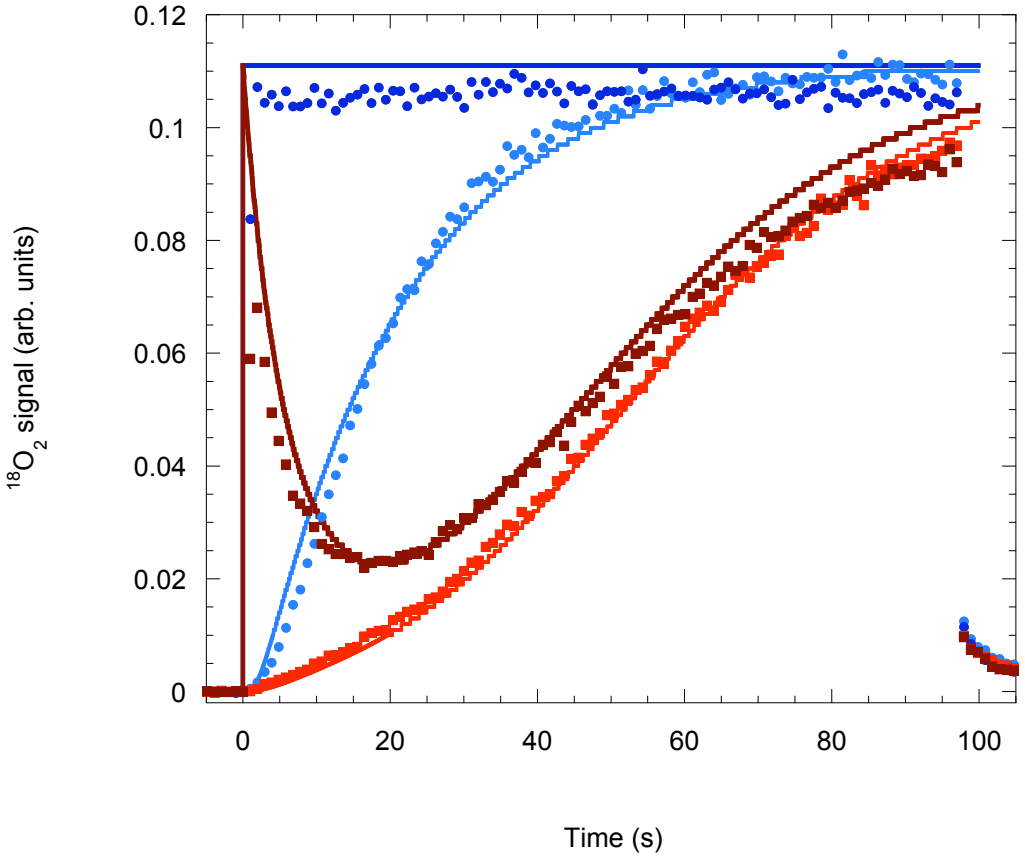

Figure 4.14: A comparison of Model 3 with the data. The $^{18}O_2$ signals from unprocessed and pre-irradiated films of pure $H_2{}^{18}O$ (light blue and dark blue, respectively) and unprocessed and pre-irradiated films of $H_2{}^{18}O$ capped with 0.1 ML CH_3OH (red and maroon, respectively) are compared with predictions by Model 3. Data, shown earlier in Figure 4.9, are represented by points; model predictions are represented by solid lines. The addition of the HO_2 scavenging reaction 10 allows the model to accurately predict suppression of O_2 production from both unprocessed and pre-processed films.

Appendix

The kinetic model used in Chapter 4 was developed by Nikolay Petrik at Pacific Northwest National Laboratory. Using the ten reaction equations described in Chapter 4, a series of differential equations were determined and solved numerically. For more details on the technique used, please see "Electron-stimulated production of molecular oxygen in amorphous solid water." by Petrik, Kavetsky, and Kimmel (*Journal of Physical Chemistry B*, 2006, volume 110, pp. 2723-2731).

$$\frac{d[OH]}{dt} = k_1 + 2k_3[H_2O_2] - k_2[OH]^2 - k_4[OH][H_2O_2] - k_6[OH][CH_3OH]$$

$$\frac{d[H_2O_2]}{dt} = k_2[OH]^2 - k_3[H_2O_2] - k_4[OH][H_2O_2]$$

$$\frac{d[HO_2]}{dt} = k_4[OH][H_2O_2] - k_5[HO_2] - k_8[HO_2][CH_3OH]$$

$$\frac{d[CH_3OH]}{dt} = -k_6[OH][CH_3OH] - k_7[CH_3OH] - k_8[HO_2][CH_3OH]$$

$$Y_{O2}(t) = \alpha k_5[HO_2]$$

$$Y_{CH3OH}(t) = \beta k_7[CH_3OH]$$

Bibliography

1. Al-Amoudi, A.; Dubochet, J.; Studer, D., Amorphous solid water produced by cryosectioning of crystalline ice at 113 K. *Journal of Microscopy-Oxford* **2002,** 207, 146-153.
2. Angell, C. A., Amorphous water. *Annual Review of Physical Chemistry* **2004,** 55, 559-583.
3. Ayotte, P.; Smith, R. S.; Teeter, G.; Dohnalek, Z.; Kimmel, G. A.; Kay, B. D., A Beaker without walls: Formation of deeply supercooled binary liquid solutions of alcohols from nanoscale amorphous solid films. *Physical Review Letters* **2002,** 88, (24).
4. Baggott, S. R.; Kolasinski, K. W.; Perdigao, L. M. A.; Riedel, D.; Guo, Q. M.; Palmer, R. E., Vacuum ultraviolet surface photochemistry of water adsorbed on graphite. *Journal of Chemical Physics* **2002,** 117, (14), 6667-6672.
5. Beltran, F. J.; Ovejero, G.; Rivas, J., Oxidation of polynuclear aromatic hydrocarbons in water .3. UV radiation combined with hydrogen peroxide. *Industrial & Engineering Chemistry Research* **1996,** 35, (3), 883-890.
6. Bernstein, M. P.; Dworkin, J. P.; Sandford, S. A.; Cooper, G. W.; Allamandola, L. J., Racemic amino acids from the ultraviolet photolysis of interstellar ice analogues. *Nature* **2002,** 416, (6879), 401-403.
7. Brovchenko, I.; Geiger, A.; Oleinikova, A., Liquid-liquid phase transitions in supercooled water studied by computer simulations of various water models. *Journal of Chemical Physics* **2005,** 123, (4).
8. Brunetto, R.; Baratta, G. A.; Domingo, M.; Strazzulla, G., Reflectance and transmittance spectra (2.2-2.4 _m) of ion irradiated frozen methanol. *Icarus* **2005,** 175, (1), 226-232.
9. Buch, V.; Bauerecker, S.; Devlin, J. P.; Buck, U.; Kazimirski, J. K., Solid water clusters in the size range of tens-thousands of H_2O: a combined computational/spectroscopic outlook. *International Reviews in Physical Chemistry* **2004,** 23, (3), 375-433.
10. Burrows, M. D.; Ryan, S. R.; Lamb, W. E.; McIntyre, L. C., Studies of H^+, H^{+2}, and H^{+3} Dissociative Ionization Fragments from Methane, Ethane, Methanol, Ethanol, and Some Deuterated Methanols Using Electron-Impact Excitation and a Time-of-Fight Method Incorporating Mass Analysis. *Journal of Chemical Physics* **1979,** 71, (12), 4931-4940.
11. Caro, G. M. M.; Meierhenrich, U. J.; Schutte, W. A.; Barbier, B.; Segovia, A. A.; Rosenbauer, H.; Thiemann, W. H. P.; Brack, A.; Greenberg, J. M., Amino acids from ultraviolet irradiation of interstellar ice analogues. *Nature* **2002,** 416, (6879), 403-406.
12. Collignon, B.; Picaud, S., Comparison between methanol and formaldehyde adsorption on ice: a molecular dynamics study. *Chemical Physics Letters* **2004,** 393, (4-6), 457-463.
13. Collings, M. P.; Dever, J. W.; Fraser, H. J.; McCoustra, M. R. S.; Williams, D. A., Carbon monoxide entrapment in interstellar ice analogs. *Astrophysical Journal* **2003,** 583, (2), 1058-1062.
14. Daschbach, J. L.; Schenter, G. K.; Ayotte, P.; Smith, R. S.; Kay, B. D., Helium

diffusion through H_2O and D_2O amorphous ice: Observation of a lattice inverse isotope effect. *Physical Review Letters* **2004,** 92, (19).
15. Delzeit, L.; Powell, K.; Uras, N.; Devlin, J. P., Ice surface reactions with acids and bases. *Journal of Physical Chemistry B* **1997,** 101, (13), 2327-2332.
16. Devlin, J. P., Structure, spectra, and mobility of low-pressure ices: Ice I, amorphous solid water, and clathrate hydrates at T < 150 K. *Journal of Geophysical Research-Planets* **2001,** 106, (E12), 33333-33349.
17. Dohnalek, Z.; Kimmel, G. A.; Ayotte, P.; Smith, R. S.; Kay, B. D., The deposition angle-dependent density of amorphous solid water films. *Journal of Chemical Physics* **2003,** 118, (1), 364-372.
18. Duvernay, F.; Chiavassa, T.; Borget, F.; Aycard, J. P., Experimental study of water-ice catalyzed thermal isomerization of cyanamide into carbodiimide: Implication for prebiotic chemistry. *Journal of the American Chemical Society* **2004,** 126, (25), 7772-7773.
19. Fisher, M.; Devlin, J. P., Defect Activity in Amorphous Ice from Isotopic Exchange Data - Insight into the Glass-Transition. *Journal of Physical Chemistry* **1995,** 99, (29), 11584-11590.
20. Garrett, B. C.; Dixon, D. A.; Camaioni, D. M.; Chipman, D. M.; Johnson, M. A.; Jonah, C. D.; Kimmel, G. A.; Miller, J. H.; Rescigno, T. N.; Rossky, P. J.; Xantheas, S. S.; Colson, S. D.; Laufer, A. H.; Ray, D.; Barbara, P. F.; Bartels, D. M.; Becker, K. H.; Bowen, H.; Bradforth, S. E.; Carmichael, I.; Coe, J. V.; Corrales, L. R.; Cowin, J. P.; Dupuis, M.; Eisenthal, K. B.; Franz, J. A.; Gutowski, M. S.; Jordan, K. D.; Kay, B. D.; LaVerne, J. A.; Lymar, S. V.; Madey, T. E.; McCurdy, C. W.; Meisel, D.; Mukamel, S.; Nilsson, A. R.; Orlando, T. M.; Petrik, N. G.; Pimblott, S. M.; Rustad, J. R.; Schenter, G. K.; Singer, S. J.; Tokmakoff, A.; Wang, L. S.; Wittig, C.; Zwier, T. S., Role of water in electron-initiated processes and radical chemistry: Issues and scientific advances. *Chemical Reviews* **2005,** 105, (1), 355-389.
21. Givan, A.; Loewenschuss, A.; Nielsen, C. J., FTIR studies of annealing processes in low temperature pure and mixed amorphous ice samples. *Journal of Physical Chemistry B* **1997,** 101, (43), 8696-8706.
22. Gunster, J.; Liu, G.; Stultz, J.; Goodman, D. W., Interaction of methanol and water on MgO(100) studied by ultraviolet photoelectron and metastable impact electron spectroscopies. *Journal of Chemical Physics* **1999,** 110, (5), 2558-2565.
23. Harris, T. D.; Lee, D. H.; Blumberg, M. Q.; Arumainayagam, C. R., Electron-Induced Reactions in Methanol Ultrathin Films Studied by Temperature-Programmed Desorption - a Useful Method to Study Radiation-Chemistry. *Journal of Physical Chemistry* **1995,** 99, (23), 9530-9535.
24. Henderson, M. A.; Otero-Tapia, S.; Castro, M. E., Electron-induced decomposition of methanol on the vacuum-annealed surface of TiO_2(110). *Surface Science* **1998,** 413, 252-272.
25. Henderson, M. A.; Otero-Tapia, S.; Castro, M. E., The chemistry of methanol on the surface: the TiO_2 (110) influence of vacancies and coadsorbed species. *Faraday Discussions* **1999**, (114), 313-329.
26. Hidaka, H.; Watanabe, N.; Shiraki, T.; Nagaoka, A.; Kouchi, A., Conversion of

H_2CO to CH_3OH by reactions of cold atomic hydrogen on ice surfaces below 20 K. *Astrophysical Journal* **2004,** 614, (2), 1124-1131.
27. Hornekaer, L.; Baurichter, A.; Petrunin, V. V.; Luntz, A. C.; Kay, B. D.; Al-Halabi, A., Influence of surface morphology on D_2 desorption kinetics from amorphous solid water. *Journal of Chemical Physics* **2005,** 122, (12).
28. Hudson, P. K.; Zondlo, M. A.; Tolbert, M. A., The interaction of methanol, acetone, and acetaldehyde with ice and nitric acid-doped ice: Implications for cirrus clouds. *Journal of Physical Chemistry A* **2002,** 106, (12), 2882-2888.
29. Jenniskens, P.; Banham, S. F.; Blake, D. F.; McCoustra, M. R. S., Liquid water in the domain of cubic crystalline ice I-c. *Journal of Chemical Physics* **1997,** 107, (4), 1232-1241.
30. Jenniskens, P.; Blake, D. F., Crystallization of amorphous water ice in the solar system. *Astrophysical Journal* **1996,** 473, (2 Pt 1), 1104-13.
31. Johari, G. P., State of water at 136 K determined by its relaxation time. *Physical Chemistry Chemical Physics* **2005,** 7, (6), 1091-1095.
32. Johari, G. P., Dielectric relaxation time of bulk water at 136-140 K, background loss and crystallization effects. *Journal of Chemical Physics* **2005,** 122, (14).
33. Kawanowa, H.; Hanatani, K.; Gotoh, Y.; Souda, R., Electron-stimulated desorption of positive ions from methanol adsorbed on a solid Ar substrate. *Surface Review and Letters* **2003,** 10, (2-3), 271-275.
34. Kimmel, G. A.; Orlando, T. M.; Cloutier, P.; Sanche, L., Low-energy (5-40 eV) electron-stimulated desorption of atomic hydrogen and metastable emission from amorphous ice. *Journal of Physical Chemistry B* **1997,** 101, (32), 6301-6303.
35. Kimmel, G. A.; Orlando, T. M.; Vezina, C.; Sanche, L., Low-Energy Electron-Stimulated Production of Molecular-Hydrogen from Amorphous Water Ice. *Journal of Chemical Physics* **1994,** 101, (4), 3282-3286.
36. Kimmel, G. A.; Stevenson, K. P.; Dohnalek, Z.; Smith, R. S.; Kay, B. D., Control of amorphous solid water morphology using molecular beams. I. Experimental results. *Journal of Chemical Physics* **2001,** 114, (12), 5284-5294.
37. Kohl, I.; Bachmann, L.; Mayer, E.; Hallbrucker, A.; Loerting, T., Water behaviour - Glass transition in hyperquenched water? *Nature* **2005,** 435, (7041), E1-E1.
38. Koza, M. M.; Geil, B.; Schober, H.; Natali, F., Absence of molecular mobility on nanosecond time scales in amorphous ice phases. *Physical Chemistry Chemical Physics* **2005,** 7, (7), 1423-1431.
39. La Spisa, S.; Waldheim, M.; Lintemoot, J.; Thomas, T.; Naff, J.; Robinson, M., Infrared and vapor flux studies of vapor-deposited amorphous and crystalline water ice films between 90 and 145 K. *Journal of Geophysical Research-Planets* **2001,** 106, (E12), 33351-33361.
40. LaVerne, J. A.; Pimblott, S. M., Effect of elastic collisions on energy deposition by electrons in water. *Journal of Physical Chemistry A* **1997,** 101, (25), 4504-4510.
41. Lepage, M.; Michaud, M.; Sanche, L., Low energy electron total scattering cross section for the production of CO within condensed methanol. *Journal of Chemical Physics* **1997,** 107, (9), 3478-3484.
42. Liu, L.; Chen, S. H.; Faraone, A.; Yen, C. W.; Mou, C. Y., Pressure dependence

of fragile-to-strong transition and a possible second critical point in supercooled confined water. *Physical Review Letters* **2005,** 95, (11).
43. McClure, S. M.; Barlow, E. T.; Akin, M. C.; Safarik, D. J.; Truskett, T. M.; Mullins, C. B., Transport in amorphous solid water films: Implications for self-diffusivity. *Journal of Physical Chemistry B* **2006,** 110, (36), 17987-17997.
44. McClure, S. M.; Barlow, E. T.; Akin, M. C.; Tanaka, P. L.; Safarik, D. J.; Truskett, T. M.; Mullins, C. B., Effect of dilute nitric acid on crystallization and fracture of amorphous solid water films. *Journal of Physical Chemistry C* **2007,** 111, (28), 10438-10447.
45. McClure, S. M.; Safarik, D. J.; Truskett, T. M.; Mullins, C. B., Evidence that amorphous water below 160 K is not a fragile liquid. *Journal of Physical Chemistry B* **2006,** 110, (23), 11033-11036.
46. Minoguchi, A.; Richert, R.; Angell, C. A., Dielectric studies deny existence of ultraviscous fragile water. *Physical Review Letters* **2004,** 93, (21).
47. Minoguchi, A.; Richert, R.; Angell, C. A., Dielectric relaxation in aqueous solutions of hydrazine and hydrogen peroxide: Water structure implications. *Journal of Physical Chemistry B* **2004,** 108, (51), 19825-19830.
48. Mishima, O.; Calvert, L. D.; Whalley, E., An Apparently 1st-Order Transition between 2 Amorphous Phases of Ice Induced by Pressure. *Nature* **1985,** 314, (6006), 76-78.
49. Mitlin, S.; Leung, K. T., Temporal evolution of an ultrathin, noncrystalline ice deposit at crystallization near 160 K studied by FT-IR reflection-absorption spectroscopy. *Canadian Journal of Chemistry* **2004,** 82, (6), 978-986.
50. Morishita, T., Anomalous diffusivity in supercooled liquid silicon under pressure. *Physical Review E* **2005,** 72, (2).
51. Notesco, G.; BarNun, A., Trapping of methanol, hydrogen cyanide, and n-hexane in water ice, above its transformation temperature to the crystalline form. *Icarus* **1997,** 126, (2), 336-341.
52. Palumbo, M. E.; Castorina, A. C.; Strazzulla, G., Ion irradiation effects on frozen methanol (CH_3OH). *Astronomy and Astrophysics* **1999,** 342, (2), 551-562.
53. Parenteau, L.; Jaygerin, J. P.; Sanche, L., Electron-Stimulated Desorption of H^- Ions Via Dissociative Electron-Attachment in Condensed Methanol. *Journal of Physical Chemistry* **1994,** 98, (40), 10277-10281.
54. Parenteau, L.; Sanche, L., Low-Energy Dissociative Electron-Attachment (0-20 Ev) on Methanol and Some Organic-Molecules. *Journal de Chimie Physique et de Physico-Chimie Biologique* **1994,** 91, (7-8), 1237-1242.
55. Petrik, N. G.; Kavetsky, A. G.; Kimmel, G. A., Electron-stimulated production of molecular oxygen in amorphous solid water. *Journal of Physical Chemistry B* **2006,** 110, (6), 2723-2731.
56. Petrik, N. G.; Kavetsky, A. G.; Kimmel, G. A., Electron-stimulated production of molecular oxygen in amorphous solid water on Pt(111): Precursor transport through the hydrogen bonding network. *Journal of Chemical Physics* **2006,** 125, (12).
57. Petrik, N. G.; Kimmel, G. A., Electron-stimulated reactions at the interfaces of amorphous solid water films driven by long-range energy transfer from the bulk. *Physical*

Review Letters **2003,** 90, (16).
58. Petrik, N. G.; Kimmel, G. A., Electron-stimulated production of molecular hydrogen at the interfaces of amorphous solid water films on Pt(111). *Journal of Chemical Physics* **2004,** 121, (8), 3736-3744.
59. Picaud, S.; Toubin, C.; Girardet, C., Monolayers of acetone and methanol molecules on ice. *Surface Science* **2000,** 454, 178-182.
60. Pimblott, S. M.; LaVerne, J. A., Production of low-energy electrons by ionizing radiation. *Radiation Physics and Chemistry* **2007,** 76, (8-9), 1244-1247.
61. Poole, P. H.; Sciortino, F.; Essmann, U.; Stanley, H. E., Phase-Behavior of Metastable Water. *Nature* **1992,** 360, (6402), 324-328.
62. Poole, P. H.; Sciortino, F.; Grande, T.; Stanley, H. E.; Angell, C. A., Effect of Hydrogen-Bonds on the Thermodynamic Behavior of Liquid Water. *Physical Review Letters* **1994,** 73, (12), 1632-1635.
63. Rowntree, P.; Parenteau, L.; Sanche, L., Electron-Stimulated Desorption Via Dissociative Attachment in Amorphous H2o. *Journal of Chemical Physics* **1991,** 94, (12), 8570-8576.
64. Sadtchenko, V.; Knutsen, K.; Giese, C. F.; Gentry, W. R., Interactions of CCl_4 with thin D_2O amorphous ice films, part I: A nanoscale probe of ice morphology. *Journal of Physical Chemistry B* **2000,** 104, (11), 2511-2521.
65. Sasaki, T.; Itai, Y.; Iwasawa, Y., Real-time observation of the dehydrogenation processes of methanol on clean Ru(001) and Ru(001)-p(2x2)-O surfaces by a temperature-programmed electron-stimulated desorption ion angular distribution/time-of-flight system. *Surface Science* **1999,** 443, (1-2), 44-56.
66. Schutte, W. A., Production of organic molecules in interstellar ices. In *Space Life Sciences: Extraterrestrial Organic Chemistry, Uv Radiation on Biological Evolution, and Planetary Protection*, Pergamon-Elsevier Science Ltd: Oxford, 2002; Vol. 30, pp 1409-1417.
67. Schwaner, A. L.; White, J. M., Electron-induced chemistry of methanol on Ag(111). *Journal of Physical Chemistry B* **1997,** 101, (49), 10414-10422.
68. Sieger, M. T.; Simpson, W. C.; Orlando, T. M., Production of O_2 on icy satellites by electronic excitation of low-temperature water ice. *Nature* **1998,** 394, (6693), 554-556.
69. Smith, R. S.; Dohnalek, Z.; Kimmel, G. A.; Stevenson, K. P.; Kay, B. D., The self-diffusivity of amorphous solid water near 150 K. *Chemical Physics* **2000,** 258, (2-3), 291-305.
70. Smith, R. S.; Huang, C.; Kay, B. D., Evidence for molecular translational diffusion during the crystallization of amorphous solid water. *Journal of Physical Chemistry B* **1997,** 101, (32), 6123-6126.
71. Smith, R. S.; Huang, C.; Wong, E. K. L.; Kay, B. D., The molecular volcano: Abrupt CCl_4 desorption driven by the crystallization of amorphous solid water. *Physical Review Letters* **1997,** 79, (5), 909-912.
72. Smith, R. S.; Kay, B. D., The existence of supercooled liquid water at 150 K. *Nature* **1999,** 398, (6730), 788-791.
73. Smith, R. S.; Zubkov, T.; Kay, B. D., The effect of the incident collision energy on the phase and crystallization kinetics of vapor deposited water films. *Journal of*

Chemical Physics **2006,** 124, (11).
74. Souda, R., Hydration of polar and nonpolar molecules at the surface of amorphous solid water. *Physical Review B* **2004,** 70, (16).
75. Stockbauer, R.; Bertel, E.; Madey, T. E., The Origin of H^+ in Electron-Stimulated Desorption of Condensed CH_3OH. *Journal of Chemical Physics* **1982,** 76, (11), 5639-5641.
76. Takano, Y.; Tsuboi, T.; Kaneko, T.; Kobayashi, K.; Marumo, K., Pyrolysis of high-molecular-weight complex organics synthesized from a simulated interstellar gas mixture irradiated with 3 MeV proton beam. *Bulletin of the Chemical Society of Japan* **2004,** 77, (4), 779-783.
77. Velikov, V.; Borick, S.; Angell, C. A., The glass transition of water, based on hyperquenching experiments. *Science* **2001,** 294, (5550), 2335-2338.
78. Wada, A.; Mochizuki, N.; Hiraoka, K., Methanol formation from electron-irradiated mixed H2O/CH4 ice at 10 K. *Astrophysical Journal* **2006,** 644, (1), 300-306.
79. Walch, S. P.; Bauschlicher, C. W.; Ricca, A.; Bakes, E. L. O., On the reaction CH_2O+NH_3 -> CH_2NH+H_2O. *Chemical Physics Letters* **2001,** 333, (1-2), 6-11.
80. Winkler, A. K.; Holmes, N. S.; Crowley, J. N., Interaction of methanol, acetone and formaldehyde with ice surfaces between 198 and 223 K. *Physical Chemistry Chemical Physics* **2002,** 4, (21), 5270-5275.
81. Wolff, A. J.; Carlstedt, C.; Brown, W. A., Studies of binary layered CH_3OH/H_2O ices adsorbed on a graphite surface. *Journal of Physical Chemistry C* **2007,** 111, (16), 5990-5999.
82. Woon, D. E., Pathways to glycine and other amino acids in ultraviolet-irradiated astrophysical ices determined via quantum chemical modeling. *Astrophysical Journal* **2002,** 571, (2), L177-L180.
83. Woon, D. E., Photoionization in ultraviolet processing of astrophysical ice analogs at cryogenic temperatures. In *Space Life Sciences: Steps toward Origin(S) of Life*, 2004; Vol. 33, pp 44-48.
84. Woon, D. E.; Park, J. Y., Photoionization of benzene and small polycyclic aromatic hydrocarbons in ultraviolet-processed astrophysical ices: A computational study. *Astrophysical Journal* **2004,** 607, (1), 342-345.
85. Wu, C. Y. R.; Judge, D. L.; Cheng, B. M.; Shih, W. H.; Yih, T. S.; Ip, W. H., Extreme ultraviolet photon-induced chemical reactions in the C_2H_2-H_2O mixed ices at 10 K. *Icarus* **2002,** 156, (2), 456-473.
86. Wu, C. Y. R.; Judge, D. L.; Cheng, B. M.; Yih, T. S.; Lee, C. S.; Ip, W. H., Extreme ultraviolet photolysis of CO_2-H_2O mixed ices at 10 K. *Journal of Geophysical Research-Planets* **2003,** 108, (E4).
87. Wu, C. Y. R.; Yang, B. W.; Judge, D. L., Total Ion Desorption Yields of H_2O, D_2O, CH_3OH, CD_3OD and Water-Methanol Mixed Ices Irradiated at 584 Angstrom. *Planetary and Space Science* **1994,** 42, (4), 273-277.
88. Yamamoto, S.; Beniya, A.; Mukai, K.; Yamashita, Y.; Yoshinobu, J., Low-energy electron-stimulated chemical reactions of CO in water ice. *Chemical Physics Letters* **2004,** 388, (4-6), 384-388.
89. Yue, Y. Z.; Angell, C. A., Clarifying the glass-transition behaviour of water by

comparison with hyperquenched inorganic glasses. *Nature* **2004,** 427, (6976), 717-720.
90. Yue, Y. Z.; Angell, C. A., Water behaviour - Reply. *Nature* **2005,** 435, (7041), E1-E2.
91. Zheng, W. J.; Jewitt, D.; Kaiser, R. I., Formation of hydrogen, oxygen, and hydrogen peroxide in electron-irradiated crystalline water ice. *Astrophysical Journal* **2006,** 639, (1), 534-548.

Vita

Minta Carol Akin was born in Fort Myers, Florida, on October 18, 1980, to Debra Everton Akin and Jerry Paul Akin. After graduating from the International Baccalaureate program at Eastside High School, Gainesville, Florida, in 1999, she attended the California Institute of Technology in Pasadena, California. Following receipt of the degree of Bachelor of Science from Caltech in 2003, she entered the Graduate School of the University of Texas at Austin.

Permanent address: 600 E. Covington Drive, Austin, Texas 78753

This dissertation was typed by the author.